Feary, D.A., Hine, A.C., Malone, M.J., et al., 2000
Proceedings of the Ocean Drilling Program, Initial Reports Volume 182

6. Site 1128[1]

Shipboard Scientific Party[2]

BACKGROUND AND OBJECTIVES

Site 1128 is located on the southern Australian upper continental rise in 3874.4 m of water (Fig. F1). This was primarily a paleoceanographic site designed to intersect pelagic sections that collectively span the entire Cenozoic succession and to constitute the deeper water component of the overall Leg 182 shelf-to-basin transect sampling strategy. Site 1128 is located on gently dipping seafloor immediately seaward of a relatively steep, eroding lower slope. The site was positioned to sample a thick stratigraphic section of presumed Cenozoic age, together with the uppermost part of the underlying presumed Mesozoic succession (Fig. F2; see "Seismic Stratigraphy," p. 36). The absence of any suitable middle to lower slope site (between 1500 and 2500 m water depth) meant that this site was a particularly important component of the depth transect. Although the sedimentary section underlying the modern continental rise appears to be laterally extensive (extending for some 350–400 km along the Great Australian Bight foot of slope) and >10 km thick, there are no stratigraphic ties to enable reliable predrill stratigraphic predictions. The estimation of depth to the Cenozoic/Mesozoic boundary was simply based on identification of a significant unconformity surface (Fig. F2) at approximately the expected depth. Anticipated lithologies at Site 1128 were pelagic nannofossil foraminifer oozes, possibly with intercalated clay-rich layers representing deposition below the carbonate compensation depth (CCD).

The principal objective at this site was to sample the Cenozoic succession in a deep oceanic setting to obtain a complete record of Circum-Antarctic Current evolution within the developing seaway between Australia and Antarctica that resulted from the Tasman Gateway opening during the Eocene. Because the condensed section at the base of the Cenozoic in the Jerboa-1 well contains lower Oligocene faunas, there was a high probability that the intermediate and deep pelagic succes-

F1. Map showing Site 1128 in relation to other Leg 182 sites and the AGSO169 site-survey seismic lines, p. 42.

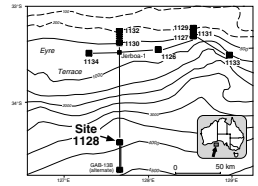

F2. Portion of seismic Line AGSO169/11e showing seismic stratigraphic sequences at Site 1128, p. 43.

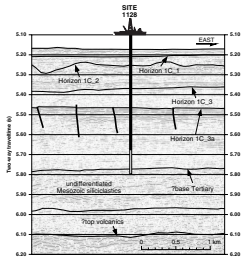

[1] Examples of how to reference the whole or part of this volume.
[2] Shipboard Scientific Party addresses.

sions would together contain a more expanded record of this critically important time of Antarctic ice-cap evolution and Southern Ocean paleoceanographic development.

Additional objectives were to

1. Determine depositional and diagenetic facies in an upper continental rise setting;
2. Recover a condensed Cenozoic section recording the history of CCD fluctuations and at least a partial history of deep-water mass variations during the evolution of the Southern Ocean;
3. Categorize the heatflow regime on the upper continental rise; and
4. Seek evidence for fluid flow within the upper part of this deep sedimentary basin.

OPERATIONS

Transit to Site 1128

The 76-nmi transit to Site 1128 required 8.5 hr at an average speed of 8.9 kt. A beacon was launched at 1100 hr on 3 November initiating Site 1128. Its signal was erratic, however, and another beacon was deployed.

Hole 1128A

The ship was stabilized on position and an advanced hydraulic piston core (APC)/extended core barrel (XCB) bottom-hole assembly (BHA) was run to the seafloor. Hole 1128A was spudded at 1900 hr on 3 November, recovering 9.31 m in Core 1H. The hole was terminated at 1930 hr on 3 November because the recovery was excessive for establishment of a good mudline.

Hole 1128B

The ship was not moved, and Hole 1128B was spudded at 1955 hr on 3 November. The bit was positioned at 3882 meters below rig floor (mbrf) and Core 1H recovered 5.66 m, indicating a water depth of 3874.6 meters below sea level (mbsl). Advanced hydraulic piston coring advanced to 137.8 meters below seafloor (mbsf) and ceased when a partial stroke on Core 15H bent the APC shoe. Cores 3H–15H were oriented, and coring continued with the XCB advancing from 137.8 to 280.6 mbsf (Table T1). The Davis-Villinger temperature probe (DVTP) was deployed after Core 16X at 145.8 mbsf. It became apparent that the jet nozzles in the bit were plugged some time after running the DVTP. The resulting increased pump pressure required to maintain circulation may have caused reduced recovery in Cores 17X and 18X (Table T1). Recovery dropped to 28.9% in the last four XCB cores (27X–30X), probably as a result of the bit overheating, despite attempts to increase circulation and pressure. Coring was terminated because of the low recovery in the last four cores and increasing drilling times. The bit cleared the seafloor at 1515 hr on 5 November, ending Hole 1128B.

T1. Site 1128 coring summary, p. 87.

Hole 1128C

The ship was moved 20 m east, and Hole 1128C was spudded with the APC at 1640 hr on 5 November. The bit was positioned at 3884 mbrf, and Core 1H recovered 7.95 m, indicating a water depth of 3874.3 mbsl. APC coring advanced to 138.3 mbsf, ceasing again with a partial stroke at Core 15H and a bent APC shoe. Cores 3H–15H were oriented and Adara tool heat-flow measurements were taken at Cores 4H, 8H, and 12H. A special nonmagnetic assembly was run on the bottom two-thirds of the APC inner core barrel on Cores 3H, 5H, 7H, 9H, 11H, and 13H (see **"Paleomagnetism,"** p. 22, and **"Appendix: Magnetics Experiment"**). Coring resumed with the XCB to the depth objective of 240.1 mbsf. The drill string was recovered at 0330 hr on 7 November, terminating Hole 1128C.

Hole 1128D

The ship was moved 20 m north of Hole 1128C, and a rotary core barrel (RCB) BHA was run to the seafloor. Hole 1128D was spudded at 1115 hr on 7 November, and the hole was drilled ahead with a center bit to 231.2 mbsf. Rotary core barrel coring advanced from 231.1 to 452.6 mbsf with 35.7% recovery. Coring was terminated when drilling times increased and recovery decreased to unacceptable levels. The hole was prepped for logging, and the end of the drill pipe was placed at 92 mbsf. The triple combination logging tool (triple combo) tool string was run but was unable to pass 96 mbsf. The tool was pulled out, and the pipe run to 112 mbsf. The triple combo was rerun through a tight spot at ~250 mbsf from 428 mbsf (24 m off bottom) to the mudline. The Formation MicroScanner (FMS)/sonic tool string was deployed and logged from 424 mbsf to the end of the pipe. Operational time constraints precluded deployment of the well seismic tool (WST). The hole was displaced with mud, the drill string was retrieved and secured, and the ship was under way to Site 1129 at 0130 on 11 November.

LITHOSTRATIGRAPHY

Introduction

Site 1128 is located on the upper continental rise, close to the toe of slope in 3874.4 m of water. Coring penetrated sediment in a small perched depression (see **"Seismic Stratigraphy,"** p. 36) within a seaward-thickening wedge of Cenozoic carbonate and terrigenous clastic sediment. Seismic data indicate that the lower part of the continental slope directly north of the site is an ~2000-m-high relatively steep incline with an irregular topography of exposed Mesozoic (see **"Seismic Stratigraphy,"** p. 36), mainly terrigenous, clastic sedimentary rocks. The upper part of the slope is a relatively smooth seaward-dipping incline that represents the outer part of the cool-water carbonate ramp. The continental slope is cut by numerous canyons.

The succession intersected at Site 1128 (Fig. **F3**) consists of 70 m of mainly Neogene pelagic carbonate sediment overlying a 380-m succession of Paleogene deep-water siliciclastic deposits. These two sediment types are separated by a zone of sediment gravity-flow deposits and a major hiatus.

F3. Sediment lithostratigraphy, **p. 44.**

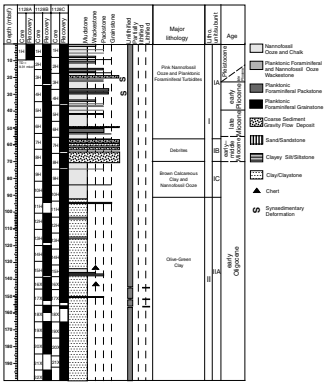

Lithostratigraphic Units

Unit I

Intervals: Sections 182-1128A-1H-1 through 1H-CC; Sections 182-1128B-1H-1 through 10H-7, 66 cm; Sections 182-1128C-1H-1 through 10H-6, 30 cm
Depth: 0–9.50 mbsf (Hole 1128A); 0–91.36 mbsf (Hole 1128B); 0–93.30 mbsf (Hole 1128C)
Age: Pleistocene–early Oligocene

Unit I is a succession of deep-water pelagic carbonate sediment, mostly nannofossil ooze, punctuated by centimeter- to meter-scale planktonic foraminifer glauconite packstones and wackestones and several coarse- to very coarse grained boulder conglomerates. The base of the unit is defined by the transition from brown calcareous clay to gray and green clay. The grainy carbonates and conglomerates have all the attributes of sediment gravity-flow deposits and are interpreted as calciturbidites and debris-flow deposits, respectively. The sediments are pink to brown throughout and characterized by extensive bioturbation.

Subunit IA

Intervals: Core 182-1128A-1H; Sections 182-1128B-1H-1 through 7H-1, 125 cm; Sections 182-1128C-1H-1 through 6H-CC
Depth: 0–9.50 mbsf (Hole 1128A); 0–54.45 mbsf (Hole 1128B); 0–55.50 mbsf (Hole 1128C)
Age: Pleistocene–late Miocene

Subunit IA is pelagic nannofossil ooze punctuated by numerous thin calciturbidites. The sediment is pink to brown in color, interrupted by discrete white intervals. These colors, which become somewhat muted with increased depth, are most probably caused by small amounts of oxidized clay. The noncarbonate component of these sediments is generally ~10% (see **"Organic Geochemistry,"** p. 27). Darker hues commonly pass gradationally into lighter hues, defining repetitive decimeter-scale units. Alternatively, color changes abruptly across obvious omission surfaces. Contacts between pink/brown units and white units are generally sharp.

Portions of the section, as thick as 3 m at ~20.0–20.4, 21.2–22.0, and 27.5–28.5 mbsf, are characterized by steeply inclined (as much as 50°) and/or contorted bedding and are interpreted to be the result of synsedimentary deformation. It is not clear whether these are syndepositional or were formed later within the sediment pile.

Pelagic Sediment. The nannofossil ooze has a mudstone to wackestone texture and is conspicuously spiculitic. Well-preserved planktonic foraminifers, generally small and in the fine to very fine sand-size range, form most of the coarser particles. Other rare grains include bioclasts, clay particles, and tunicate sclerites (see **"Site 1128 Smear Slides,"** p. 79). White sediment is typically totally homogenized through bioturbation, whereas pink/brown sediment, although extensively burrowed, displays multi-tiered trace fossils with discrete *Zoophycos, Chondrites,* and *Planolites*.

Calciturbidites. These white to gray grainy sediments have a packstone or grainstone texture and are generally fine- to medium-grained sand. Most are graded turbidites with sharp to eroded bases that gradually pass upward from grainstone to packstone into nannofossil ooze

(Fig. F4). Less common grain flows are composed of grainstone throughout and have sharp bases and tops. Units range in thickness from <1 cm to >2 m, with thicker beds usually composed of stacked turbidites. Virtually all the calciturbidites can be correlated between Holes 1128B and 1128C, and they show only minor thickness changes.

The sediment is typically dominated by the tests of planktonic foraminifers and lesser but conspicuous glaucony grains. Glaucony ranges from dark green/black to light pale green and typically has a well-developed botryoidal texture. Some sediment contains numerous limonite/goethite grains, many of which are clearly altered glaucony, whereas others have an indeterminate origin. Other important particles, although usually present in trace amounts, are angular to subangular quartz grains (clear and iron stained) and sedimentary rock fragments, particularly fine- to very fine grained green sandstone. These carbonate sands also occur in isolated burrows, suggesting either infiltration down from overlying turbidites or burrow filling by otherwise bypassing sediment. Other sand-sized grains include benthic foraminifers, sponge spicules, and occasional infaunal echinoid spines.

Coarse-Grained Sediment Gravity Flows. One interval 19 m below the top of the succession is an ~1.2-m-thick sandy conglomerate (Fig. F5). This deposit is mostly a planktonic foraminifer sand with granule-sized pieces of bryozoans (mostly delicate branching growth forms; cf. *Nevianopora* and *Hornera*), serpulid worm tubes, benthic foraminifers (mostly nodosariids), and fine-grained green sandstone. The middle portion contains cobble-sized clasts of compacted nannofossil ooze with a wackestone texture, together with planktonic foraminifers. This unit appears to represent several stacked beds.

Subunit IB

Intervals: Sections 182-1128B-7H-1, 125 cm, through 8H-2, 55 cm; Sections 182-1128C-7H-1 through 8H-4, 55 cm
Depth: 54.45–64.75 mbsf (Hole 1128B); 55.50–70.05 mbsf (Hole 1128C)
Age: early Miocene–late Miocene

This interval consists of large clasts, fine sediment, and deformed strata (Figs. F6, F7). Although there are differences between the two holes, there is a general similarity in stratigraphy, and the interval is divisible into two zones.

The upper zone is a series of three meter-scale polymict conglomerates and pebbly mudstones separated by black clay and nannofossil ooze. The lower zone from Hole 1128C is deformed nannofossil ooze and black clay with basal conglomerates. The conglomerates are mainly matrix supported, with clasts in the coarse pebble to cobble grade and a calcareous ooze matrix. Clasts represent a large variety of lithologies from different stratigraphic levels. They consist mainly of claystone and mudstone lithologies, but siltstone and sandstone are also present.

Clasts are well segregated. Some are slightly compacted but not severely deformed, although clast boundaries locally show shearing. A succession of clasts in Sections 182-1128C-7H-1 and 7H-2 are considerably wider than the core diameter (6.6 cm), extending over 20–30 cm in thickness and showing an inclination of 35°–45°. They seem to represent elongated slabs. Consolidation ranges from very soft to moderately consolidated to lithified. This last type is mainly seen in a few specimens of relatively hard green sandstones, with most clasts being poorly to moderately consolidated. Most fragments are randomly oriented, al-

F4. A calciturbidite of planktonic foraminifers and glaucony grading up into nannofossil ooze, Subunit IA, p. 47.

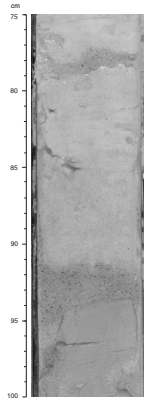

F5. The upper part of a sediment gravity flow, Subunit IA, p. 48.

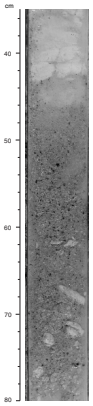

F6. Conglomerates and deformed strata, Subunit IB, p. 49.

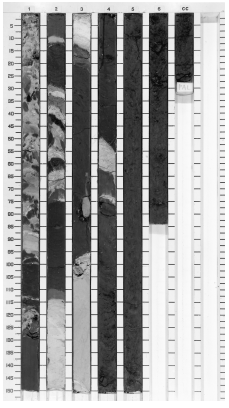

though some beds show a crude subhorizontal clast fabric. Steeply inclined to vertical clast orientations are common.

The matrix consists of massive, nonbioturbated, light gray to white nannofossil and foraminiferal ooze. The clast/matrix ratio varies considerably from very matrix-rich beds, which may be described as pebbly mudstones, to almost clast-supported beds. The well-consolidated greenish black clay occurs in Sections 182-1128C-7H-2 through 7H-CC. It contains scattered vertical or inclined pebble- to cobble-sized clasts of nannofossil ooze and green sandstone. A 55-cm-thick clast? of nannofossil ooze occurs in the clay at the base of Section 182-1128C-7H-3. The lower 340 cm of the greenish black clay unit shows burrow mottling and a poorly developed banding or layering.

The clasts occur in what seem to be fairly well-defined beds, some of which are amalgamated, as indicated by abrupt changes in overall clast size or composition. Bed thickness is on the order of 0.3–1.5 m, and bed boundaries are mainly well defined. Some very matrix rich beds have lower and upper portions dominated by whitish ooze-like matrix that is difficult to distinguish from the enclosing nannofossil and foraminiferal oozes. A few beds show very sharp boundaries with signs of syndepositional shearing. Vertical trends in clast size or clast/matrix ratios of individual beds are difficult to evaluate because of the large clast size compared to the width of the core (6.6 cm). Basal inverse grading and top coarse-tail grading seem, however, to be present in some beds.

The ages of the clasts are known only in a reconnaissance fashion, and further study is needed. Nannofossil ooze clasts analyzed from Subunit IB are middle and late Miocene in age (see **"Biostratigraphy,"** p. 11). Lithostratigraphic similarities between the sandstone clasts and Cretaceous sediment encountered at Site 1126 suggest that the terrigenous clastic materials may be of Cretaceous age.

F7. Deformed strata, Subunit IB, **p. 50.**

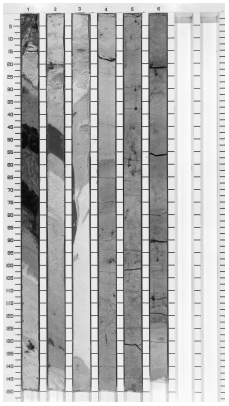

Subunit IC

Intervals: Sections 182-1128B-8H-2, 55 cm, through 10H-7, 66 cm; Sections 182-1128C-8H-4, 55 cm, through 10H-6, 30 cm
Depth: 64.75–91.360 mbsf (Hole 1128B); 70.05–93.30 mbsf (Hole 1128C)
Age: early Oligocene

This fine-grained unit is composed of clay and ooze punctuated by several small sediment gravity-flow deposits. The sediment is transitional in character, varying from clay rich in nannofossils to nannofossil ooze with a high clay content. The unit is usually a dull brown to gray color with a yellow to red hue, punctuated by some white units of nannofossil ooze. There are few obvious sediment gravity-flow deposits. Overall, the sediment grades from red at the top to gray toward the base. The interval is characterized by striking alternations of dark and light units, 0.5–1.0 m thick, that pass gradually into one another or are separated by sharp omission surfaces.

Pelagic muds are usually subequal in carbonate and clay content, with the calcareous portion dominated by nannofossils, whereas the biosiliceous component is mostly abundant sponge spicules. Although many sediments are totally mud size, those with a "wackestone" texture (silty muds) also contain benthic and planktonic foraminifers, lesser sponge spicules, bioclasts, tunicate sclerites, and trace amounts of glauconey and quartz. Calcareous nannofossils in most of this interval are poorly preserved and show some evidence of corrosion (see **"Biostratigraphy,"** p. 11).

Sediment gravity-flow deposits make up a very small proportion of these sediments (Fig. F3), consisting of centimeter-thick calciturbidites similar to those in the overlying Unit I.

Unit II

Intervals: Sections 182-1128B-10H-8 through 30X-CC (total depth); Sections 182-1128C-10H-6, 30 cm, through 26X-CC (total depth); Sections 182-1128D-1R-1 through 6R-2, 105 cm
Depth: 91.36–280.70 (bottom of hole) mbsf (Hole 1128B); 93.30–242.80 mbsf (Hole 1128C); 231.20 (top of hole)–281.85 mbsf (Hole 1128D)
Age: early Oligocene

This part of the succession is a uniform green, slightly calcareous clay that is locally interrupted, particularly in the upper parts, by a few beds of redeposited planktonic foraminiferal and nannofossil ooze (Fig. F8). The sediment is divided on the basis of composition into three subunits: an upper clay, an intermediate clayey chalk, and a lower claystone. The unit is light to dark green in color. Bright green millimeter-scale laminations are present throughout.

F8. Burrowed transition from white nannofossil ooze upward into bioturbated green clay, Subunit IIA, p. 51.

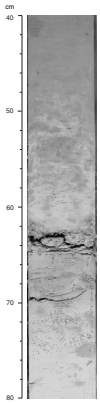

Subunit IIA

Intervals: Sections 182-1128B-10H-8 through 24X-6; Sections 182-1128C-11H-2, 60 cm, through 23X-CC
Depth: 91.36–222.10 mbsf (Hole 1128B); 93.30–221.30 mbsf (Hole 1128C)
Age: early Oligocene

This unconsolidated slightly calcareous clay is thoroughly bioturbated, with burrows manifest as mottles and a few discrete trace fossils. The sediment is clay with trace amounts of angular quartz and glaucony silt and a variable carbonate component, generally less than 20 wt% (see "Organic Geochemistry," p. 27). The carbonate component is dominated by coccoliths with accessory small planktonic foraminifers. Many such skeletons are corroded by dissolution. Accessory biosiliceous components are volumetrically dominated by sponge spicules with lesser discoasters, radiolarians, diatoms, and silicoflagellates. Sponge spicules are commonly concentrated in small subcentimeter burrows.

The carbonate intervals are white and either nannofossil ooze with a mudstone to wackestone texture, planktonic foraminiferal ooze with a packstone texture, or layers that grade upward from planktonic foraminiferal ooze to nannofossil ooze. Most are less than 0.5 m thick, except for one 6.0-m-thick layer at ~135 mbsf. The grading suggests that most of these intervals are turbidites.

Subunit IIB

Intervals: Sections 182-1128B-24X-7 through 26X-CC; Sections 182-1128D-1R-1 through 1R-CC
Depth: 222.10–242.80 mbsf (Hole 1128B); 221.30–240.80 mbsf (Hole 1128D)
Age: late Eocene–early Oligocene

This clayey chalk is partially lithified and contains chert layers and numerous discrete multigeneration ichnofossils. The most prominent of

these trace fossils are *Planolites, Chondrites, Zoophycos, Terebelina,* and *Thalassinoides*. Pyrite locally fills some small burrows.

Subunit IIC

Intervals: Sections 182-1128B-27X-1 through 30X-CC; Sections 182-1128D-2R-1 through 6R-2, 105 cm
Depth: 242.80–280.70 mbsf (total depth; Hole 1128B); 240.80–281.85 mbsf (Hole 1128D)
Age: late Eocene–early Oligocene

This poorly recovered sediment is a moderately consolidated clay in the upper part of the interval and a lithified claystone below 260 mbsf. This unit is an olive-green clay rich in sponge spicules with ~30% carbonate (see **"Organic Geochemistry,"** p. 27), mainly in the form of nannofossils. The section contains four centimeter-thick carbonate beds, mudstone or wackestone in texture, composed of nannofossils and pelagic foraminifers and interpreted as calciturbidites. Numerous centimeter-thick chert layers are present. Ichnofossils are superbly preserved and dominated by *Zoophycos*.

Unit III

Interval: Sections 182-1128D-6R-2, 105 cm, through 6R-CC
Depth: 281.85–288.90 mbsf
Age: late Eocene

This 2-m-thick unit stands out from the enclosing sediment because of its light-colored, coarse-grained character. Although thin, the unit is distinguished because it is so different from sediment above and below and because it marks a major change in overall sediment composition. The unit is composed of a lower glauconitic sandstone, an intermediate cross-laminated sandstone grading upward to a carbonate nannofossil wackestone (Fig. **F9**), and an upper glauconitic sandstone with water-escape structures grading upward to a nannofossil carbonate mudstone (Fig. **F10**). The sandstones, interpreted as turbidites, are separated by green burrowed claystone.

F9. Cross-laminated glauconitic sand in the basal part of a turbidite, Unit III, **p. 52.**

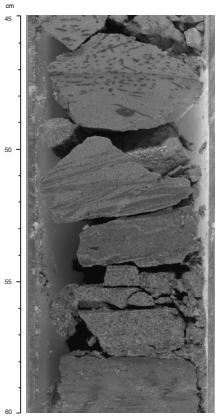

Unit IV

Interval: Sections 182-1128D-7R-CC through 23R-CC
Depth: 288.90–452.60 mbsf
Age: early?–middle Eocene

This unit is composed of green, highly burrowed, silty clay to sandy siltstone. Two subunits are distinguished. Subunit IVA is silty clay and claystone; Subunit IVB, a clayey siltstone to sandy siltstone. Although extensively burrowed, there are short sections with millimeter-scale laminations.

F10. Burrowed nannofossil ooze with numerous horizontal *Zoophycos* burrows, Unit IV, **p. 53.**

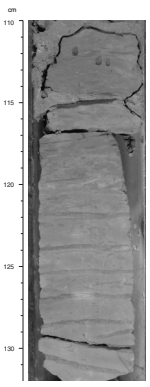

Subunit IVA

Interval: Sections 182-1128D-7R-CC through 14R-CC
Depth: 288.90–365.30 mbsf
Age: middle Eocene

The green silty clay of this unit is mostly partially lithified but grades into a lithified claystone below 355 mbsf. Although trace fossils are characteristically flattened and compacted throughout, *Zoophycos, Chon-*

drites, Paleophycus, and *Planolites* are still distinguishable. The claystones contain silt-sized quartz and glauconite with biotite, opaque minerals, and clay flakes present in trace amounts. Opaline diatoms are common. Some of the sediment contains rare sponge spicules, radiolarians, and planktonic foraminifers. There are a few centimeter-scale chert layers between 140 and 160 mbsf.

The section is punctuated by occasional centimeter-scale sandstone Ta-Tc turbidites at ~335 mbsf. These sandstones are fine sand-sized lithified arkose with angular quartz grains, glauconite grains, intraclasts, lithoclasts, and planktonic foraminifers (see **"Site 1128 Thin Sections,"** p. 81). Sediment is normally graded with the coarser lithoclast and glauconite grains at the base, planktonic foraminifers in the middle, and silt-sized quartz grains at the top. The matrix is locally partially silicified with alteration rims around glauconite and phosphatic grains. There are also traces of bryozoans, sponge spicules, and benthic foraminifers. Other terrigenous grains consist of traces of opaque minerals, biotite, microcline, and plagioclase.

Subunit IVB

Interval: Sections 182-1128D-15R-1 through 23R-CC
Depth: 365.30–452.60 mbsf
Age: early?–middle Eocene

The sediment is mostly clayey siltstone with silt- to occasional fine sand-sized grains of glaucony, quartz, mica, unidentified opaque minerals, and trace amounts of sponge spicules. Burrowing is extensive throughout. The basal 5 m is coarser grained, grading downward from sandy siltstone to silty sandstone. The sandy sediment near the base has centimeter-thick brown-colored layers and contains abundant quartz and feldspar grains, mica, glaucony, and minor silicified benthic foraminifers.

Discussion

Eocene and Lower Oligocene Terrigenous Clastic Sediment (Units II, III, and IV)

These Eocene and lowermost Oligocene clays, siltstones, and basal sandstones, with their almost total lack of calcareous material except for a few layers with corroded microfossils, suggest deep-water deposition below the CCD. The green color and extensive bioturbation of the sediment throughout most of this section, except for the base of Subunit IVB, indicate dysoxic depositional conditions.

Overall, Unit IV fines upward from basal sandy silts to pelagic clays at the top, indicating gradual fining of terrigenous clastic sediment delivery. This may be due in large part to climate. The middle Eocene in much of southern Australia was a time of abundant rainfall, coastal rainforests, and much runoff (Kemp, 1978; Macphail et al., 1994). Fluvial siliciclastic and paralic lignite deposits are common onshore. Sedimentation became more marine and carbonate rich toward the end of the late Eocene as climate became more semiarid. The fining-upward trends observed in this interval may reflect this change as a result of fluvial systems delivering less coarse sediment to the ocean.

The succession of sandstone-carbonate turbidites of Unit III, resulting from either seismicity or sea-level fall, signals a change in depositional style. The uppermost Eocene and lowermost Oligocene green

sediments of Unit II are variably calcareous and similar to shallower Neogene pelagic sediments. The thick section of clays and clayey chalks most probably accumulated near the lysocline, as indicated by the corroded and partially dissolved calcareous nannofossils and overall paucity of planktonic foraminifers (see "Biostratigraphy," p. 11). The green color and diverse trace fossil assemblage indicate a continuing dysoxic seafloor environment.

The upper Eocene–lowermost Oligocene record contains numerous chert bands, in most cases representing silicified clay. The upper Eocene in shallow-water facies across southern Australia was characterized by biosiliceous deposition, particularly spiculites, spongiolites, and silicified chalks. This similarity implies some sort of oceanographic control on silica deposition during this time.

Lower Oligocene and Neogene Clays and Carbonates (Unit I)

These fine-grained sediments are transitional in color in the lower part, from gray upward to brown, reflecting a gradual oxygenation of the seafloor and presumably more vigorous mixing and ventilation of the entire water column. The pink nannofossil oozes are classic pelagic sediments composed mostly of fine coccolith plates derived from the postmortem disintegration of calcareous phytoplankton (cf. Scholle, 1983). The accessory planktonic foraminifers are well preserved, indicating accumulation above the calcite lysocline. Numerous siliceous sponge spicules were probably derived from upslope because there are no sponge body fossils or root mats. One possible source is the zone of prolific sponge growth near the shelf edge and upper slope (James et al., 1992).

The presence of bryozoans in coarser conglomerates also suggests a link to a relatively shallow-water sediment source. Delicate branching bryozoans, like those in the resedimented material, accumulate today on the upper slope and characterize sediments between water depths of 200 and 350 m (Bone and James, 1993). Likewise, the lack of material characteristic of slightly downslope environments (~350–600 m water depth) like those encountered at Site 1127 implies sediment bypassing, possibly by travel down submarine canyons and gullies. Nevertheless, the presence of green terrigenous sand grains and lumps of compacted nannofossil ooze suggests erosion and acquisition of some deeper material as the flows moved downslope. Local synsedimentary deformation of the pelagic sediment points to periodic slumping or mass movement, presumably caused by oversteepening or seismicity.

Upper? Miocene Coarse-Sediment Gravity-Flow Deposits

This assemblage of matrix-supported, soft to hard sediment clasts with exotic lithologies such as black clay and green sandstone, together with abundant soft-sediment deformation and evidence of local shear with a fine-grained locally derived matrix of pelagic carbonate, indicates a complex accumulation process involving downslope movement. The three main lithologies are (1) graded foraminiferal packstone, (2) nonbioturbated, unlithified foraminiferal wackestone, and (3) matrix-supported, unlithified pebble and cobble conglomerates with clasts composed of a variety of strongly colored consolidated clays and oozes. The graded packstone beds indicate deposition by turbidity currents, and the interbedded nannofossil and foraminiferal oozes indicate depo-

sition at deep bathyal to abyssal water depths. The nonbioturbated wackestones were probably deposited from mudflows or short-traveled turbidity currents. The conglomerates were deposited from viscous debris flows, and benthic foraminifers in the clasts and matrix suggest a middle to upper bathyal source. The size of clasts and other features in such deposits is best seen and interpreted at the large outcrop scale; two cores can only hint at the precise nature of these sediments. Nevertheless, the relatively intact nature of the materials, even though commonly poorly lithified, implies that their origin is local and that they were derived from immediately upslope environments. On balance, this interval is interpreted as a series of debrites whose origin is relatively local, but which has sampled rocks possibly as old as Paleogene or Cretaceous.

The timing of the events is somewhat constrained by upper Miocene sediment directly overlying these deposits. The late middle Miocene–late Miocene was a period of prolonged low eustatic sea level (Haq et al., 1987). In southern Australia, however, it is also a time when the southern continental margin underwent tilting and uplift, exposing Paleogene and lower–middle Miocene shallow-water sediments (Lowry, 1970). The coincidence of the mass flows with this uplift episode suggests that the two events may be linked and that the triggering mechanism for movement was seismic.

The event that presumably removed upper Oligocene–lower Miocene sediment might be due to either submarine erosion/corrosion before the resedimentation event or removal of the underlying section by erosion during mass flow deposition.

BIOSTRATIGRAPHY

Introduction

Drilling at Site 1128 revealed the presence of two major biostratigraphic units, which were dated by nannofossils and planktonic foraminifers as upper Miocene–Pleistocene (0–55 mbsf) and lower Eocene–lower Oligocene (70–427 mbsf). The Neogene and Paleogene successions are separated by a series of spectacular debrites (55–70 mbsf) containing mixed Oligocene and Miocene nannofossils and planktonic foraminifers. Planktonic foraminifer data indicate a hiatus above a slump at the lower/upper Pliocene boundary and a major unconformity of ~20 m.y. at the Miocene/Oligocene boundary at ~70 mbsf. Nannofossil data further indicate possible hiatuses in the Neogene: two within the Pliocene (missing Zones NN17 and NN16 at ~24 mbsf and missing Zone NN13 at ~34 mbsf) and one within the Miocene (missing Zone NN10 at ~49 mbsf). Both nannofossil and planktonic foraminifer data show that the Miocene/Oligocene unconformity beneath the debrite spans a gap of at least 18 m.y. as the whole upper Oligocene is missing. The unconformity may represent an even larger hiatus as the age of the sediment above the debrite is <11.4 Ma. Seismic Horizons 1C_1 and 1C_2 detected on seismic profiles may correspond to a suspected hiatus in the upper lower Pliocene and to the major unconformity at the Miocene/Oligocene boundary, respectively. Changes in benthic foraminiferal assemblages are also noted at these levels.

Preservation of calcareous nannofossils and planktonic foraminifers is generally good down to ~45 mbsf, although it deteriorates downhole because of partial dissolution. Below 70 mbsf, nannofossils and plank-

tonic foraminifers show increasing signs of dissolution and disappear at some levels, suggesting deposition near the lysocline and the CCD. Benthic foraminifers are generally abundant and relatively well preserved down to 55 mbsf, although they become rare below 70 mbsf and some intervals are barren in the lower part of Hole 1128D.

Five main benthic foraminiferal assemblages are distinguished. A diversified Pleistocene–upper Miocene calcareous assemblage indicates abyssal paleodepths above the CCD and relatively well oxygenated conditions. Displaced heterogeneous assemblages are also found within the same interval in turbidites. Below this interval, a series of displaced exotic assemblages occur within the debrites. An impoverished lower Oligocene–lower upper Eocene calcareous assemblage is indicative of lower bathyal to abyssal paleodepths near the lysocline. Fine-grained turbidites within this latter interval contain redeposited assemblages from the shelf. An impoverished lower upper–upper middle Eocene calcareous assemblage also indicates lower bathyal to abyssal paleodepths near the lysocline. Finally, an impoverished upper middle–upper lower Eocene agglutinated assemblage indicates deposition below the CCD.

Sedimentation rates are relatively low for the Pleistocene and Pliocene interval in comparison with rates recorded at shallower sites for coeval sediments. A marked increase in sedimentation rates is registered in the Paleogene succession, reaching ~50–60 m/m.y. in the lower Oligocene and ~40–45 m/m.y. in the Eocene.

Calcareous Nannofossils

An upper Pleistocene–lower/middle Eocene succession of calcareous nannofossil assemblages is recorded from Site 1128, where core recovery was good for most of the Pleistocene–Oligocene but much poorer for the Eocene. The Pliocene–Miocene seems to be punctuated by four hiatuses. The most significant of these is associated with a mixed assemblage in a thin ~3-m-thick unit—all the middle Miocene and a greater part of the lower Miocene are at least partly missing. In contrast, assemblages from the cores below indicate an expanded lower Oligocene. Another substantial disconformity marks the Neogene/Paleogene boundary—at least the entire upper Oligocene section seems to be missing. A poor Eocene record of nannofossils resulted from the combination of the generally poor core recovery and the occurrence of numerous barren levels (Fig. F11).

Evidence of severe nannofossil dissolution abounds in the lower Oligocene and Eocene section, suggesting deposition near the CCD. Barren intervals in much of the middle Eocene (Fig. F11) suggest deposition well below the CCD. The quality of nannofossil preservation in the lower Oligocene section fluctuates but remains generally poor, indicating fluctuation of the CCD.

F11. Calcareous nannofossil and planktonic foraminifer zones, and benthic foraminiferal assemblages, p. 54.

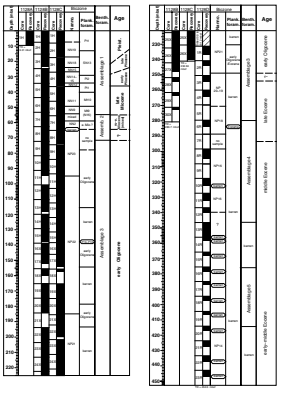

Pleistocene

Sample 182-1128B-1H-CC (5.63 mbsf) contains a well-preserved assemblage of calcareous nannofossils indicative of upper Zone NN19 of Pleistocene age, but with a minor reworked component. In situ species include *Coccolithus pelagicus, Gephyrocapsa caribbeanica, Gephyrocapsa oceanica,* small *Gephyrocapsa* spp. (including *G. aperta*), *Helicosphaera carteri, Helicosphaera hyalina, Pseudoemiliania lacunosa* (both circular and oval forms), *Reticulofenestra asanoi,* and *Rhabdosphaera clavigera;* the reworked Neogene *Discoaster variabilis* is also present. Assemblages readily

assignable to Zone NN19 are also recorded from Samples 182-1128B-2H-CC and 3H-3, 18–22 cm (15.5–16.88 mbsf). These contain evidence of minor reworking not only from the Neogene but also from the upper Paleogene and Upper Cretaceous (e.g., *Dictyococcites bisectus, D. variabilis,* and *Gartnerago obliquum*).

The occurrence of *R. asanoi* in the upper part of Zone NN19 at this site is confirmed in assemblages from Samples 182-1128B-1H-CC (4.95 mbsf) and 182-1128A-1H-CC (9.28 mbsf). Both *Calcidiscus macintyrei* and *Helicosphaera sellii* make their simultaneous appearance downhole in Sample 182-1128C-2H-CC (16.74 mbsf), suggesting lower Zone NN19 at this level.

Pliocene

Zone NN18 (late Pliocene age) is indicated by the presence of rare *Discoaster brouweri,* in association with the dominant taxa *Reticulofenestra minuta* and *Reticulofenestra minutula,* and the common occurrence of *C. pelagicus, P. lacunosa,* and *C. macintyrei* in Sample 182-1128B-3H-CC (23.19 mbsf).

Two intra-Pliocene disconformities are proposed on the basis of the apparent absence of Zones NN17 and NN16 (mostly late Pliocene age) and Zone NN13 (early Pliocene age) from the calcareous nannofossil succession. Nannofossil assemblages recovered indicate Zone NN15 from Sample 182-1128C-3H-CC (26.61 mbsf); the combined Zones NN14–NN15 from Sample 182-1128B-4H-4, 56–63 cm (29.78 mbsf), and 4H-CC (33.99 mbsf); and Zone NN12 from Sample 182-1128C-3H-CC (35.75 mbsf) (Fig. **F11**). The Zone NN15 assemblage contains common *Discoaster surculus;* few *Discoaster asymmetricus, Discoaster pentaradiatus,* and *P. lacunosa;* and rare *Discoaster tamalis* and *Reticulofenestra pseudoumbilicus*. Evidence of reworking in Zone NN15, particularly from Paleogene sediments, is indicated by the presence of common *Cyclicargolithus floridanus, D. bisectus,* and *Sphenolithus moriformis*. The assignment to the combined Zones NN14–NN15 is based on the presence of few to common *D. tamalis* and *R. pseudoumbilicus,* and the association of few *Amaurolithus ninae* and common *D. asymmetricus* in Sample 182-1128B-4H-4, 56–63 cm, together with abundant (acme of) *D. asymmetricus* in Sample 182-1128B-4H-CC.

The Zone NN12 assemblage of early Pliocene age, recorded from Sample 182-1128C-3H-CC, contains *A. ninae, Calcidiscus leptoporus, C. macintyrei, C. pelagicus, Ceratolithus acutus, D. pentaradiatus, D. surculus, D. variabilis, H. carteri, R. pseudoumbilicus, R. minuta,* and *R. minutula.*

Miocene

Signs of severe dissolution and notable enrichment of *Discoaster* specimens are observed in the assemblages from Samples 182-1128B-5H-CC (43.7 mbsf) and 6H-3, 98–103 cm (47.68 mbsf), which are placed in Zone NN11 of late Miocene age. The association of common *Amaurolithus amplificus, A. ninae, Discoaster intercalaris, D. variabilis, R. pseudoumbilicus,* and rare *Discoaster quinqueramus* in Sample 182-1128B-5H-CC indicates upper Zone NN11. A similar upper Zone NN11 association was also recorded from Sample 182-1128C-5H-5, 45–60 cm (42.95 mbsf), with rare *Reticulofenestra umbilicus,* reworked from Paleogene sediments.

Amaurolithus amplificus, A. ninae, and *D. quinqueramus* are not found in Sample 182-1128B-6H-3, 98–103 cm (55.8 mbsf), and instead rare

Discoaster berggrenii and common *Minylitha convallis* together indicate lower Zone NN11. Discoasters in the assemblage below from Sample 182-1128B-6H-CC (53.56 mbsf) are heavily calcified. However, it was possible to identify the index species for Zone NN9, *Discoaster hamatus*. This suggests that Zone NN10 is either missing or condensed in the interval between 55.8 (Zone NN11) and 53.56 mbsf (Zone NN9).

Samples below 53.56 mbsf (Zone NN9), taken from a lithostratigraphic unit consisting of a series of debrites down to 70.0 mbsf in Hole 1128C (see **"Lithostratigraphy,"** p. 3), contain lower–middle Miocene calcareous nannofossil assemblages, although one sample is barren. Samples 182-1128C-6H-CC (55.15 mbsf) and 7H-2, 143–147 cm (58.43 mbsf), contain a mixed assemblage. The dominant elements of this assemblage, including *Chiasmolithus altus, Cyclicargolithus abisectus, C. floridanus, D. bisectus, Helicosphaera obliqua, Reticulofenestra lockeri,* and *Zygrhablithus bijugatus,* are derived from Paleogene sediments. The lesser elements are also reworked, but from relatively younger sediments (e.g., *Sphenolithus heteromorphus* from low in the Miocene). The remaining elements are probably in situ, consisting of *C. macintyrei, Dictyococcites antarcticus, D. variabilis, H. carteri, R. pseudoumbilicus, Scyphosphaera* spp., and *Triquetrorhabdus rugosus*. Their abundance and diversity indicate a middle–late Miocene age.

Sample 182-1128B-7H-CC (62.35 mbsf) from the debrite unit contains a poorly to moderately preserved assemblage with heavily calcified discoasters. This assemblage includes *Coccolithus miopelagicus, Coronocyclus nitescens, C. floridanus, Discoaster deflandrei, Discoaster trinidadensis, H. carteri, Helicosphaera euphratis, H. obliqua,* and *S. moriformis,* suggesting Zone NN2 of early Miocene age. Minor reworking from Paleogene sediments is indicated by the occurrence of *Chiasmolithus oamaruensis*.

The evidence of intense reworking and mixing of nannofossils in the interval between 55.15 and 58.43 mbsf is associated with a substantial hiatus in the nannofossil record. The ~9.5-m interval between Samples 182-1128B-6H-CC (53.56 mbsf; Zone NN9) and 7H-CC (62.35 mbsf; Zone NN2) is likely to include at least one substantial disconformity. This interval is too short to accommodate all the middle Miocene and the greater part of the lower Miocene. Sample 182-1128C-7H-CC (64.12 mbsf), less than 2 m below Zone NN2 samples and also from the debrite unit, is barren.

Oligocene

Sample 182-1128B-8H-6, 79–83 cm (70.99 mbsf), contains an assemblage indicative of Zone NP23 of early Oligocene age, whereas the assemblage from Sample 182-1128B-7H-CC is early Miocene in age (Zone NN2). This suggests that most of the basal Miocene and upper Oligocene is either condensed in the intervening ~8.4-m interval or, more likely, partially or completely missing. The main components of the poorly preserved Zone NP23 assemblage in Sample 182-1128B-8H-6, 79–83 cm, include *C. altus, C. nitescens, C. abisectus, D. bisectus, D. deflandrei, S. moriformis,* and *Sphenolithus predistentus*.

Lower Oligocene assemblages, assignable to combined Zones NN23–NN21, occur in Samples 182-1128C-9H-CC (84.42 mbsf) through to 26X-CC (240.36 mbsf). Nannofossil debris and signs of partial dissolution are abundant in these assemblages, suggesting deposition near the CCD. The assemblage from Sample 182-1128C-9H-CC shows the effects of strong dissolution; it is dominated by *Discoaster* spp. (the *D. deflan-*

drei "group"), *C. floridanus* and *D. bisectus* and contains specimens of *Chiasmolithus* (rims only), *S. predistentus* (distal spines only), and *Coccolithus eopelagicus*. Better preserved assemblages occur at a few levels, suggesting fluctuations of the CCD and some transportation from shallower sites, as hemipelagic species are usually present in the better preserved assemblages. One such assemblage, readily assignable to Zone NP22, is found in Sample 182-1128C-15X-CC (84.42 mbsf). It contains *Blackites spinosus, Braarudosphaera bigelowii, C. altus, Clausicoccus fenestratus, C. floridanus, D. bisectus, Discoaster scrippsae, Discoaster nodifer, Helicosphaera* sp. cf. *H. recta, Lanternithus*? *minutus, Pontosphaera multipora, Reticulofenestra hillae, R. lockeri, R. umbilicus, S. moriformis,* and *Z. bijugatus*. Another example is from Samples 182-1128D-1R-CC (236.73 mbsf) and 2R-CC (243.87 mbsf), where the assemblages (Zone NP21) remain relatively diverse, despite showing signs of severe dissolution. The main elements of these assemblages include *B. spinosus, C. altus, C. oamaruensis, C. fenestratus, C. eopelagicus, C. formosus, D. bisectus, D. deflandrei, D. nodifer, Isthmolithus recurvus, Pontosphaera pulcheroides, Reticulofenestra hampdenensis, R. hillae, R. lockeri, R. umbilicus,* and *Z. bijugatus*. In addition to these, *Lanternithus minutus, Pontosphaera plana,* and *Reticulofenestra oamaruensis* are present in Sample 182-1128D-2R-CC. The co-occurrence of *R. hampdenensis* and *R. oamaruensis* above the extinction of *Discoaster saipanensis* typifies the lower part of Zone NP21 in southern Australia (S. Shafik, unpubl. data).

Eocene

Preservation deteriorates rapidly in the upper Eocene section, and most of the lower cores below Sample 182-1128D-12R-CC are barren. Poor preservation is mainly caused by dissolution. The highest occurrence of *D. saipanensis* is in Sample 182-1128B-28X-CC (254.66 mbsf), in association with *C. altus, C. oamaruensis, D. bisectus, I. recurvus,* and *R. hampdenensis*. This indicates upper Zone NP19–NP20. The better preserved assemblages in Samples 182-1128D-4R-CC (263.94 mbsf) and 5R-CC (268.71 mbsf) include the hemipelagic *L. minutus* and *Z. bijugatus*. In Sample 182-1128D-5R-CC, *D. saipanensis* and *Cribrocentrum reticulatum* co-occur, suggesting the lower part of Zone NP19–NP20.

The assemblage from Sample 182-1128D-6R-CC (284.03 mbsf) is poorly preserved, although *C. oamaruensis, C. eopelagicus, D. bisectus, D. saipanensis,* and *R. umbilicus* are identifiable, suggesting Zone NP18 of late Eocene age. A similar assemblage is recorded from Sample 182-1128D-7R-CC (289.01 mbsf).

The assemblage from Sample 182-1128D-8R-2, 5–6 cm, is relatively diverse, and the occurrence of *Chiasmolithus grandis, Chiasmolithus solitus, C. reticulatum, D. bisectus, D. saipanensis, Helicosphaera dinesenii/H. reticulata,* and *Neococcolithites dubius* indicate Zone NP16 of middle Eocene age. Poor core recovery coupled with inadequate sampling of Core 182-1128D-8R probably accounts for the absence of Zone NP17 from our record. With the exception of the barren Sample 182-1128D-10R-CC (322.46 mbsf), assemblages of Zone NP16 continue to occur downhole to Sample 182-1128D-13R-3, 110–111 cm.

The assemblage from Sample 182-1128D-8R-2, 5–6 cm, which contains warmer water species such as *H. dinesenii/H. reticulata,* recalls other assemblages from Zone NP16 recorded at Site 1126 (see **"Biostratigraphy,"** p. 12, in the "Site 1126" chapter) and in the eastern part of the Great Australian Bight (Shafik, 1990). Coeval assemblages from southeastern Australia (western Otway Basin) lack warm-water indicators

(Shafik, 1983), suggesting that the flow of a warm-water surface current in the middle Eocene along the southern Australian margin diminished away from the Indian Ocean (Shafik, 1990).

Samples 182-1128D-13R-CC (355.93 mbsf) to 23R-CC (444.37 mbsf) are barren except for Sample 182-1128D-21R-CC (427.32 mbsf), which yielded *C. solitus, C. eopelagicus, Coccolithus formosus, Discoaster barbadiensis,* and *Discoaster sublodoensis*. These indicate Zone NP14, which straddles the lower/middle Eocene boundary.

Planktonic Foraminifers

Planktonic foraminifers indicate that Site 1128 recovered two major biostratigraphic units: upper Miocene–Pleistocene (0–55 mbsf) and Eocene–lower Oligocene (70–>290 mbsf). A debrite separates these packages (~55–70 mbsf) and contains clasts of upper Miocene, middle Miocene, and Oligocene sediments, indicating probable upper Miocene deposition from sediment gravity flows. A major unconformity associated with the debrite (see **"Lithostratigraphy,"** p. 3) is indicated by Miocene Zone Mt9 above and lower Oligocene assemblages beneath the debrite. The hiatus is estimated to be ~20 m.y. in duration. The Pliocene/Pleistocene boundary lies between 15 and 25 mbsf, although the temperate nature of the assemblage means that it is not possible to resolve whether the boundary is a disconformity. Separated by two distinct assemblages, the Pliocene/Miocene boundary falls near 40 mbsf and appears to be gradational. With the exception of several levels, planktonic foraminifers become absent or very rare in lower Oligocene and Eocene sediments further downhole, suggesting a depositional environment near the lysocline and CCD.

Preservation and Abundance

Planktonic foraminifers are generally abundant with moderate to good preservation in the upper 36 m of the section. They are common to few with mostly moderate to poor preservation between 36 and 63 mbsf, and they occur only as traces to rare with poor preservation below 63 mbsf (although there are several important exceptions). Select intervals near 135–138 mbsf in both Holes 1128B and 1128C, one sample at 94.63 mbsf in Hole 1128C, and one sample at 243.87 mbsf in Hole 1128D have common planktonic foraminifers with poor to moderate preservation. Core recovery fell from >90% above 240 mbsf to 29% and 36% below 240 mbsf in Holes 1128B and 1128D, respectively, significantly degrading the continuity of the fossil record.

Quaternary

A typical warm temperate Quaternary assemblage is found in the first cores of Holes 1128A, 1128B, and 1128C (Samples 1128A-1H-CC, 7–10 cm, from 9.28 mbsf; 182-1128B-1H-CC, 14–17 cm, from 5.63 mbsf; and from the surface to 182-1128C-1H-CC, 11–13 cm, from 7.93 mbsf). The assemblage is comprised of abundant *Globorotalia inflata, Globigerina quinqueloba, Globigerina falconensis,* and *Globigerinoides ruber* with few *Orbulina universa, Neogloboquadrina pachyderma* (dextral), *Globorotalia truncatulinoides, Globorotalia crassaformis, Globigerinella siphonifera, Globigerinita glutinata,* and *Globigerina bulloides*. The section is placed in the subtropical Zone Pt1 on the basis of the presence of *G. truncatulinoides*. However, the base of the zone as defined by Berggren et al. (1995) could

not be applied because *Globigerinoides fistulosus* and *Globigerinoides extremus* were not observed. We placed the base at the first appearance of *G. truncatulinoides* (between 5.63 and 15.50 mbsf at Hole 1128B and between 7.93 and 16.74 mbsf at Hole 1128C), following the definition of Jenkins (1993) and Chaproniere et al. (1995) for the estimated regional base of the Pleistocene.

Upper Pliocene

The upper Pliocene assemblage represents somewhat cooler temperatures than the overlying Pleistocene assemblage. It includes abundant *Gt. inflata, Gg. quinqueloba, G. falconensis,* and few *G. ruber, Globigerinita glutinata, Globigerina bulloides, G. crassaformis,* and *N. pachyderma* (dextral). The upper Pliocene fits the definition of Zone SN13, the *Gt. inflata* Zone of Jenkins (1985, 1993) because it contains abundant *Gt. inflata* without *G. truncatulinoides*. The zone generally corresponds in time to Zones Pl5 and Pl6 of Berggren et al. (1995) (Chaproniere et al., 1995). Samples 182-1128B-2H-CC, 21–24 cm (15.5 mbsf), to 3H-CC, 21–24 cm (23.19 mbsf), and 182-1128C-2H-CC, 15–18 cm (16.74 mbsf), to 3H-6, 24–28 cm (25.24 mbsf), are placed in this zone. The base of the upper Pliocene sequence rests disconformably on a slump (~27–29 mbsf) that contains a lower Pliocene assemblage.

Lower Pliocene

The lower Pliocene assemblage represents somewhat warmer temperatures than the upper Pliocene assemblage. It includes abundant *Globigerinita glutinata* and *Globigerina juvenilis* and few to rare *Globorotalia puncticulata, G. crassaformis, G. ruber, Gg. quinqueloba, G. falconensis,* and *Globigerina bulloides*. Also present are *Zeaglobigerina decoraperta, Zeaglobigerina apertura, Zeaglobigerina woodi, O. universa, Neogloboquadrina humerosa, Neogloboquadrina acostaensis, Globorotalia scitula, Zeaglobigerina nepenthes,* and *Globorotalia margaritae.*

The section can be divided into subtropical Zones Pl2 and Pl1 on the basis of the last occurrences of *G. margaritae* in Samples 182-1128B-4H-4, 58–63 cm (29.78 mbsf), and 182-1128C-3H-CC, 0–3 cm (26.61 mbsf), and *Z. nepenthes* in Sample 182-1128C-4H-CC, 55–58 cm (35.75 mbsf). A combined Zone Pl1–Pl2 is recognized at Hole 1128B where *Z. nepenthes* is absent, although *Z. apertura* is present with *G. margaritae* in Sample 182-1128B-5H-2, 101–105 cm.

Miocene

The Miocene/Pliocene boundary is placed at the first appearance of *Globorotalia sphericomiozea* in Samples 182-1128B-6H-3, 98–103 cm (47.68 mbsf), and 182-1128C-5H-CC, 21–24 cm (46.52 mbsf). Berggren et al. (1995) suggested that it is a suitable proxy for the boundary in temperate regions on the basis of the work of Hodell and Kennett (1986). A combined Zone Pl1–Mt10 is recognized in Sample 182-1128C-5H-6, 34–38 cm (44.34 mbsf), where *Globoconella conomiozea* makes its last appearance in the hole, although *G. crassaformis* is still present. The presence of fossils with two distinctly different preservation states supports mixing between two assemblages.

The upper Miocene assemblage includes *Z. nepenthes, Z. woodi, Z. decoraperta, Sphaeroidinellopsis disjuncta, O. universa, N. acostaensis, G. margaritae,* and *Globorotalia menardii*. The fossils are poorly preserved, with

numerous partially dissolved and broken tests. Zones Mt10 and Mt9 are divided on the basis of the first occurrence of *Globorotalia conomiozea,* and Mt9 is further distinguished by the occurrence of *Globorotalia conoidea* with neither *Globorotalia conomiozea* nor *Neogloboquadrina mayeri*. Samples 182-1128B-5H-CC, 11–13 cm (43.70 mbsf), and 182-1128C-5H-CC, 21–24 cm (46.52 mbsf), are placed in Zone Mt10; Sample 182-1128C-6H-2, 104–108 cm (48.54 mbsf), is assigned to Zone Mt9; and Samples 182-1128B-6H-3, 98–103 cm (47.68 mbsf), and 6H-CC, 19–21 cm (53.56 mbsf), are assigned to a composite Zone Mt10–Mt9.

Four paleontologic samples were taken within the interval of dramatic sediment gravity flow deposits (debrites) observed between 55 and 70 mbsf (see **"Lithostratigraphy,"** p. 3). Three samples, each from a different lithology, were placed in different Miocene zones, namely Zone Mt9, composite Zone Mt10–Mt9, and the middle Miocene (Samples 182-1128C-6H-CC, 10–13 cm, from 55.15 mbsf; 7H-2, 143–147 cm, from 58.43 mbsf; and 182-1128B-7H-CC, 21–24 cm, from 62.58 mbsf, respectively). One additional sample (Sample 182-1128C-7H-CC, 29–32 cm, 64.12 mbsf) lay within the debrite. It was barren of foraminifers, but contained abundant siliceous microfossils similar to those observed in the lower Oligocene siliceous unit found beneath the gravity flows. Preliminary results indicate that the various debrite lithologies include discrete packages of Oligocene, middle Miocene, and some upper Miocene sediment. The Quaternary to uppermost Miocene sequence above the debrite appears undisturbed and in proper stratigraphic order.

Oligocene

A prominent lithologic change from carbonate-rich to clayey siliceous sediments occurs at ~70 mbsf. Planktonic foraminifers are sparse, and many samples are barren or contain only a trace of tests. The site probably lies alternately near and below the CCD during deposition of this siliceous ooze. A few intermittent intervals contain some age-diagnostic planktonic foraminifers, indicating that the interval from 70 to >200 mbsf mainly belongs in the lower Oligocene. The core-catcher samples from Cores 182-1128C-8H (73.95 mbsf), 182-1128B-8H (72.47 mbsf), and 9H (81.82 mbsf), and Sample 182-1128B-11H-2, 93–97 cm (93.63 mbsf), contain a poorly preserved assemblage with *Catapsydrax dissimilis, Chiloguembelina* sp., *Globorotaloides suteri,* and *Subbotina angiporoides*. Samples 182-1128C-11H-1, 113–117 cm (94.63 mbsf), 13H-2, 14–18 cm (114.14 mbsf), and the core-catcher samples from Cores 182-1128B-15H (137.76 mbsf), 182-1128C-15H (138.30 mbsf), 16X (148.10 mbsf), and 17X-5, 43–47 cm (152.53 mbsf), contain a typical lower Oligocene assemblage characterized by *Tenuitella gemma, Tenuitella munda, Tenuitella angustiumbilicata, Tenuitella juvenilis, Tenuitella praestainforthi, S. angiporoides, Globorotaloides testarugosa, Globorotaloides suteri, Globigerina officinalis, Chiloguembelina cubensis, Globigerina euapertura, Guembelitria triseriata,* and *Zeaglobigerina ampliapertura*.

Eocene–Oligocene

Samples between 236 and 244 mbsf at Site 1128 contain an assemblage that cannot be positively distinguished as either Oligocene or Eocene. The assemblage includes poorly preserved specimens of *Tenuitella* spp., *Subbotina gortanii, C. dissimilis, Globorotaloides suteri, S. angiporoides, G. officinalis, C. cubensis,* and *G. testarugosa*. No planktonic

foraminifers were found deeper than 285 mbsf at Site 1128. Biostratigraphy from most of the section in Hole 1128D relied on calcareous nannofossils, which indicate that the lower part of the sediment sequence at Site 1128 was mainly middle–late Eocene in age.

Benthic Foraminifers

Benthic foraminifers were studied from every core-catcher sample at Holes 1128B and 1128D. Additional samples were also analyzed from core-catcher samples at Hole 1128C and from selected intervals at Holes 1128B and 1128C, where the lithology differed markedly from core-catcher samples. Benthic foraminifers are generally abundant and well preserved in the upper parts of Hole 1128B and Hole 1128C (Cores 182-1128C-1H through 7H). However, abundance and diversity decrease dramatically and preservation is generally poor below Core 182-1128C-7H (63 mbsf) and in all samples examined from Hole 1128D. The following core-catcher samples were found to be barren: Samples 182-1128D-4R-CC and 13R-CC through 15R-CC, and Section 182-1128D-21R through Sample 182-1128D-23R-CC. Approximately 100–300 benthic foraminifers were picked from the >63-µm fraction, except in samples in which benthic foraminifer abundance was low. The benthic foraminiferal assemblages studied include mainly calcareous taxa. However, an assemblage containing only agglutinated taxa with organically cemented tests was found in the lower part of Hole 1128D (Cores 182-1128D-16R through 20R). Five benthic foraminiferal asssemblages are distinguished within the Cenozoic succession at Site 1128.

Assemblage 1 (Pleistocene–Late Miocene)

Cores 182-1128B-1H through 6H and 182-1128C-1H through 6H

This diversified assemblage is characterized by the occurrence of few to common *Pyrgo murrhina* and the rare to few occurrence of *Melonis sphaeroides* and *Melonis barleeanum*. Also present as rare to common constituents are *Planulina wuellerstorfi, Globocassidulina subglobosa, Oridorsalis umbonatus, Cibicidoides mundulus, Uvigerina hispidocostata, Pullenia bulloides, Eggerella bradyi, Stilostomella lepidula, Triloculina trihedra, Astronion pusillum, Bulimina alazanensis, Stilostomella* spp., *Loxostomum* spp., *Bolivina* spp., *Cibicidoides* spp., and *Pleurostomella* spp., as well as various nodosariids. Tests within this assemblage are generally well preserved, showing no obvious sign of partial dissolution. Included within Assemblage 1 are useful bathymetric indicators such as *M. sphaeroides,* which provides a reliable index for abyssal depths (Hasegawa, 1984; van Morkhoven et al., 1986), *P. wuellerstorfi,* considered to be primarily a lower bathyal to abyssal dweller (van Morkhoven et al., 1986), and *P. murrhina,* characteristically found in middle bathyal to abyssal deposits (van Morkhoven et al., 1986). The composition of Assemblage 1 indicates deposition above the CCD, which is in accordance with the consistently high $CaCO_3$ values recorded in this interval (see **"Organic Geochemistry,"** p. 27). Heterogeneous bathyal faunas are also recorded between Cores 1H and 6H at Holes 1128B and 1128C in Samples 182-1128B-4H-4, 58–63 cm; 182-1128B-4H-CC; 182-1128B-6H-CC; 182-1128B-6H-3, 98–103 cm; and 182-1128C-6H-2, 104–108 cm. These obviously displaced faunas are interpreted as having been transported by turbidity flows. More detailed work will clarify the provenance and the frequency of such flows.

Assemblage 2 (Middle Miocene–Early? Miocene)

Intervals 182-1128B-7H through 8H-6 and 182-1128C-7H through 8H-4

This assemblage is found within a lithostratigraphic unit that includes a series of debrites in intervals 182-1128B-7H-1, 125 cm, through 8H-2, 55 cm, and 182-1128C-7H through 8H-4, 55 cm (see "Lithostratigraphy," p. 3). Nannofossil and planktonic foraminiferal assemblages within this unit contain mixed Miocene and Oligocene taxa, which reflect the exotic provenance of some of the clasts. The following displaced benthic foraminifers are recorded: *P. wuellerstorfi, Siphonina tenuicarinata, Rectuvigerina multicostata, Rectuvigerina striata, Bulimina alazanensis, Bulimina aculeata, Hanzawaia ammophila, G. subglobosa, O. umbonatus, Cibicidoides mundulus, U. hispidocostata, Pullenia bulloides, Karreriella bradyi, Stilostomella subspinosa, Laticarinina pauperata, Pullenia* spp., *Cibicidoides* spp., *Stilostomella* spp., *Uvigerina* spp., *Bolivina* spp., and *Trifarina* spp., as well as various nodosariids. It is interesting to note that *M. sphaeroides,* the indicator for abyssal paleodepths, is absent from any of the samples examined. Most of the taxa recorded within this interval are typical of lower to upper bathyal paleodepths. However, a more detailed study is needed to determine the provenance of the clasts within the debrites and to establish the timing of deposition within a regional framework.

Assemblage 3 (Early Oligocene–Early Late Eocene)

Intervals 182-1128B-8H-CC through 30X and 182-1128C-8H-CC through 28X, and Cores 182-1128D-1R through 5R

A major lithologic change from carbonate-rich sediments to calcareous claystones occurs within Core 8H from Holes 1128B and 1128C. This represents a major unconformity spanning a gap of at least 18 m.y. between the Miocene and lower Oligocene, as shown by nannofossil and planktonic foraminifer data. Below a transitional unit composed of calcareous clay and clayey nannofossil ooze (intervals 182-1128B-8H, 55 cm, through 11H and 182-1128C-8H4, 55 cm, through 11H-2, 60 cm), the dominant lithology consists of green, variably calcareous claystones with minor calcareous turbidites, decreasing in frequency downhole. The washed residues from the green claystones contain abundant sponge spicules and radiolarians, as well as a poorly preserved, impoverished benthic foraminiferal assemblage. The benthic foraminiferal assemblage consists of rare specimens of *Cibicidoides subhaidingeri, Astronion pusillum, O. umbonatus, Stilostomella subnodosa, Stilostomella aculeata, K. bradyi, G. subglobosa, L. pauperata, Pleurostomella* spp., *Cibicidoides* spp., *Stilostomella* spp., *Pullenia* spp., *Gyroidinoides* spp., and some nodosariids. Samples from the base of the interval (Cores 182-1128D-3R through 5R) also contain fragments of thick-walled *Rhabdammina* sp. The major faunal change observed between Assemblages 2 and 3 is probably coincident with sequence boundary 1C_2 recognized on seismic lines (see "Seismic Stratigraphy," p. 36).

The composition of the assemblage suggests that it originated from a lower bathyal to abyssal environment, probably near the lysocline, as shown by evidence of strong dissolution in the planktonic foraminifer tests and nannofossils from this interval. The benthic foraminifers from Assemblage 3 tend to have robust, heavily calcified tests and are thus probably resistant to dissolution, even in close proximity to the lysocline. The fluctuating but generally low $CaCO_3$ values recorded within

this interval (see "Organic Geochemistry," p. 27) also suggest paleodepths near the lysocline for this site. The paucity of benthic foraminifers in Assemblage 3 may be caused by dysoxic conditions at the seafloor, as indicated by the green color of the sediment (see "Lithostratigraphy," p. 3), and/or may reflect high sedimentation rates. Interestingly, biosiliceous radiolarian-rich sediments are commonly associated with impoverished benthic foraminiferal assemblages in the deep sea during the Cretaceous and Paleogene (Kuhnt et al., 1989; Kaminski et al., 1992).

Several samples from fine-grained calcareous turbidites within this interval were also analyzed in an attempt to determine the origin of the turbidites (Samples 182-1128B-11X-CC; 26X-4, 94–98 cm; 27X-3, 100–103 cm; 15X-CC; 182-1128C-15-3, 100–104 cm; 17X-5, 43–47 cm; and 182-1128D-2R-CC). In contrast to samples from the green claystones, these yielded relatively well-preserved benthic foraminiferal assemblages with few to abundant small specimens (63–150 µm) of *Patellina corrugata, Spirillina* spp., *Stilostomella* spp., *Bolivina* spp., *Trifarina* spp., and various nodosariids. The uniformity in test size and the presence of typically shallow-water indicators such as *P. corrugata* and *Spirillina* spp. indicate that the tests were originally derived from the shelf, before being redeposited into the basin and sorted by distal turbidity currents.

Assemblage 4 (Early Late–Late Middle Eocene)

Cores 182-1128D-6R through 12R

This impoverished, poorly preserved assemblage is characterized by the occurrence of few to common *Rhabdammina* sp. and *Cibicidoides* spp. and by the rare presence of *Nuttallides truempyi, O. umbonatus, Glomospira charoides, Pullenia* spp., and some nodosariids. Also found in the samples are abundant radiolarians and sponge spicules. According to Tjalsma and Lohmann (1983), *N. truempyi* had a bathymetric range from middle or lower bathyal to abyssal during the Eocene. *Nuttallides truempyi* was also recorded within the same stratigraphic interval in Assemblage 4B at Site 1126, but in a more proximal setting than at Site 1128. Paleodepths at Site 1128 were much greater than at Site 1126 in the middle and upper Eocene, as shown by the strong dissolution of nannofossils and the virtual absence of presumably dissolved planktonic tests. However, the presence of calcareous benthic foraminifers within Assemblage 4 indicates deposition near the lysocline, although not below the CCD. The rarity of benthic foraminifers within this assemblage may be caused by dysoxic conditions at the seafloor, perhaps related to high biosiliceous productivity in surface waters and/or to high sedimentation rates causing dilution of benthic foraminiferal tests. *Nuttallides truempyi,* with a last occurrence in the upper Eocene in Zone P17 (Berggren and Miller, 1989), is a stratigraphically significant taxon within Assemblage 4.

Assemblage 5 (Late Middle–Late Early Eocene)

Cores 182-1128D-16R through 20R

Assemblage 5 is found between two barren intervals at the base of Hole 1128D and represents a very impoverished assemblage containing only thick-walled *Rhabdammina* fragments. Preservation is generally poor and abundance is low. Also present within the same samples are abundant radiolarians and sponge spicules. The lack of calcareous tests

within this interval indicates deposition below the CCD. This is supported by the extremely low $CaCO_3$ values (0–0.99 wt%) recorded within this interval (see "Organic Geochemistry," p. 27). Dysoxic conditions at the seafloor, indicated by the green sediment color (see "Lithostratigraphy," p. 3), and/or an increased siliciclastic flux into the restricted basin during the middle and lower upper Eocene (see "Lithostratigraphy," p. 3) may account for the scarcity of benthic foraminifers within this assemblage.

Sedimentation Rates

Sediment accumulation rates were calculated from preliminary biostratigraphic and paleomagnetic data from Site 1128, and the results are presented in Figure F12. The datum levels used to calculate sedimentation rates are listed in Table T2.

The Pleistocene–Pliocene registered a sedimentation rate of ~11 m/m.y. This is a relatively low rate when compared with sedimentation rates averaging between ~240 m/m.y. and ~31 m/m.y. recorded for coeval sections at Sites 1127 and 1126, respectively. There is a sharp decrease in sedimentation rates from ~10–15 m/m.y. for the lower Pliocene–upper Miocene section. A thin debrite (~14 m thick) containing clasts bearing upper Miocene, middle Miocene, and Oligocene assemblages separates the upper Miocene section above from the Paleogene unit below. The gravity-flow event apparently removed most of the basal Miocene and upper Oligocene, an interval spanning more than 18 m.y.

Sedimentation rates are low (~18 cm/m.y.) in the upper lower Oligocene and increase to 50–67 m/m.y. in the lower Oligocene. In contrast, the rate for the upper Eocene is 4 m/m.y. Because of poor recovery for the remainder of the Eocene and the occurrence of barren intervals, the sedimentation rate calculated for this part of the section (40–45 m/m.y.) should be considered with caution.

F12. Sedimentation rate curve from datum levels for Site 1128, p. 55.

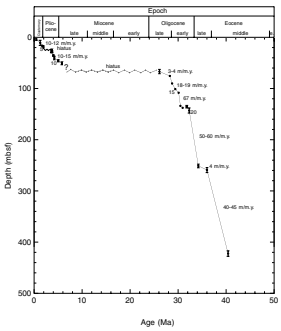

T2. Datum levels used to calculate the sedimentation rate, p. 90.

PALEOMAGNETISM

All cores from Holes 1128B, 1128C, and 1128D with sufficient recovery to make long-core measurements feasible were measured as half cores using the 2-G 760-R magnetometer. Measurements were made of natural remanent magnetization (NRM) and after 20-mT demagnetization. An experimental nonmagnetic APC assembly was used to obtain alternate cores in Hole 1128C from 3H to 13H. The nonmagnetic corer produced a significant reduction in the acquisition of a "radial" coring-induced contamination (see "Appendix: Magnetics Experiment"). Discrete samples for NRM and rock magnetic analysis were taken from both soft sediments cored by APC and from biscuits in the XCB and RCB cores. The analyses were performed using the methods discussed in "Paleomagnetism," p. 12, in the "Explanatory Notes" chapter.

Long-Core Measurements

Long-core measurement provided two almost continuous records from Holes 1128B and 1128C for the uppermost 250 mbsf. Neogene sediments have relatively high remanence intensities, averaging ~6 mA/m. Notably lower intensities, ranging from 8×10^{-4} to 2×10^{-5} A/m, are present in the Oligocene and Eocene pelagic clays that predominate be-

low 140 mbsf. Although the quality of the record varied from excellent in the vicinity of ~100 mbsf to fair in deeper cores, a reliable record of inclination was obtained. Variable recovery from Hole 1128D made a continuous record impossible, although clearly reversed and normal inclinations were evident.

Discrete Samples

Analysis of NRM by standard Kirschvink-Zijderveld techniques yielded satisfactory results from both soft sediments and lithified material, as illustrated in Figure F13. In the uppermost Figure F13A, results from a soft sediment sample show that a soft upward moment demagnetizes to yield a progressively steeper downward (reverse polarity) magnetization, with a maximum angular deviation angle of 1.6. The second sample is from an RCB biscuit that has acquired a stronger soft upward magnetization and again gives way on demagnetization to a reversed magnetization.

Rock magnetic analysis revealed subtle differences in magnetic properties of APC cores. This is illustrated in Figure F14, in which results from Cores 182-1128B-3H-2 and 13H-2 are compared. In the nannofossil oozes that predominate in the upper cores, isothermal remanent magnetization (IRM) acquisition is consistent with fine-grained magnetite, as are the demagnetization characteristics. The ratio of anhysteretic remanent magnetization (ARM) to IRM suggests single-domain grain size. Deeper in the section, in the calcareous clays of Section 13H-2, the alternating field decay of the natural and laboratory-induced magnetizations suggest that the bulk of the remanence is carried by a phase of relatively low coercivity such as magnetite, although inductions of 300 mT are not sufficient to reach saturation. The ratios of ARM:IRM for the calcareous clays are lower than in the shallow samples. These ratios and the lower coercivity of the NRM would imply small multidomain grain sizes (in excess of several micrometers) rather than the submicrometer size of bacterial magnetite. The higher coercivities in the IRM in the calcareous clay (Section 1H-2) may indicate that small amounts of hematite are present.

F13. AF demagnetization behavior of soft sediment and lithified discrete samples, p. 56.

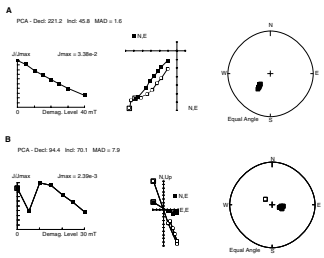

F14. Plots of demagnetization of NRM, ARM, and IRM, and of the acquisition of IRM, p. 57.

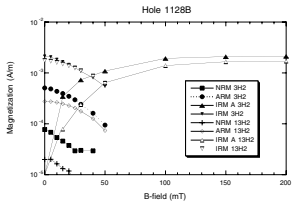

Susceptibility Records

The magnetic susceptibility data obtained from the multisensor track (MST) for Hole 1128B are shown in Figure F15. Above the debrites in lithostratigraphic Unit I, there is a trend of decreasing susceptibility with depth, which is interrupted by short wavelength peaks and a strong peak centered at 40 mbsf. This peak is associated with a high in the natural gamma log and a color change from lighter to darker green, although the source of the high susceptibility values has not been established. The shorter wavelength troughs reflect the contrast between the low-susceptibility packstones and turbidites, compared with the nannofossil ooze, whereas wackestones are associated with higher susceptibility peaks. The remainder of lithostratigraphic Unit I, including the debrites, have intermediate susceptibilities between 20 and 40 × 10^{-5} SI. Within the calcareous clays of lithostratigraphic Unit II, the susceptibility falls from values of 40 × 10^{-5} SI to ~5 × 10^{-5} SI at 240 mbsf. Frequency dependence of susceptibility is low to moderate (2%–10%), except for samples in the deepest cores of Hole 1128D, in which values reach 17%, indicating a higher concentration of superparamagnetic magnetite. Within lithostratigraphic Unit II, higher susceptibility val-

F15. Magnetic susceptibility of cores from Hole 1128B, p. 58.

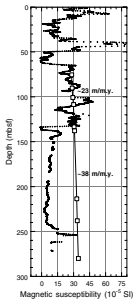

ues are observed in the interval from 70 to 130 mbsf than in the interval from 140 to 240 mbsf. Susceptibility is higher by a factor of ~5, coinciding with lower sedimentation rates. At 250 mbsf a minor peak appears to correlate with the occurrence of siltstones.

Magnetostratigraphy

The two records for Holes 1128B and 1128C are similar and permit tentative correlation with the geomagnetic polarity time scale in the Pliocene–Pleistocene to a depth of 54 mbsf, at which point the section is dominated by gravity-flow deposits, and no meaningful record can be obtained. This Pliocene–Pleistocene section is illustrated in Figure F16 from Holes 1128B and 1128C. In Hole 1128C the long wavelength pattern of normal from 0 to ~15 mbsf, reversed from 15 to ~40 mbsf, followed by a return to dominantly normal polarity, appears to be a manifestation of the Brunhes-Matuyama-Gauss sequence. The Jaramillo and Olduvai normal zones in the Matuyama are tentatively interpreted to be at 16 and 26–27 mbsf. However, the occurrence of other brief intervals of normal polarity preclude indisputable identification. In the normal interval interpreted as the end of the Gauss, the Kaena appears at 46 mbsf. The record in Hole 1128B is less clear, but the Brunhes/Matuyama boundary is evident at 14 mbsf. The Jaramillo Subchron is possibly between 20 and 22 mbsf, and the Olduvai Subchron is possibly between 28 and 32 mbsf.

Below 70 mbsf a sequence of reversals is clearly evident in the pelagic clays (Fig. F17). A long period of reversed polarity occurs from ~138 to 213 mbsf and has been correlated with Chron C12r, the longest reversed chron in the time frame indicated by biostratigraphic data. The well-defined short reverse interval centered at 82 mbsf, bounded by two intermediate-length normal chrons, is similar to the reversal sequence of Chron C10n. The correlation suggested in Figure F17 implies that a moderate change in sedimentation rate occurs toward the end of Chron C12r, with a faster sedimentation rate in the lowermost Oligocene. It also suggests that the Eocene/Oligocene boundary lies at a depth of ~250 mbsf, although it cannot be better defined because of poor recovery in this critical interval.

Recovery was limited in Hole 1128D, and thus paleomagnetic results are difficult to interpret. However, the results are strongly biased toward normal directions from ~280 mbsf to the bottom of the core at 450 mbsf, which may correspond to the dominantly normal polarity sequence of the upper and upper middle Eocene.

In summary, the magnetostratigraphy above the debrites is interpreted as recording C1n to C2An in the Pliocene–Pleistocene and below the debrites we interpret C9r to C13r from mid-Oligocene to the Eocene/Oligocene boundary. In the RCB cores, the long predominantly normal polarity is tentatively interpreted as a record of the predominantly normal upper and middle Eocene section. However, it must be recognized that this is an equivocal magnetostratigraphic interpretation.

F16. Pliocene–Pleistocene magnetostratigraphy from Holes 1128B and 1128C, p. 59.

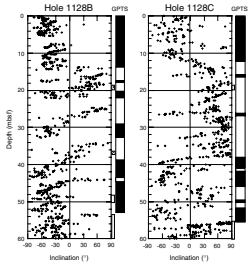

F17. Magnetostratigraphy and correlation with the geomagnetic polarity time scale, p. 60.

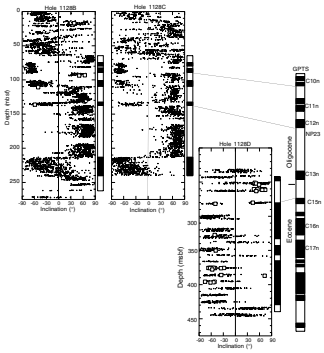

COMPOSITE DEPTHS

Introduction

Construction of the composite section from Holes 1128B and 1128C indicates that a nearly complete record of the Pleistocene–lower Oligocene sedimentary section at Site 1128 was recovered. Comparison of the amount of overlap between cores from adjacent holes was used to verify the degree of section continuity (see **"Composite Depths,"** p. 14, in the "Explanatory Notes" chapter). Using the Splicer software, sedimentary features and physical properties present in adjacent holes were aligned so that they occur at approximately the same depth. The alignment was performed downward from the mudline, and an offset value was added to the mbsf depth of each core to create a meters composite depth (mcd) for each core. Table **T3** (also in **ASCII format**) relates mbsf to mcd for each core and section at Holes 1128B and 1128C and provides offset values for the conversion of mbsf to mcd.

Data Input

The primary lithologic parameters used to create the composite section were magnetic susceptibility (MS) data collected by the MST on whole-round cores, gamma-ray attenuation (GRA) bulk density data (also acquired by the MST), color reflectance data (400 nm) measured on split cores, and natural gamma radiation (NGR) emissions data collected by the MST (Fig. **F18**). For specifics regarding these data collection procedures and parameters, see **"Physical Properties,"** p. 30. Unlike at the shallower sites of Leg 182, the MS of the sediments at Site 1128 was quite high, and the resulting data were very useful for correlation. *P*-wave velocity data collected by the MST were of poor quality as a result of numerous voids in the cores and, therefore, were not used for correlation purposes.

Biostratigraphic data aided in correlations by providing additional datums that were compared between holes (Table **T4;** see **"Biostratigraphy,"** p. 11). Planktonic foraminifers were particularly useful in constraining correlative intervals of the recovered section. Because most biostratigraphic samples were taken from core catchers, the stratigraphic error is generally on the order of 9.5 m (the distance between core catchers in two consecutive cores). However, in some cases, more detailed investigations were performed that reduced the stratigraphic error of a biostratigraphic range and allowed for increased confidence in correlations. Occasionally, overlapping biostratigraphic ranges permitted the recognition of correlative intervals between holes to an accuracy of 1–2 m. An example is the overlap of the range of the *C. macintyrei* last appearance datum in the top of Core 182-1128B-3H and the bottom of Core 182-1128C-2H, which constrains the tie between these two cores, in addition to providing an excellent time-stratigraphic horizon (1.67 Ma at 17–18.75 mcd) (Table **T4**).

Magnetostratigraphic datums also aided in correlation between holes (see **"Magnetostratigraphy,"** p. 24). Chron boundaries were identified throughout the recovered section except from the interval between 57 and 75 mcd where the record is disrupted by the debrite unit (Fig. **F19;** Table **T5**). The stratigraphic error on the chron boundaries is estimated to be ~±0.2 m.

T3. Site 1128 core and section depths in mcd and mbsf, **p. 91.**

F18. Composite depth section produced using Splicer software, **p. 61.**

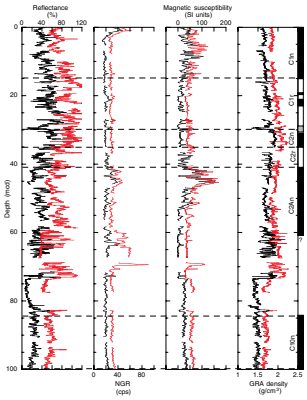

T4. Site 1128 biostratigraphic data used for correlations, **p. 96.**

F19. Spliced section of smoothed color reflectance data produced using Splicer software, **p. 64.**

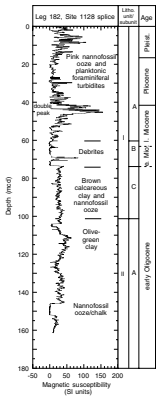

T5. Site 1128 magnetostratigraphic datums, **p. 97.**

Composite Section Construction

Differential core distortion was not a significant problem at Site 1128, in contrast to the shallower water sites, because of the relatively low concentration of hydrocarbon and hydrogen sulfide (H_2S) gas within the sediments. The data records from both holes are quite similar and easily aligned. Core overlap between holes averaged ~2 m where recovery was high and allowed for a statistical evaluation of ties used to create the composite section. However, correlations below ~160 mcd were hindered by poor core recovery, resulting from the presence of multiple chert layers interbedded with calcareous wackestone (see "Lithostratigraphy," p. 3). Recovery and correlation improved again below ~180 mcd (Fig. F18).

The Pliocene/Pleistocene boundary occurs at ~17 mcd (~15 mbsf in both holes), based upon biostratigraphic data (Fig. F19). The Pliocene/Miocene boundary occurs at ~42 mcd (39.5 mbsf in both holes). The upper Miocene–Pleistocene section corresponds to lithostratigraphic Subunit IA and is characterized by pink nannofossil ooze, interbedded with numerous turbidites consisting dominantly of planktonic foraminifers. The turbidites exhibit high color reflectance and low NGR activity and MS. These small features, ranging from tens of centimeters to >1 m thick, can be readily correlated between holes, based on the high similarity of data peak characteristics. At 40–50 mcd, a 10-m-thick high-amplitude peak doublet occurs in the NGR and MS data and corresponds to lows in the color reflectance data (Figs. F18, F19). This doublet provides a prominent correlation marker in both holes and corresponds to two layers of dark wackestone separated by a turbidite.

At 60–72 mcd, a debrite unit occurs that is prominent in all of the data and corresponds to lithostratigraphic Subunit IB. The top of the debrite is present in Core 182-1128B-7H, but it is missing between Cores 182-1128C-6H and 7H and, therefore, does not provide a useful correlative horizon. The base of the debrite occurs at 73 mcd, is present in both holes and provides a good correlation horizon. There appears to be a section within the debrite that was not recovered in either hole; therefore, correlations between holes within the debrite zone are not possible. Below the debrite bed, sediments are a more uniform calcareous clay to nannofossil ooze (lithostratigraphic Subunit IC; lower Oligocene), which grade downward to an olive green clay (lithostratigraphic Subunit IIA) at 104 mcd. These units exhibit lower amplitude, but still easily correlated, oscillations in all of the data. Another prominent, large-scale feature occurs at 146–153 mcd in both holes. This unit is a nannofossil ooze, probably a thick turbidite, exhibiting very high and uniform reflectance and density values and very low and uniform NGR and MS values. The base and top of this distinctive unit provide excellent correlation horizons.

Overall, the composite section indicates excellent agreement between the depositional records in Holes 1128B and 1128C, with the one exception being the debrite discussed above. Although there exists a small gap in the composite section within the debrite, recovery of the rest of the section is complete to 162 mcd (Fig. F19; Table T6, also in ASCII format). The composite section continues below this, but the spliced section could not be continued because of large gaps in recovery. Correlations are still readily apparent in the data to 260 mcd, the total depth of Hole 1128C. The mcd scale expansion relative to the mbsf scale is ~10%.

T6. Site 1128 splice tie points, p. 98.

ORGANIC GEOCHEMISTRY

At Site 1128, in addition to routine monitoring of hydrocarbon gases for safety, analyses were conducted for inorganic carbon, total carbon, nitrogen, and sulfur. The analytical procedures are described in "Organic Geochemistry," p. 16, in the "Explanatory Notes" chapter.

Volatile Hydrocarbons

Concentrations of volatile hydrocarbons were routinely determined from every core in Holes 1128B and 1128D using standard ODP headspace sampling procedures. Only low concentrations of methane were detected; the maximum concentration was 6.2 ppm, and most samples have <3 ppm (Table T7). No heavier hydrocarbon gases (C_{2+}) were detected.

T7. Headspace gas compositions, p. 99.

Inorganic and Organic Carbon, Sulfur, and Nitrogen

Inorganic carbon concentrations were converted to calcium carbonate percentages (see "Organic Geochemistry," p. 16, in the "Explanatory Notes" chapter). Calcium carbonate content has a bimodal pattern with increasing depth in Holes 1128B and 1128D (Table T8; Fig. F20). High carbonate values (75–90 wt%) are generally present in the upper 50 mbsf of Hole 1128B, decreasing from 50.3 to 138.4 mbsf to a low of 2.1 wt%. From 138.4 mbsf to the base of Hole 1128B, the carbonate content exhibits a second mode with a maximum concentration of 68 wt%. In Hole 1128D, with increasing depth from 241.4 mbsf, the carbonate content decreases from 52.6 wt% and generally has very low values (0–1 wt%) from 353 mbsf to total depth.

T8. $CaCO_3$, C_{org}, N, and S data, Holes 1128B and 1128D, p. 100.

Organic carbon (C_{org}) is low throughout Hole 1128B. With the exception of two samples having values of 0.32 and 0.41 wt%, C_{org} concentrations are all <0.16 wt% from Hole 1128B (Table T8; Fig. F20). Because C_{org} values are 0 wt% from 200 to 276 mbsf and methane concentrations in the headspace samples in this depth range are barely above background level, organic carbon was not analyzed in samples from Hole 1128D.

F20. $CaCO_3$ and C_{org} contents in samples from Holes 1128B and 1128D, p. 65.

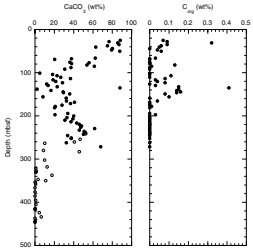

Sulfur is present in only five samples in Hole 1128B, with values ranging from 0.05 to 0.21 wt%. Nitrogen was not detectable in any sample. Sulfur and nitrogen were not analyzed in samples from Hole 1128D.

INORGANIC GEOCHEMISTRY

Interstitial Waters

Whole-round cores for interstitial water analysis were taken from Hole 1128B at a rate of two samples per section from the upper four cores, one per core down to Core 182-1128B-6H and every other core thereafter, recovery permitting. No samples were taken from Hole 1128C. Samples from Hole 1128D were taken at a rate of one sample every other core, recovery permitting. Samples were analyzed according to the procedures outlined in the "Inorganic Geochemistry," p. 18, in the "Explanatory Notes" chapter. These data are presented in Table T9 and Figures F21, F22, F23, F24, and F25.

T9. Interstitial water geochemistry, p. 101.

Salinity and Chlorinity

Salinity shows an increase from 34 to 35 at a depth of 11.7 mbsf in Hole 1128B. Below 11.7 mbsf the salinity remains constant to a depth of 236.8 mbsf. Between Cores 182-1128B-26X and 28X, near the base of Hole 1128B, there was a marked drop in salinity from 35 to 32. This decrease is also evident in Hole 1128D, and a salinity of ~32 is maintained to a depth of 434.8 mbsf in Core 182-1128D-22R (Fig. F21). The concentration of Cl^- increases from 563 to 571 mM by Core 182-1128B-6H and remains relatively constant (561 and 565 mM) to a depth of 236.8 mbsf. The increase in Cl^- and salinity in the upper portion of Hole 1128B is probably related to the increase in seawater salinity that occurred during the last sea-level lowstand (McDuff, 1978), with high-salinity waters characteristic of the last glacial period diffusing downward into older sediments. Between Cores 182-1128B-26X and 28X, the Cl^- concentration falls abruptly to 534 mM. Changes in chlorinity are not directly related to variations in salinity in the lower portion of Site 1128 (Fig. F22), implicating controls other than evaporation on the pore-water salinity (see "Discussion," p. 29).

Calcium, Magnesium, Potassium, Lithium, Silica, and Strontium

The concentrations of Mg^{2+} and K^+ decrease with increasing depth, whereas concentrations of Ca^{2+}, Li^+, $H_4SiO_4^0$, and Sr^{2+} increase (Figs. F23, F24; Table T9). The concentration of Mg^{2+} decreases from a value of 52.1 mM in Core 182-1128B-1H to 42.9 mM in Core 182-1128B-26X at a depth of 236.8 mbsf. Below this depth an abrupt decrease in concentration occurs at the bottom of Hole 1128B and continues in Hole 1128D. This abrupt change between Cores 182-1128B-26X and 28X is also manifested as a decrease in the concentration of K^+ and an increase in the concentrations of Ca^{2+} and Li^+ (Fig. F24). The concentration of Sr^{2+} shows an increase to 117 µM by a depth of 30.7 mbsf and subsequently a gradual increase throughout the remainder of Holes 1128B and 1128D. The concentration of Sr^{2+} does not appear to change significantly between Cores 182-1128B-26X and 28X. The concentration of $H_4SiO_4^0$ shows a steady rise from the normal bottom-water concentrations to a maximum of 1126 µM at 198.3 mbsf. Exceptions to this increase are three samples in Cores 182-1128B-4H and 5H that all have $H_4SiO_4^0$ concentrations similar to those measured in Core 182-1128B-1H. The most probable explanation for the low $H_4SiO_4^0$ in these samples is that they reflect penetration of bottom water into the formation. However, although slight anomalies were noted in other parameters at this depth (Table T9), none of the other chemical parameters measured are particularly diagnostic of bottom seawater and therefore the origin of the $H_4SiO_4^0$ concentrations in these samples remains enigmatic.

Sulfate, Alkalinity, Ammonium, and pH

The concentration of SO_4^{2-} gradually decreases to a value of 21.6 mM in Core 182-1128B-26X. Consistent with the change in several of the other elements, SO_4^{2-} shows a large decrease in concentration between 236.8 and 253.3 mbsf. The concentration of SO_4^{2-} decreases to 2.9 mM by the base of Hole 1128D. Although the decrease in SO_4^{2-} in the lower

F21. Concentration depth profiles, p. 66.

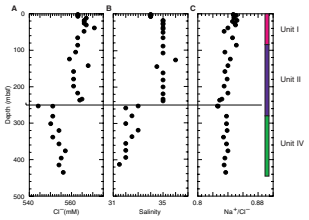

F22. Salinity vs. Cl^-, p. 67.

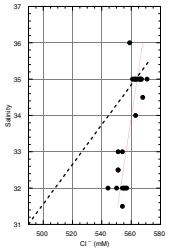

F23. Concentration depth profiles of cations, p. 68.

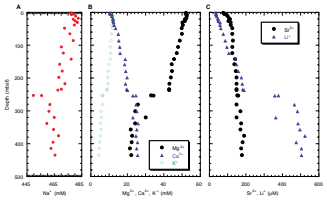

F24. Concentration depth profile of H_4SiO_4, p. 69.

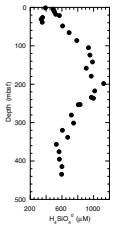

portion of Hole 1128D is associated with a slight increase in alkalinity, there is no noticeable smell of H_2S that might suggest the reduction of SO_4^{2-} by bacteria. However, the decrease in SO_4^{2-} is associated with an increase in the concentration of NH_4^+ (Table T9), indicating that the decrease in the concentration of SO_4^{2-} was originally linked to the oxidation of organic material. The apparent absence of H_2S at the present time could reflect the removal of H_2S by diffusion or through the formation of solid iron sulfide phases.

Alkalinity increases to a value of 4.52 mM by a depth of 21.2 mbsf, approximately coincident with the initial increase in Sr^{2+}. Below this depth there is a reduced rate of increase to 236.8 mbsf in Core 182-1128B-26X. At this depth there is an abrupt increase in alkalinity, which is coincident with the changes in other geochemical parameters noted previously. The pH, measured using the punch-in electrode method, showed a consistent decline with depth until 86.1 mbsf in Core 182-1128B-10H, where hardness of the core precluded further use of this technique (Fig. F25). In contrast, pH measured using the normal ODP method (see "Inorganic Geochemistry," p. 18, in the "Explanatory Notes" chapter) showed a great deal of variability.

F25. Variations in pH and interstitial water compositions, p. 70.

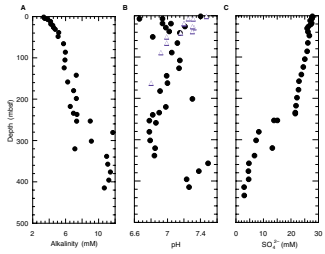

Discussion

Because Sr^{2+} is added to pore fluids by the recrystallization of biogenic forms of aragonite and calcite (Baker et al., 1982), the low increase in the concentration of Sr^{2+} with increasing depth at Site 1128 indicates a relatively low rate of carbonate recrystallization. The steepest gradient in Sr^{2+} occurs in the upper 20–30 mbsf, accompanied by an increase in the concentration of alkalinity and a decrease in the concentration of SO_4^{2-}. This interval appears to be the most active region of carbonate recrystallization, with reduced carbonate saturation probably being linked to the diagenesis of organic material. Changes in the concentrations of Ca^{2+}, Mg^{2+}, and K^+ deeper in Holes 1128B and 1128D are probably a result of clay mineral alteration, rather than the result of diagenetic reactions involving carbonates. Clay mineral diagenesis consumes Mg^{2+} and K^+ and produces Ca^{2+} (Gieskes, 1973). Perhaps the most significant aspect of the pore-water geochemistry at Site 1128 is the abrupt change in most of the pore-water parameters (except Sr^{2+}) between Cores 182-1128B-26X and 28X. This change is observed near the transition between lithostratigraphic Units II and IV (see "Lithostratigraphy," p. 3). Differences in pore-water parameters probably result from the presence of relatively impermeable barriers to vertical diffusion and the existence of a separate hydrological unit in the older sediments. Although no such barriers were recovered during coring, the downhole logs (see "Downhole Measurements," p. 33) revealed a section between 250 and 280 mbsf that contained numerous relatively impermeable layers, with the potential to act as impediments to vertical movement of ions. The pore fluids in the lower unit, therefore, are being altered by local diagenetic reactions. The products of these reactions are impeded from exchanging with the overlying units. As mentioned above, the salinity and chlorinity are decoupled in this unit (Fig. F22). This arises as a result of the loss of cations and anions through precipitation and adsorption reactions. This hypothesis can be tested by summing the mass of cations and anions and comparing the total with measured salinity. This comparison shows that salinity determined by the two methods agrees within the error of the analytical methods used

(see "Inorganic Geochemistry," p. 18, in the "Explanatory Notes" chapter). The low chlorinity of this unit, however, is probably not a result of diagenesis and may reflect the chlorinity of some continentally derived fluid or the dewatering of clays under compaction.

X-Ray Mineralogy

The sediments at Site 1128 are composed of low-Mg calcite (LMC), quartz, and clay minerals (Fig. F26; Table T10, also in ASCII format). No samples were analyzed above Core 182-1128B-4H. Lithostratigraphic Unit I is composed predominantly of LMC, with the exception of the slumped unit in Cores 182-1128B-7H and 8H that contains high concentrations of clay minerals and quartz (see "Lithostratigraphy," p. 3). In contrast, Unit II is composed predominantly of noncarbonate minerals, the main component of which is clay. In Unit IV the main component is quartz.

PHYSICAL PROPERTIES

Introduction

Measurements of physical properties at Site 1128 followed the procedures outlined in "Physical Properties," p. 19, in the "Explanatory Notes" chapter. These included nondestructive measurements of *P*-wave velocity (every 4 cm; Table T11, also in ASCII format), GRA bulk density (every 4 cm; Table T12, also in ASCII format), MS (every 8 cm; Table T13, also in ASCII format), and NGR (every 16 cm; Table T14, also in ASCII format) using the MST. The *P*-wave logger (PWL) was activated only on APC cores. Thermal conductivity was measured in unconsolidated sediment at a frequency of one per core (Table T15, also in ASCII format), with three samples per core analyzed after deployments of the Adara temperature tool and the DVTP (Table T15). A minimum of two discrete *P*-wave velocity measurements per section were made on the working half of the split cores (Table T16, also in ASCII format), and the measurement frequency was increased to five per section after the PWL was turned off. Standard index properties (Table T17, also in ASCII format) and undrained shear strength (only in unconsolidated sediments) (Table T18, also in ASCII format) were measured at a frequency of one per section.

The following sections describe the downhole variations in sediment physical properties and their relationships to lithology and downhole logging measurements. Variations in MS are described within "Paleomagnetism," p. 22.

Index Properties, *P*-Wave Velocity, Natural Gamma Radiation, and GRA Densiometry

Sediment physical properties at Site 1128 closely reflect lithologic variations observed in the recovered sediments and provide essential data for core-log correlation (Figs. F27, F28). An offset was seen between the discrete bulk density measurements and the GRA densiometry measurements of the MST in the upper 138 mbsf of the sediment section (Fig. F28). This offset was corrected using the equation of Boyce (1976) as described in "Index Properties," p. 21, in the "Explanatory Notes" chapter.

F26. Variations in the ratio of low-Mg calcite and quartz, p. 71.

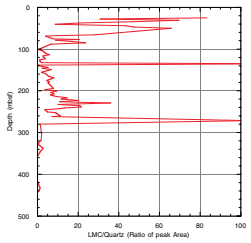

T10. XRD data, p. 102.

T11. *P*-wave velocity measurements, p. 104.

T12. GRA densiometry measurements, p. 105.

T13. Magnetic susceptibility measurements, p. 106.

T14. Natural gamma-ray measurements, p. 107.

T15. Thermal conductivity measurements, p. 108.

T16. Discrete *P*-wave velocity measurements, p. 109.

T17. Index properties measurements, p. 110.

T18. Undrained shear strength measurements, p. 111.

A close correlation was seen between the downhole logging data (see "Downhole Measurements," p. 33) and sediment physical properties (Fig. F29). Natural gamma radiation values from both whole core and downhole logging measurements show an excellent correlation that supports the integrity of both data sets (Fig. F29). Index properties and GRA bulk densities have similar patterns to the downhole logging data, although values are generally lower (Fig. F29). This difference probably results from the fact that in situ density includes the influence of sediment overburden and hydrostatic pressure, whereas laboratory measurements do not. A similar effect is seen in the *P*-wave velocities (Fig. F29), particularly above 250 mbsf, where in situ velocities are higher than those measured on discrete samples. Similar data trends have been observed during other ODP legs (e.g., Leg 166; Eberli, Swart, Malone, et al., 1997)

Physical properties data can be divided into five units on the basis of trends in the measured parameters. Physical properties Unit (PP Unit) 1 (0–69 mbsf) is characterized by high variability in all data sets and corresponds to a lithostratigraphic sequence dominated by turbidites and debris flows (see "Lithostratigraphy," p. 3). Values of NGR average ~5 cps, with distinct peaks of as much as 60 cps (39–43 and 45–69 mbsf; Fig. F28). The upper peak (25 cps) occurs with a corresponding peak in MS (140 SI units) and a distinct peak in NGR in the downhole logs (see "Downhole Measurements," p. 33). This downhole spectral gamma peak appears to be mainly caused by high thorium concentrations, indicating that terrigenous sediments in the section are the cause of the NGR and MS shifts. The lower and much larger NGR peak (Figs. F27, F28) corresponds to a significant interval of debrites within lithostratigraphic Subunit IB. This interval also has increased bulk density (as much as 1.9 g/cm^3), increased MS (80 SI units), and variable *P*-wave velocity (1.5–1.8 km/s) (Figs. F27, F28). A distinct peak in bulk density (as much as 1.85 g/cm^3), correlated to decreased porosity (48%), is seen near 32 mbsf (Fig. F27). Sediments in this interval have increased cohesiveness, as expressed by greater shear strength (Fig. F30). No change in lithology can be identified to explain this density increase. The lower limit of PP Unit 1 is characterized by abrupt shifts in all physical properties parameters measured and marks the base of the debrite unit (see "Lithostratigraphy," p. 3).

Physical properties Unit 2 (69–139 mbsf) is characterized by low variability in all data sets, punctuated by distinct offsets (1–5 m) corresponding to sharply bounded turbidites. The three most prominent turbidite layers occur at 94, 115, and 132–139 mbsf (Fig. F27) and are characterized by reduced NGR (5 cps), reduced MS (0 SI units), increased bulk density (1.8 g/cm^3), and increased *P*-wave velocity (1.76 km/s). All these changes are characteristic of intervals of high calcium carbonate content (~90%; see "Organic Geochemistry," p. 27). Between the turbidite layers, NGR values range from 5 to 20 cps, MS is nearly constant at 30 SI units, bulk density ranges from 1.47 to 1.57 g/cm^3, and *P*-wave velocity is nearly constant at 1.55 km/s (Figs. F27, F28). The base of the unit occurs at the bottom of the thickest turbidite layer between 132 and 139 mbsf (Fig. F28).

Physical properties Unit 3 (139–231 mbsf) is characterized by an interval of low and nearly constant values for all physical properties parameters measured (NGR = ~12 cps; MS = ~5 SI units; bulk density = ~1.5 g/cm^3; and *P*-wave velocity = ~1.55 km/s) (Figs. F27, F28). This PP unit corresponds to lithostratigraphic Unit II, a sequence of monotonous olive-green clay (see "Lithostratigraphy," p. 3). Sediment homo-

F27. *P*-wave velocity, bulk densities, porosity, magnetic susceptibility, and NGR measurements, p. 72.

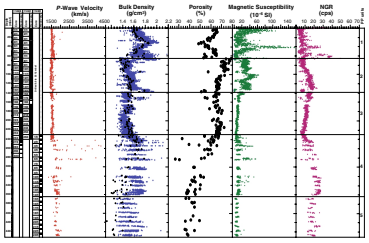

F28. NGR, magnetic susceptibility, bulk densities, and *P*-wave velocities from the upper 270 m at Site 1128, p. 73.

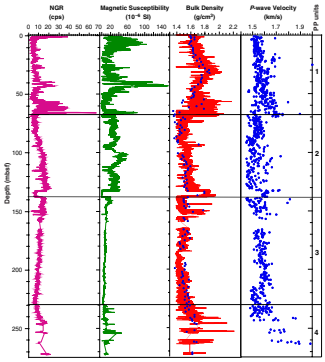

F29. Downhole logging data and physical properties measurements, p. 74.

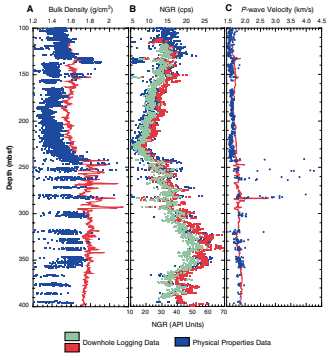

F30. Sediment consolidation, p. 75.

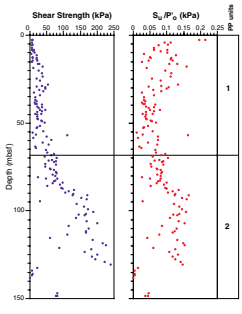

geneity was also reflected in downhole logs (Fig. F29) (see "Downhole Measurements," p. 33) as an interval of low variability in all parameters.

An increase in NGR (8–20 cps), MS (5–55 SI units), bulk density (1.5–1.8 g/cm^3), and *P*-wave velocity (1.6–4.3 km/s) and a decrease in porosity (65%–25%) occur at the upper boundary of PP Unit 4 (231–363 mbsf), below which all parameters show increased variability reflecting alternations of indurated and unindurated sediment (Fig. F27). This unit correlates with logging Units 2–4 (see "Downhole Measurements," p. 33), and lithostratigraphic Subunit IIC, Unit III, and Subunit IVA (see "Lithostratigraphy," p. 3). Incomplete core recovery within this interval made it difficult to further divide PP Unit 4. Within PP Unit 4, sediments are lithified above 282 mbsf and partially lithified below 284 mbsf (see "Lithostratigraphy," p. 3). This decrease in lithification is reflected in sediment physical properties by reduced variability of *P*-wave velocity and an overall decrease in bulk density (1.7–1.52 g/cm^3) (Fig. F27). Decreased lithification was accompanied by a decrease in calcium carbonate content, which resulted in increased NGR (6–23 cps). The base of PP Unit 4 is marked by a shift to lower values in bulk density, MS, and NGR (Fig. F27).

The upper boundary of PP Unit 5 (363–452 mbsf) correlates well with the transition to lithostratigraphic Subunit IVB (see "Lithostratigraphy," p. 3) and logging Unit 5 (see "Downhole Measurements," p. 33). Within this unit all measured parameters show a constant trend for the rest of the recovered interval, reflecting the homogenous nature of the sediments (Fig. F27). This constant trend is also seen in downhole logging data (see "Downhole Measurements," p. 33).

Shear Strength

Undrained peak and residual shear strength were measured on unconsolidated sediments from 0 to 150 mbsf (Fig. F30). Shear strength at Site 1128 shows an overall downhole increase (5–240 kPa) caused by compaction, punctuated by increased variability below 50 mbsf. This variability is caused in part by alternations in sediment lithification. However, in some intervals it may also result from drilling disturbance and cracking of the sediment before sediment failure, resulting in lower values for peak strength. A prominent layer of low shear strength occurs between 132 and 139 mbsf in PP Unit 2 within a turbidite interval (Fig. F30).

An estimate of sediment consolidation can be made by comparing the range of shear strengths measured at Site 1128 to those of a gravimetrically or "normally" consolidated sedimentary section by calculating the ratio of undrained shear strength (S_u) to overburden stress (P'_o). Overburden pressure is calculated from bulk density and overlying sediment thickness assuming hydrostatic pore fluid pressures. The S_u/P'_o ratio in normally consolidated sediments is usually between 0.22 and 0.25. All sediments at Site 1128 fall below this range and, thus, appear to be underconsolidated (Fig. F30). Sediment underconsolidation can result from processes such as retarded dewatering of the sediment in response to rapid deposition and low interparticle friction or cohesion.

Thermal Conductivity

Thermal conductivity values at Site 1128 range from 0.62 to 1.28 W/(m·K) (Fig. F31; Table T14). In general, thermal conductivity data correlate well with other sediment physical properties, particularly bulk density (Fig. F31). Physical properties Unit 1 is an exception to this relationship, having only a moderate correlation to other physical properties data sets (Fig. F31) caused by high sediment variability occurring as a result of slumping within the upper sedimentary section (see "Lithostratigraphy," p. 3).

F31. Thermal conductivity and bulk density measurements, p. 76.

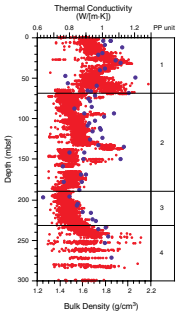

In Situ Temperature Measurements

Three Adara and one DVTP in situ temperature measurements were made at Site 1128. There was some variation in estimates of mudline temperatures, which ranged from 1.52° to 2.48°C with an average of 1.92°C (Table T19, also in ASCII format). Measurements made at Core 182-1128C-4H were affected by postemplacement movement of the probe. Despite this disturbance, a value for in situ temperature was determined using data before and after the disturbance.

T19. In situ formation temperature estimates, p. 112.

In situ measurements provide a linear temperature-depth relationship that defines a geothermal gradient of 53°C/km (r^2 = 0.985; Fig. F32). This relatively high value can be explained by the low thermal conductivity of the sediments at Site 1128. The geometric mean of thermal conductivity between 0 and 200 mbsf (Fig. F31) was used to determine heat flow (0.94 ± 0.05 W/[m·K]). Using this value and the geothermal gradient determined above, heat flow is estimated to be 49.8 mW/m². This value is close to the global average for continental and oceanic heat flows and is close to the values of 56 and 63 mW/m² reported for the Ngalia and Alice Springs/Amadeus Basins of the Central Australia Archean Shield by Lambeck (1986).

F32. Variation of formation temperature with depth, p. 77.

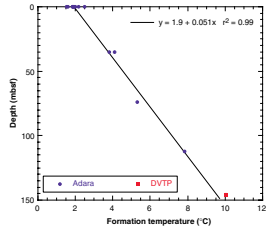

DOWNHOLE MEASUREMENTS

Logging Operations

After completion of drilling operations at Hole 1128D, the hole was prepared for logging (see "Operations," p. 2). An initial logging attempt was made with the base of pipe at 90 mbsf. This proved to be too shallow and resulted in a niche being carved into the sidewall as the pipe moved in the complex ~3-m heave. After this initial attempt, the lower limit of the BHA was placed at 110 mbsf for both logging runs (Fig. F33). Two logging tool strings were run in the following order: (1) triple combo, phasor dual induction–spherically focused resistivity tool (DITE-SFL), hostile environment lithodensity sonde, accelerator porosity sonde (APS), hostile environment natural gamma-ray sonde; and (2) FMS/sonic (see "Logging Tools and Tool Strings," p. 27, in the "Explanatory Notes" chapter). Neither logging run reached the total depth drilled (452.5 mbsf), with the first run touching down at 424 mbsf and the second at 419 mbsf (Fig. F33). Because of time constraints, the geologic high-resolution magnetic tool and WST were not run.

F33. Logging runs at Hole 1128D, p. 78.

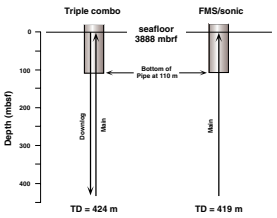

Data Quality

The diameter of the borehole was within the limits of both FMS (38 cm) and triple combo (42 cm) calipers for the entire interval logged and, with only a few exceptions, data quality was good. The caliper record showed the presence of a tight spot in the upper part of the section (252 mbsf), and some small-scale washouts between 242 and 295 mbsf, resulting from thinly bedded alternations of indurated and unindurated sediments (Figs. F34, F35). Extremely high porosities in some unconsolidated layers resulted in poor statistical validity of the APS data, despite the high-resolution (275 m/hr) logging speed. The DITE-SFL malfunctioned, resulting in several unrepeatable small spikes in the deep-resistivity log below 337 mbsf. Despite a functioning wireline heave compensator, ship movement affected the FMS data. Shipboard processing of the FMS was able to remove some of the influences of heave, although postcruise processing will be needed to entirely remove these effects. The analog modes on the sonic tool performed poorly because of the slow formation velocities, which were confirmed by discrete physical properties measurements (see "Physical Properties," p. 30). The sonic digital tool (DTCO output) provided good quality data, except within a few meters of the pipe.

Preliminary Observations

Downhole data trends in the logging data at Site 1128 are closely correlated to lithologic and sediment physical properties data. As sediment recovery below 250 m was variable, averaging only ~34%, the downhole logs provided valuable stratigraphic information and enabled more accurate placement of lithostratigraphic boundaries. Downhole logging data, when correlated to the incomplete core record during postcruise analysis, will provide a more complete understanding of depositional processes occurring from the lower middle Eocene to Holocene on the upper continental rise adjacent to the cool-water carbonate margin in the Great Australian Bight.

The compatibility of wireline log and physical properties data measured on both whole-core and discrete samples attests to the integrity of the logging data sets (see "Physical Properties," p. 30). Overall, downhole measurement trends show the effects of compaction overprinted with the influence of diagenesis and sediment redeposition. Compaction effects cause a gradual increase in sonic velocity and bulk density and a decrease in porosity with depth (Figs. F34, F35). Variations in the importance of diagenesis and sediment redeposition enable the downhole logs to be divided into four units on the basis of general trends in the data.

Logging Unit 1 (0–242 mbsf) was divided into two subunits. Subunit 1A (0–154 mbsf) is characterized by relatively uniform values in all parameters measured, with the exception of gamma radiation, which shows a general increase throughout the unit (Figs. F34, F35). Uniform values within logging Unit 1A are punctuated by excursions of decreased gamma radiation and photoelectric effect (PEF) and increased porosity, bulk density, resistivity, and sonic velocity. These excursions represent thin units (5–8 m) of redeposited nannofossil ooze, with the most prominent of these layers occurring at 133 and 153 mbsf (Figs. F34, F35). The upper part of Subunit 1A (0–110 mbsf) includes the section logged by the spectral gamma-ray (SGR) within the pipe (Fig. F36). The SGR variations within this upper interval correlate well with those

F34. Geophysical logs from the triple combo, p. 79.

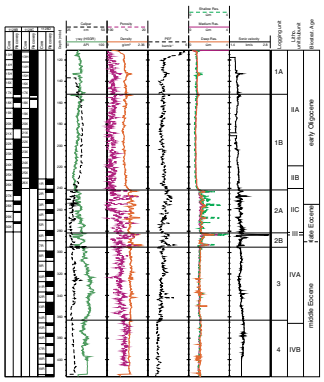

F35. Spectral gamma-ray logs for the open-hole logged interval, p. 80.

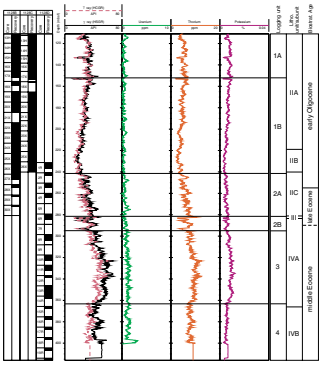

F36. Spectral gamma-ray logs for the interval logged through pipe, p. 81.

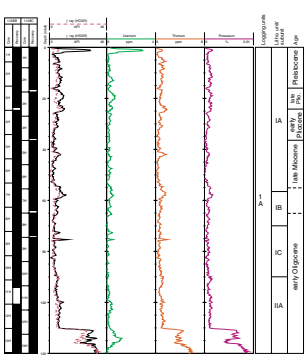

from the MST NGR record (see "Physical Properties," p. 30). Despite this correlation, the low amplitude of the SGR signal in pipe precluded any unequivocal division of units in the top 100 mbsf of the section. The base of logging Subunit 1A correlates with the first appearance of debris flows and redeposited layers within the upper part of the sedimentary section (see "Lithostratigraphy," p. 3).

Logging Subunit 1B (154–242 mbsf) is characterized by a downhole decrease in gamma-ray values and nearly constant values for all other logs (Figs. F34, F35). This decrease in gamma radiation is mainly because of a loss of thorium (Fig. F35), indicating downhole dilution of clay minerals. This conclusion is supported by the close correlation of decreased gamma-ray values with increased calcium carbonate content between 160 and 255 mbsf (see "Organic Geochemistry," p. 27). The generally homogenous logging values in logging Subunit 1B are related to monotonous, dominantly unlithified, homogenous clays and chalks, which become increasingly lithified below 203 mbsf (see "Lithostratigraphy," p. 3). This increased lithification was not observed in the porosity and density logs but correlates moderately well with a slight increase of sonic velocity near 203 mbsf (Fig. F34). The base of logging Unit 1 correlates well with the base of lithostratigraphic Subunit IIB (see "Lithostratigraphy," p. 3).

The top of logging Unit 2 (242–295 mbsf) occurs at a sharp change in character in all data sets, with an increase in density, sonic velocity, and resistivity and a decrease in gamma radiation and porosity (Figs. F34, F35). All data sets within logging Unit 2 have high variability corresponding to an equivalent interval of high variability in physical properties data from recovered sediments (see "Physical Properties," p. 30). This variability in lithology and sedimentation was imaged in FMS data as well-bedded alternations of conductive and resistive layers. Logging Unit 2 can be divided into two subunits on the basis of the nature of variability seen in the data. Logging Subunit 2A correlates with lithostratigraphic Subunit IIC, which is composed of claystone with chert and variable lithification. Within logging Subunit 2A, peaks in the different logs are not well correlated, as the thin-bedded turbidites and cherts each result in different log responses (Fig. F34). However, data peaks in logging Subunit 2B correlate well between parameters and reflect thickly deposited nannofossil ooze turbidites. These sharply bounded, high-carbonate turbidites result in decreased gamma radiation and porosity and increased density, resistivity, PEF, and sonic velocity (Fig. F34). Nannofossil ooze turbidites alternate with high gamma-ray, low density, reduced velocity, conductive intervals corresponding to terrigenous-rich sandstones (see "Lithostratigraphy," p. 3). The presence of terrigenous-rich intervals is reflected by an increase in thorium and potassium within SGR values of logging Subunit 2B (Fig. F35). Logging Subunit 2B correlates well with lithostratigraphic Unit III, although low recovery prevented the accurate placement of the lower boundary of this lithostratigraphic unit. The downhole logs indicate that this boundary was 11 m lower than described from core data (see "Lithostratigraphy," p. 3). The base of logging Unit 2 is marked by a return to less variable values in all parameters (Figs. F34, F35).

Logging Unit 3 (295–362 mbsf) corresponds to lithostratigraphic Subunit IVA, which is composed of relatively monotonous silty clays and claystones. Increased thorium and potassium concentrations within logging Unit 3 reflect an increased concentration of terrigenous sediment between 295 and 262 mbsf (Fig. F35). This conclusion is supported by X-ray diffraction data from this interval, which shows an in-

crease of noncarbonate sediment in samples measured (see "Inorganic Geochemistry," p. 27). Bulk density and resistivity are relatively constant throughout logging Unit 3, with the exception of a density peak at 342 mbsf correlating to a peak in PEF (Fig. F34). This layer was described in the recovered sediments as an interval of coarse terrigenous-rich sandstones (see "Lithostratigraphy," p. 3). Within logging Unit 3, gamma-ray values increase gradually between 295 and 338 mbsf, and then decrease in a stepwise fashion toward the base of the unit (Figs. F34, F35). Sonic velocity is relatively constant downhole until a slight increase near 350 mbsf, coincident with an increase in sediment induration (see "Lithostratigraphy," p. 3).

Logging Unit 4 (363–414 mbsf) has consistent values for all parameters, with the exception of gamma radiation and porosity that exhibit some cyclic variability (Figs. F34, F35). An interval of increased carbonate content is seen between 363 and 378 mbsf, as indicated by decreased gamma-ray values and a closer correspondence of porosity and density traces that have been plotted so that the two curves will overlie each other in a clean limestone (Fig. F34). The close correspondence of porosity and density curves for the remainder of the interval indicate calcium carbonate contents in logging Unit 4 are greater than in Unit 3 (Fig. F34). Terrigenous components are also present in the sediments of logging Unit 4, as shown by the moderately high thorium concentrations (Fig. F35). These conclusions are supported by the limited recovery of an indurated clayey siltstone in this interval (see "Lithostratigraphy," p. 3).

Acoustic impedance was calculated (Fig. F37) using downhole velocity and density data and passed through a 5-m smoothing function to produce a resolution comparable to that of the site-survey seismic data (see "Seismic Stratigraphy," p. 36). Two prominent peaks in impedance occur near 130 and 152 mbsf, which correlate well with reflectors occurring above Horizon 1c_h3. The Horizon 1c_h3 reflector (173 mbsf) is not obvious in the impedance data and, thus, may result from interference effects (Fig. F37). A prominent shift in impedance near 236 mbsf does not appear as a significant reflector in the seismic data. The most significant impedance peak occurs near 282 mbsf (Fig. F37) and corresponds to the lower boundary of lithostratigraphic Unit II. The remainder of the impedance record shows peaks that correlate with prominent reflectors below Horizon 1c_3a.

F37. Acoustic impedance log, p. 82.

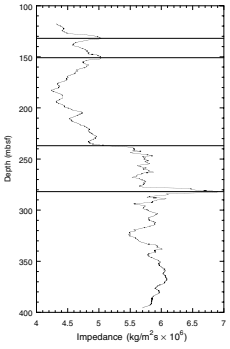

F38. Seismic site-survey tracks for Site 1128 in relation to other Leg 182 sites and the AGSO169 site-survey seismic lines, p. 83.

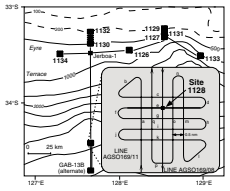

F39. Portion of seismic Line AGSO169/01e showing seismic stratigraphic sequences at Site 1128, p. 84.

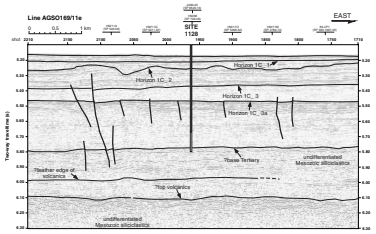

SEISMIC STRATIGRAPHY

Introduction

The seismic sequences intersected on the upper continental rise at Site 1128 (Fig. F38) could not be tied to the regional Cenozoic seismic stratigraphy established on the slope and shelf (sequences defined in Feary and James, 1998, reprinted as Chap. 2) before drilling because of the lack of appropriate seismic tie lines. Instead, a local seismic stratigraphy was established for the presumed Cenozoic portion of the continental rise succession using the high-resolution site-survey seismic data (Fig. F39). These data shows that the succession extending down to Horizon 1C_2 was deposited in a "ponded" upper continental rise basin overlying a major unconformity/hiatus surface. Viewed on a regional basis, it is clear that this small basin was formed by local compression of the underlying succession between Horizons 1C_2 and 1C_3a (Fig.

F39). Sequence geometry and the presence of folds and dislocation surfaces indicate that this local compression resulted from large-scale downslope movement. The dislocation surfaces show that movement must have occurred on a décollement surface or surfaces within the succession underlying Horizon 1C_3a, most probably in the vicinity of 300 mbsf.

Time–Depth Conversion

Because of the considerable time required to carry out a check-shot survey in this water depth, the planned deployment of the WST was abandoned. As a result, the time–depth relationship for sequence boundaries and horizons located on seismic data has been estimated principally on the basis of the integrated sonic trace (Fig. F40), derived from interval transit-time data. Therefore, the time–depth relationship must be considered to be an approximate estimate only. Because the integrated sonic trace does not extend to the sediment surface, its location in the time domain cannot be determined accurately. However, the strong likelihood that Horizons 1C_2 and 1C_3a correlate respectively with the top Oligocene (base debrite at 70 mbsf) and Eocene–Oligocene (at ~260 mbsf) unconformities provides an increased level of confidence for the proposed correlation (Fig. F41). This correlation shows that the best-fit time–depth relationship defined by the integrated sonic trace (Fig. F40A) falls within and toward the upper limit of the envelope defined by the six stacking velocity curves from the immediate vicinity of Site 1128, with a relatively small difference (≤13 m) between predicted and actual depths to boundaries/horizons (Table T20).

F40. Predicted and corrected depths and interval velocities, p. 85.

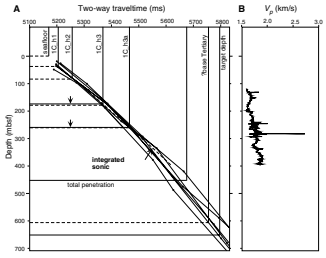

F41. Lithostratigraphic units, seismic sequences, biostratigraphic hiatuses, and ages, p. 86.

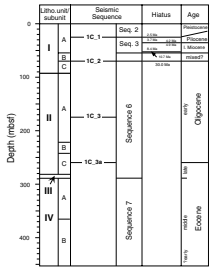

T20. Differences between depths to seismic horizons and corrected depths, p. 113.

Seismic Sequence Characteristics

The data collected at Site 1128, particularly lithostratigraphic and biostratigraphic information, offer the opportunity to interpret the site data within a more regional context and also allow a description of the characteristics of seismic sequences intersected at this site (see "Lithostratigraphy," p. 3, and "Biostratigraphy," p. 11). Downhole and seismic data can be correlated (Fig. F41) using the high-resolution site-survey seismic data collected by the Australian Geological Survey Organisation (AGSO) in 1996 (Feary, 1997); therefore, it is possible to describe and interpret the sequences intersected at Site 1128 in terms of the seismic stratigraphy established on the slope and shelf (Feary and James, 1998, reprinted as Chap. 2).

Sequence 2

The base Sequence 2 boundary correlates with continental rise Horizon 1C_1, present as an unconformity surface within the upper continental rise ponded basin. Onlap patterns at the base of this sequence indicate that this sequence boundary should represent a hiatus surface. Compared with the >500-m thickness of Sequence 2 at the shelf edge, this sequence is extremely thin (25 m) at Site 1128. Reflections within this interval are evenly stratified with low to moderate amplitude. Biostratigraphic data indicate that the succession overlying Horizon 1C_1 is of Pleistocene–late Pliocene age, and lithostratigraphic data indicate that this interval consists of pelagic nannofossil ooze containing abundant spicules, interbedded with thin calciturbidites (below seismic reso-

lution) consisting of foraminiferal packstone and grainstone. The basal hiatus surface corresponds to ~1.2 m.y.

Sequence 3

Biostratigraphic and lithostratigraphic data indicate that the interval between Horizons 1C_1 and 1C_2 consists of a 30-m-thick coherent interval, equivalent to slope and shelf seismic Sequence 3, overlying a 15-m-thick debrite interval. The coherent interval correlates to the lower portion of lithostratigraphic Subunit IA, of late Miocene age, and the debrite interval to lithostratigraphic Subunit IB. The evenly stratified, low–moderate amplitude reflection character of the Sequence 3 interval is identical to the overlying Sequence 2 succession, and lithostratigraphic data indicate that it similarly consists of pelagic nannofossil ooze interbedded with thin calciturbidites. There is no indication on seismic data of the hiatus surface at the upper Miocene/lower Pliocene boundary, toward the middle of Sequence 3 (Fig. **F41**).

The transition from Sequence 3 ooze down into the debrite unit correlates with a poorly defined disconformity surface on seismic data, and the hiatus surface toward the base of Sequence 3 is probably also represented by this indistinct discontinuity. Reflections are very indistinct within the debrite unit, although there are subtle indications of low amplitude reflections downlapping to the south onto the Horizon 1C_2 surface. By analogy with the clastic sediments intersected at the base of Site 1126, clasts of terrigenous clastic sediment within the debrite are of probable Cretaceous age. Their presence indicates derivation of at least some of the debrite material from Cretaceous strata shown on seismic data to outcrop at the seafloor on the middle and lower continental slope. The source of the Oligocene and middle and upper Miocene clasts also present within the debrite unit is unknown, although the absence of abyssal paleodepth indicators within the benthic foraminiferal assemblage in this unit is consistent with derivation from upslope.

Sequence 6

Biostratigraphic data indicate that the intervals between Horizons 1C_2 and 1C_3 (104 m thick) and between Horizons 1C_3 and 1C_3a (86 m thick), corresponding to the lower Oligocene, should be correlated with slope and shelf seismic Sequence 6 (Fig. **F41**). In addition, the 28-m-thick upper Eocene interval immediately underlying Horizon 1C_3a is also equivalent to the basal part of Sequence 6. This sequence therefore includes a diverse range of lithofacies from several units and subunits, including the spicule-dominated clay and nannofossil-dominated ooze alternations of lithostratigraphic Subunit IC; the variably calcareous, spicule-dominated clay, claystone, and clayey chalk of Unit II, interbedded with calciturbidites of planktonic foraminiferal and nannofossil ooze; and the glauconitic sandstone turbidites of Unit III. Horizon 1C_3a, correlated with the Eocene/Oligocene boundary at 260 mbsf, corresponds to the transition from moderately consolidated clay down into lithified claystone.

Horizon 1C_2, forming the boundary between the lithostratigraphic Subunit IB debrite and the underlying succession correlated to Sequence 6, is one of the most dramatic surfaces visible on seismic data on the continental rise. On the upper continental rise, this surface displays relief of as much as 70 m, principally as a result of faulting and folding of the underlying units between Horizons 1C_2 and 1C_3a (Fig.

F39). As noted above, seismic geometry indicates that this faulting and folding is a reflection of large-scale downslope movement that appears to have affected the entire 190-m interval between these two horizons, as well as some undetermined component of the succession beneath Horizon 1C_3a that may extend to the base of Sequence 6.

The upper part of Sequence 6 at Site 1128, between Horizons 1C_2 and 1C_3, consists of relatively evenly stratified, continuous to semicontinuous reflections, with mostly low amplitudes except for two higher-amplitude, continuous reflectors estimated to occur at ~95–105 and ~135–140 mbsf. This upper reflector may correlate with a grainstone interval at 95 mbsf, and the lower reflector may correlate with grainstone or chert layers at 135–137 mbsf (see "Lithostratigraphy," p. 3). The uniform mudstone interval between Horizons 1C_3 and 1C_3a is relatively featureless on seismic data, consisting of low-amplitude, semicontinuous reflections. By contrast, the interval underlying Horizon 1C_3a is characterized by high-amplitude, semicontinuous to continuous, evenly stratified reflections. This may result from some combination of variable lithification, the presence of grainstone calciturbidites, or the presence of chert layers resulting from preferential silicification.

Sequence 7

The thick middle Eocene interval at Site 1128 (>163 m), corresponding to lithostratigraphic Unit IV, correlates with seismic Sequence 7 on the shelf and slope. As is the case upslope, Sequence 7 in the continental rise setting consists of a siliciclastic facies suite. In this environment, Sequence 7 is dominated by silty clay to sandy siltstone, coarsening downward to a silty sandstone intersected at the deepest extent of Site 1128 penetration. Unlike the markedly progradational seismic geometry of Sequence 7 on the shelf and slope, the equivalent sequence on the upper continental rise is characterized by evenly stratified, continuous to semicontinuous, low- to moderate-amplitude reflections.

REFERENCES

Baker, P.A., Gieskes, J.M., and Elderfield, H., 1982. Diagenesis of carbonates in deep-sea sediments—evidence from Sr^{2+}/Ca^{2+} ratios and interstitial dissolved Sr^{2+} data. *J. Sediment. Petrol.,* 52:71–82.

Berggren, W.A., Kent, D.V., Swisher, C.C., III, and Aubry, M.-P., 1995. A revised Cenozoic geochronology and chronostratigraphy. *In* Berggren, W.A., Kent, D.V., Aubry, M.-P., and Hardenbol, J. (Eds.), *Geochronology, Time Scales and Global Stratigraphic Correlation.* Spec. Publ.—Soc. Econ. Paleontol. Mineral. (Soc. Sediment. Geol.), 54:129–212.

Berggren, W.A., and Miller, K.G., 1989. Cenozoic bathyal and abyssal calcareous benthic foraminiferal zonations. *Micropaleontology,* 35:308–320.

Bone, Y., and James, N.P., 1993. Bryozoans as carbonate sediment producers on the cool-water Lacepede Shelf, Southern Australia. *Sediment. Geol.,* 86:247–271.

Boyce, R.E., 1976. Definitions and laboratory techniques of compressional sound velocity parameters and wet-water content, wet-bulk density, and porosity parameters by gravimetric and gamma-ray attenuation techniques. *In* Schlanger, S.O., Jackson, E.D., et al., *Init. Repts. DSDP,* 33: Washington (U.S. Govt. Printing Office), 931–958.

Chaproniere, G.C.H., Shafik, S., Truswell, E.M., MacPhail, M.K., and Partridge, A.D., 1995. Cainozoic. In *Australian Phanerozoic Time Scale.* Aust. Geol. Surv. Org., 10.

Eberli, G.P., Swart, P.K., Malone, M.J., et al., 1997. *Proc. ODP, Init. Repts.,* 166: College Station, TX (Ocean Drilling Program).

Feary, D.A., 1997. ODP pollution prevention and safety panel: Leg 182 safety package—Cenozoic cool-water carbonates of the Great Australian Bight. *Aust. Geol. Surv. Org.,* 28.

Feary, D.A., and James, N.P., 1998. Seismic stratigraphy and geological evolution of the Cenozoic, cool-water, Eucla Platform, Great Australian Bight. *AAPG Bull.,* 82:792–816.

Gieskes, J.M., 1973. Interstitial water studies, Leg 15: alkalinity, pH, Mg, Ca, Si, PO_4, and NH_4. *In* Heezen, B.C., MacGregor, I.D., et al., *Init. Repts. DSDP,* 20: Washington (U.S. Govt. Printing Office), 813–829.

Haq, B.U., Hardenbol, J., and Vail, P.R., 1987. Chronology of fluctuating sea levels since the Triassic. *Science,* 235:1156–1167.

Hasegawa, S., 1984. Note on the taxonomy and paleoecology of *Melonis pompilioides* and its allied taxa from Japan. *In* Oertli, H.J. (Ed.), *Benthos '83, 2nd Int. Symp. on Benthic Foraminifera* (Pau, 1983), 299–304.

Hodell, D.A., and Kennett, J.P., 1986. Late Miocene-early Pliocene stratigraphy and paleoceanography of the South Atlantic and southwest Pacific Oceans: a synthesis. *Paleoceanography,* 1:285–311.

James, N.P., Bone, Y., von der Borch, C.C., and Gostin, V.A., 1992. Modern carbonate and terrigenous clastic sediments on a cool-water, high-energy, mid-latitude shelf: Lacepede, southern Australia. *Sedimentology,* 39:877–903.

Jenkins, D.G., 1985. Southern mid-latitude Paleocene to Holocene planktic foraminifera. *In* Bolli, H.M., Saunders, J.B., and Perch-Nielsen, K. (Eds.), *Plankton Stratigraphy:* Cambridge (Cambridge Univ. Press), 263–282.

————, 1993. Cenozoic Southern mid- and high-latitude biostratigraphy and chronostratigraphy based on planktonic foraminifera. *In* Kennett, J.P., and Warnke, D.A. (Eds.), *The Antarctic Paleoenvironment: A Perspective on Global Change.* Antarct. Res. Ser., 60:125–144.

Kaminski, M.A., Gradstein, F.M., and Geroch, S., 1992. Uppermost Jurassic to Lower Cretaceous deep-water benthic foraminiferal assemblages from Site 765 on the Argo Abyssal Plain. *In* Gradstein, F.M., Ludden, J.N., et al., *Proc. ODP, Sci. Results,* 123: College Station, TX (Ocean Drilling Program), 239–269.

Kemp, E.M., 1978. Tertiary climatic evolution and vegetation history in the southeast Indian Ocean region. *Palaeogeogr., Palaeoclimatol., Palaeoecol.,* 24:169–208.

Kuhnt, W., Kaminski, M., and Moullade, M., 1989. Deep-water agglutinated benthic foraminiferal assemblages of the upper Cretaceous North Atlantic and its marginal seas. *Geol. Rundsch.,* 78:1121–1140.

Lambeck, K., 1986. Crustal structure and evolution of the Central Australian Basins. *In* Dawson, J.B., Carswell, D.A., Hall, J., and Wedephol, K.H. (Eds.), *The Nature of the Lower Continental Crust.* Geol. Soc. Spec. Publ. London, 24:133–145.

Lowry, D.C., 1970. Geology of the Western Australian part of the Eucla Basin. *Bull.–Geol. Surv. West. Aust.,* 122.

Macphail, M.K., Alley, M.F., Truswell, E.M., and Sluiter, I.R.K., 1994. Early Tertiary vegetation: evidence from spores and pollen. *In* Hill, R.S. (Ed.), *History of the Australian Vegetation, Cretaceous to Recent:* Cambridge (Cambridge Univ. Press), 18–261.

McDuff, R., 1978. Interstitial water studies, Leg 42-A. *In* Hsü, K.J., Montadert, L., et al., *Init. Repts. DSDP,* 42: Washington (U.S. Govt. Printing Office), 561–568.

Scholle, P.A., Arthur, M.A., and Ekdale, A.A., 1983. Pelagic environments. *In* Scholle, P.A., Bebout, D.G., and Moore, C.H. (Eds.), *Carbonate Depositional Environments.* AAPG Mem., 33:620–691.

Shafik, S., 1983. Calcareous nannofossil biostratigraphy: an assessment of foraminiferal and sedimentation events in the Eocene of the Otway Basin, southeastern Australia. *BMR J. Aust. Geol. Geophys.,* 8:1–17.

————, 1990. The Maastrichtian and early Tertiary record of the Great Australian Bight Basin and its onshore equivalents on the Australian southern margin: a nannofossil study. *BMR J. Australian Geol. Geophys.,* 11:473–497.

Tjalsma, R.C., and Lohmann, G.P., 1983. Paleocene-Eocene bathyal and abyssal benthic foraminifera from the Atlantic Ocean. *Micropaleontol. Spec. Publ.,* 4.

van Morkhoven, F.P.C.M., Berggren, W.A., Edwards. A.S., 1986. Cenozoic cosmopolitan deep-water benthic foraminifera. *Mèmoire du Bulletin des Centres de Recherches Exploration-Production Elf-Aquitaine,* 11: Pau (Société Nationale Elf Aquitaine), 329–426.

Figure F1. Map showing the location of Site 1128 on the upper continental rise at the base of the Eucla slope, in relation to other Leg 182 sites and the Australian Geological Survey Organisation Survey 169 (AGSO169) seismic lines.

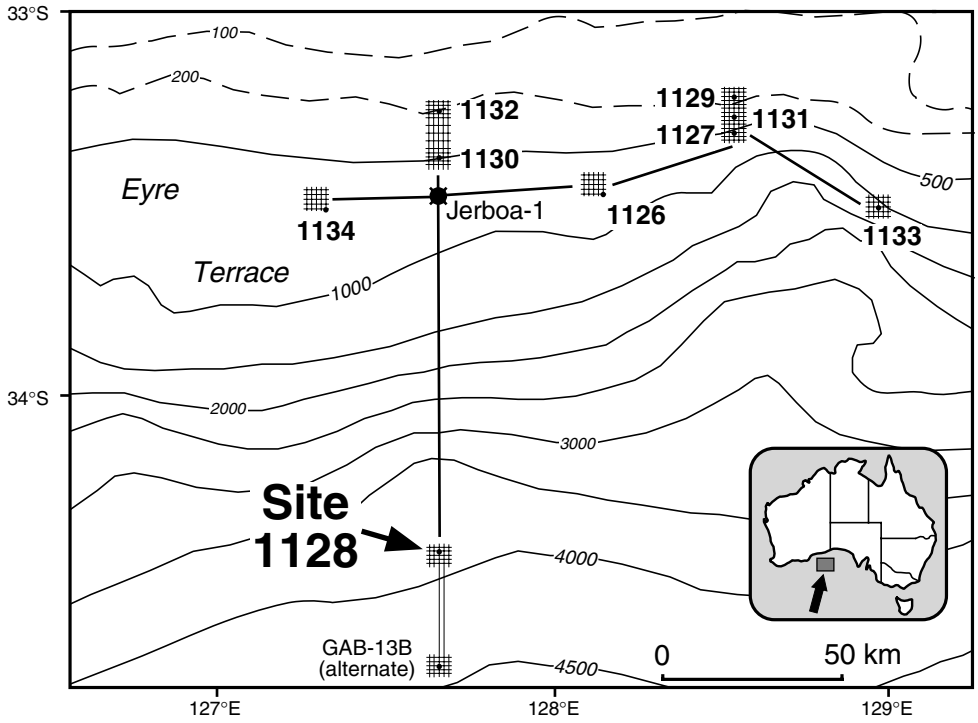

Figure F2. Portion of seismic Line AGSO169/11e illustrating the seismic stratigraphic interpretation at Site 1128 and showing sequences that were planned (shown in white) and actually intersected (shown in black) at this site.

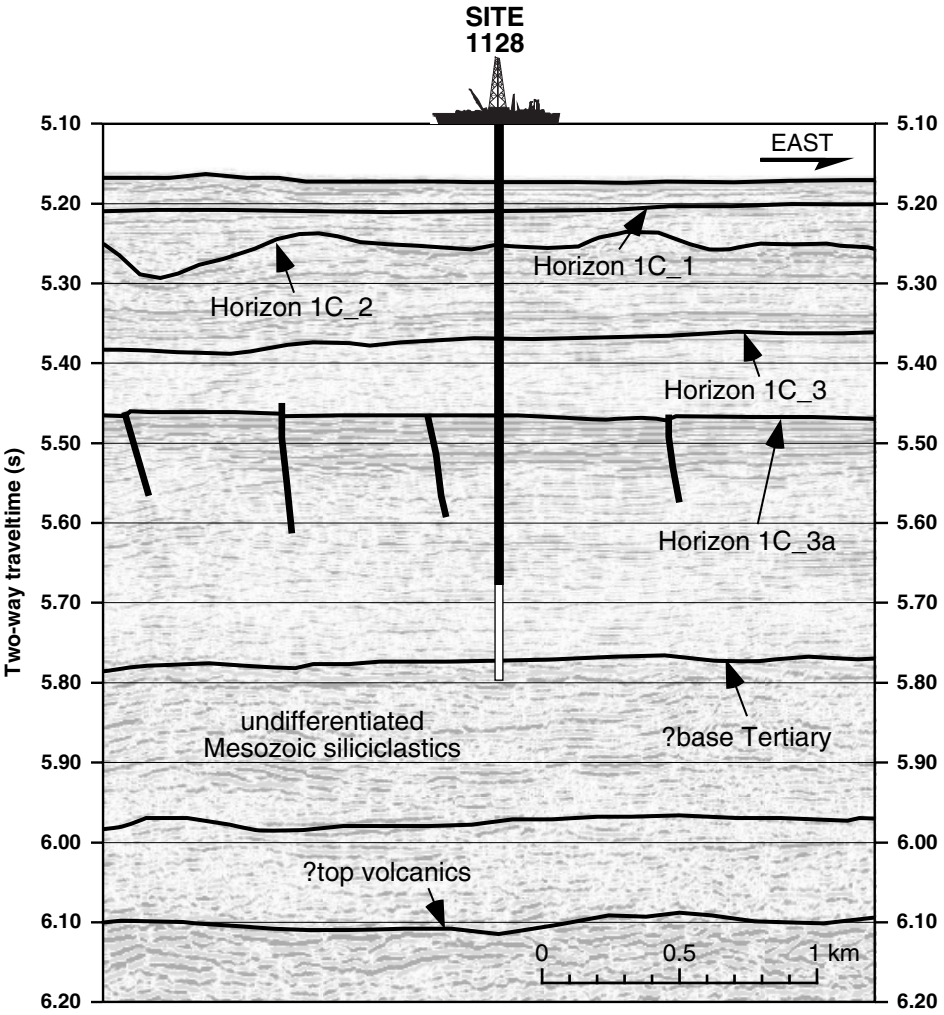

Figure F3. Summary of sediment lithostratigraphy at Site 1128. Ages are from **"Biostratigraphy,"** p. 11. (Continued on next two pages.)

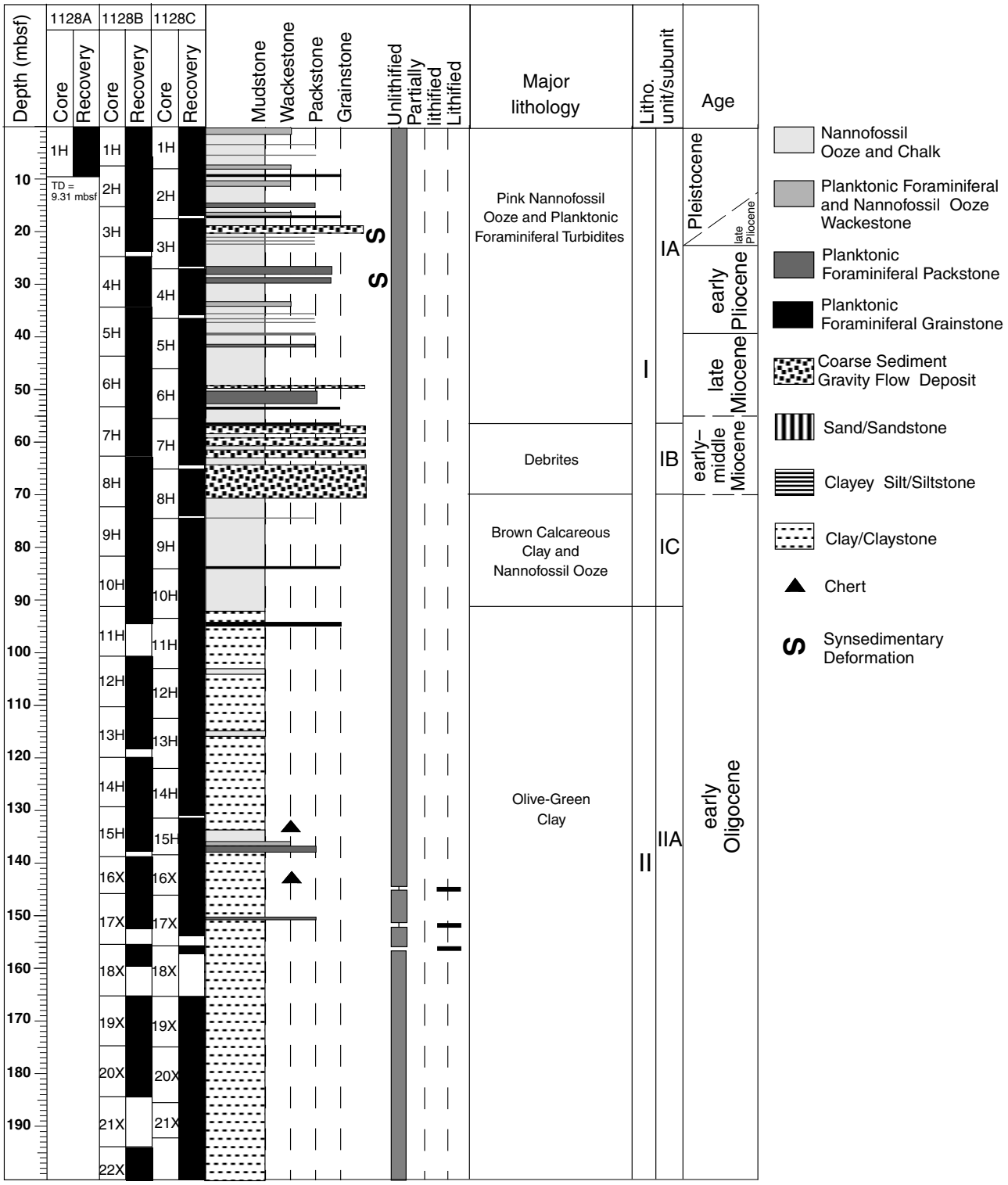

Figure F3 (continued).

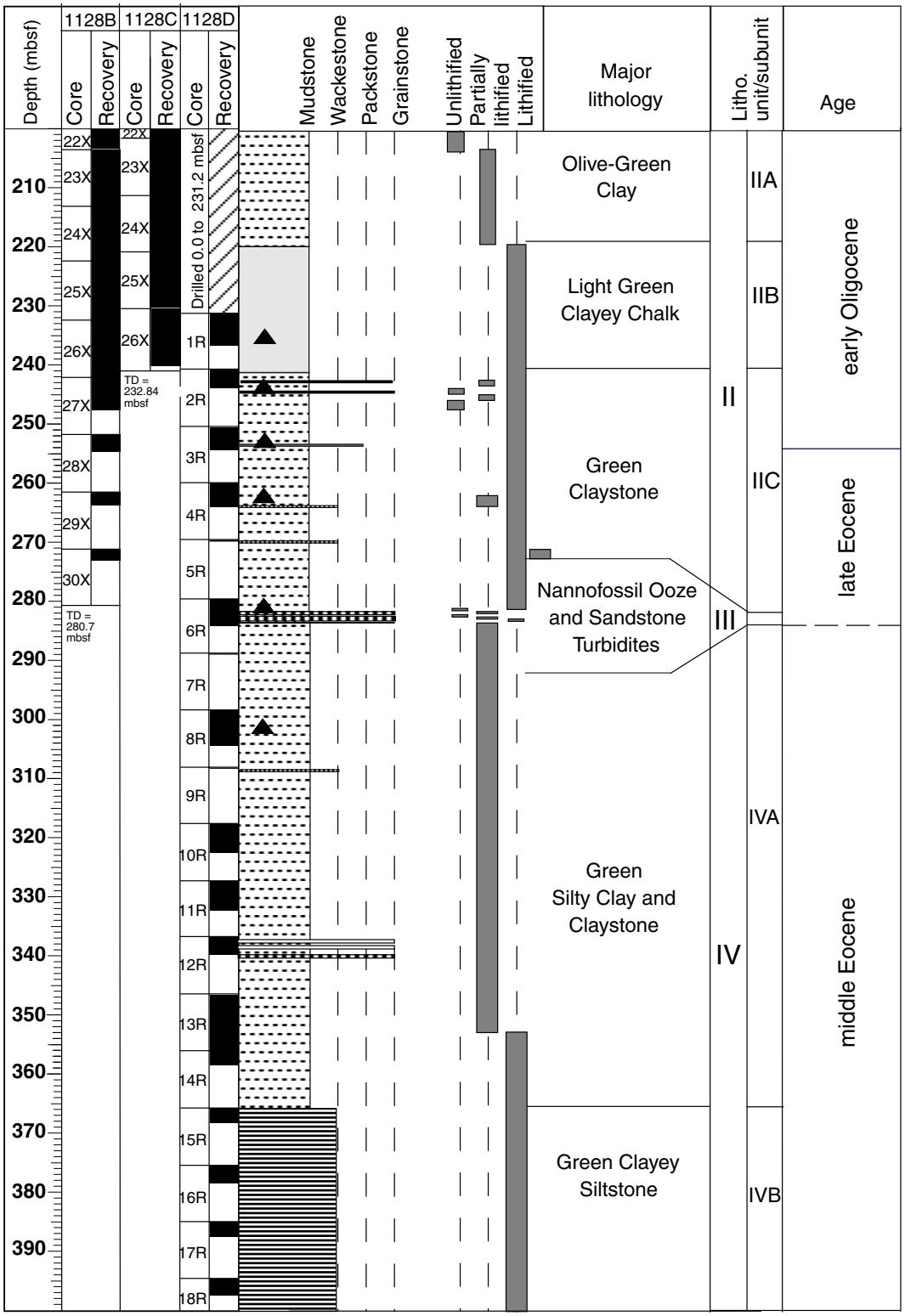

Figure F3 (continued).

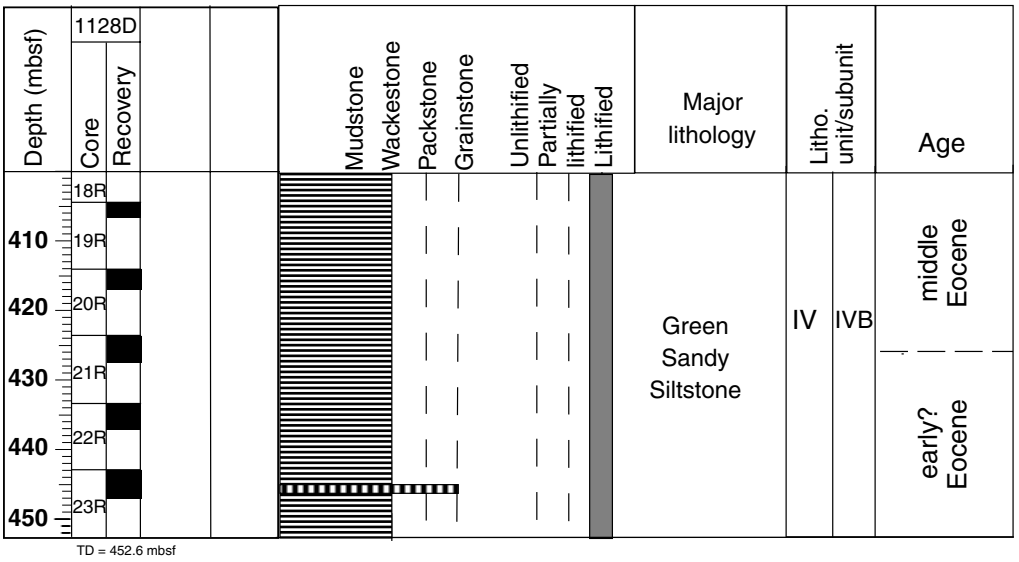

Figure F4. A calciturbidite in Subunit IA composed of planktonic foraminifers and glaucony (dark grains) grading upward into nannofossil ooze (interval 182-1128B-1H-2, 75–100 cm).

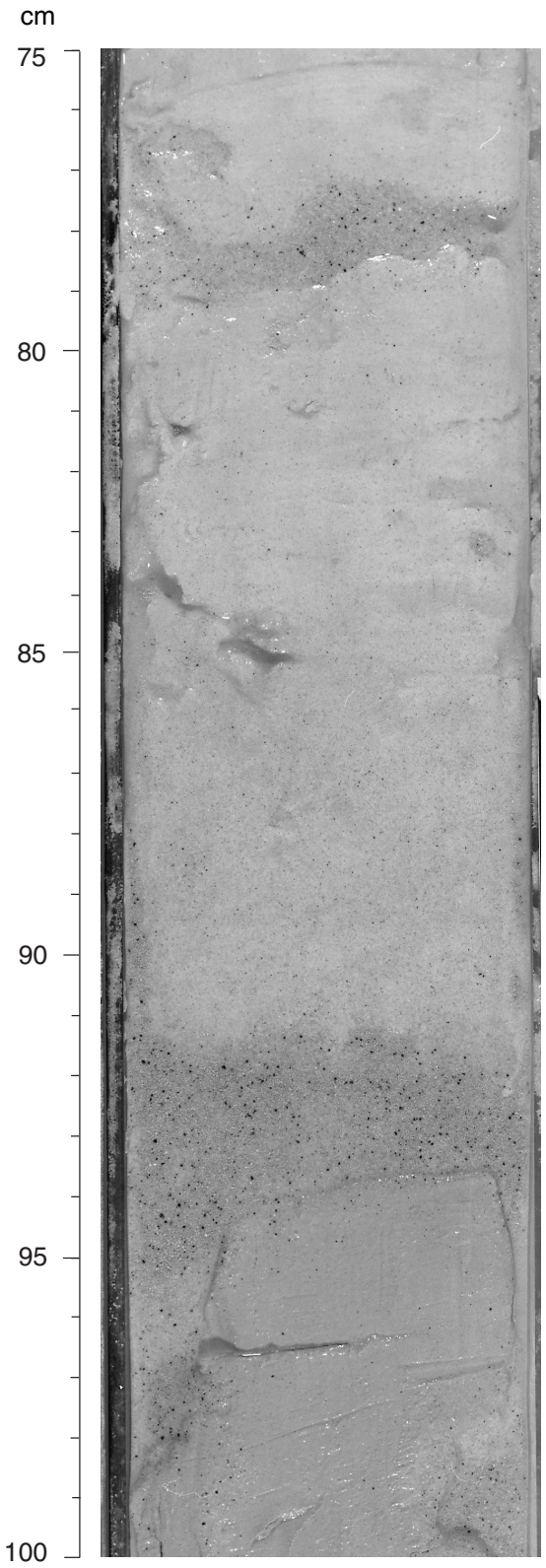

Figure F5. The upper part of a sediment gravity flow from Subunit IA containing delicate branching bryozoans and pieces of consolidated white nannofossil ooze (interval 182-1128B-3H-3, 35–80 cm).

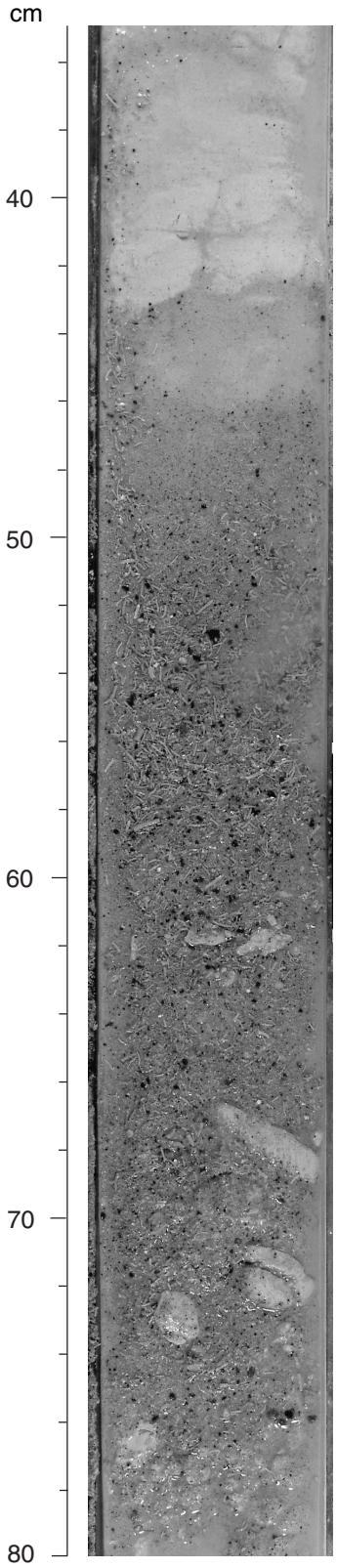

Figure F6. Conglomerates and deformed strata in Subunit IB (Core 182-1128C-7H).

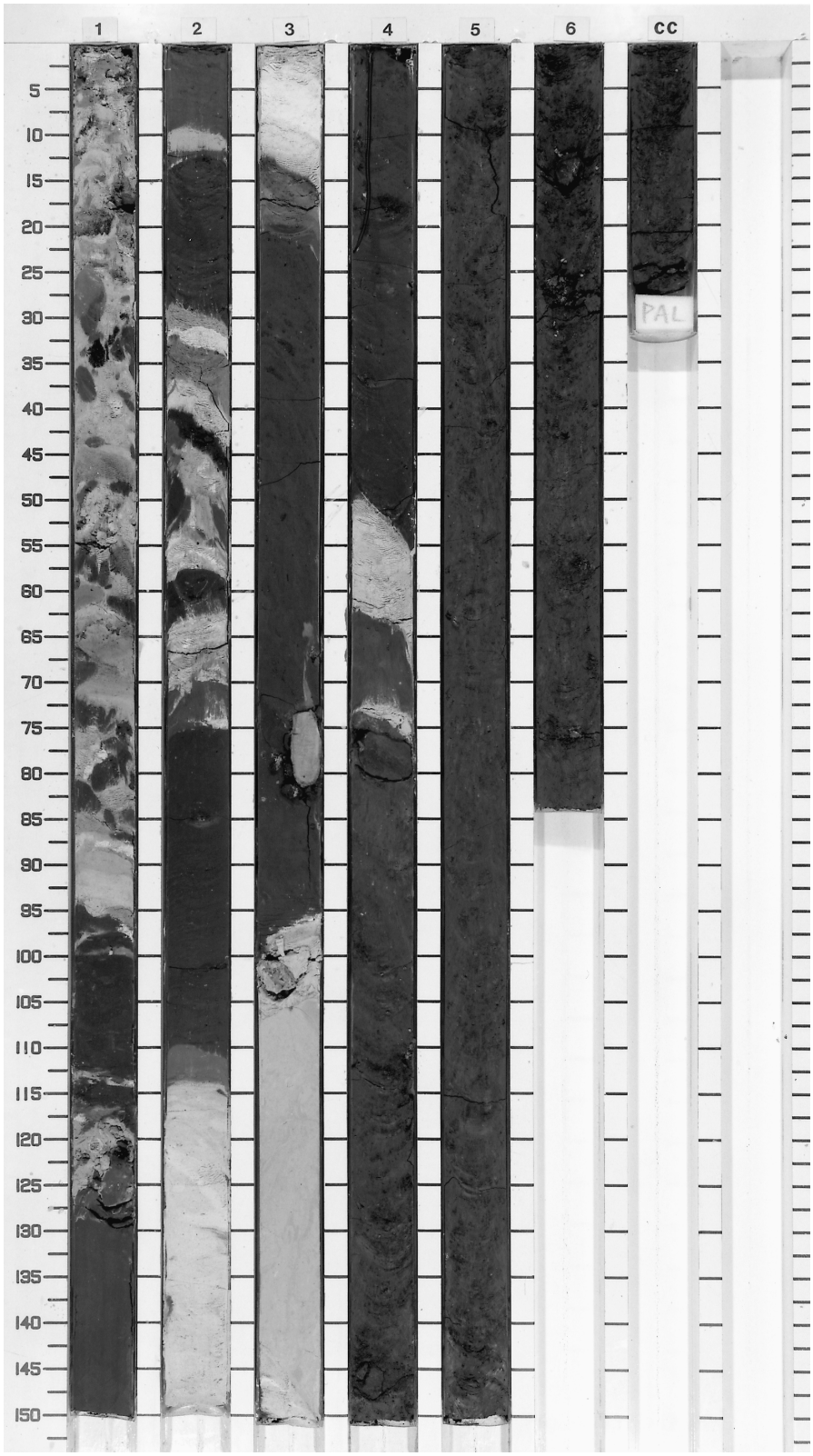

Figure F7. Deformed strata in Subunit IB (Core 182-1128C-8H).

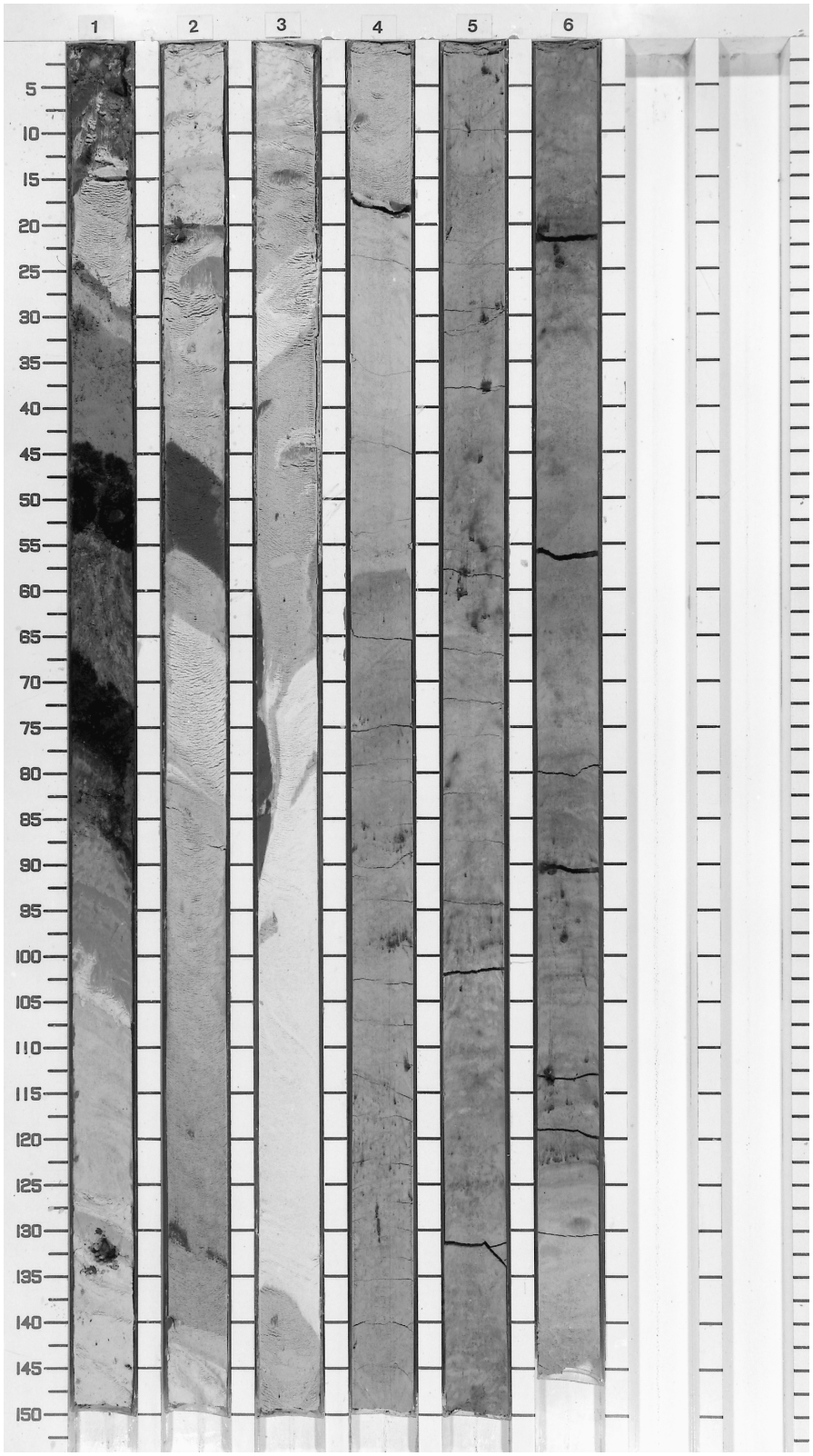

Figure F8. Burrowed transition from white nannofossil ooze upward into bioturbated green clay in Subunit IIA (interval 182-1128C-15H-1, 40–80 cm).

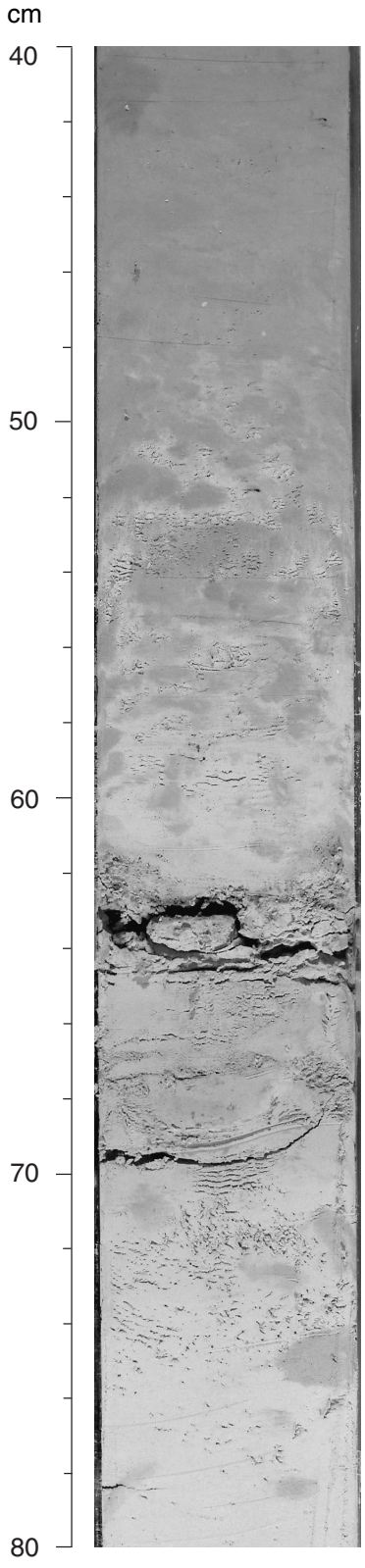

Figure F9. Cross-laminated glauconitic sand in the basal part of a turbidite in Unit IV (interval 182-1128D-12R-1, 45–60 cm).

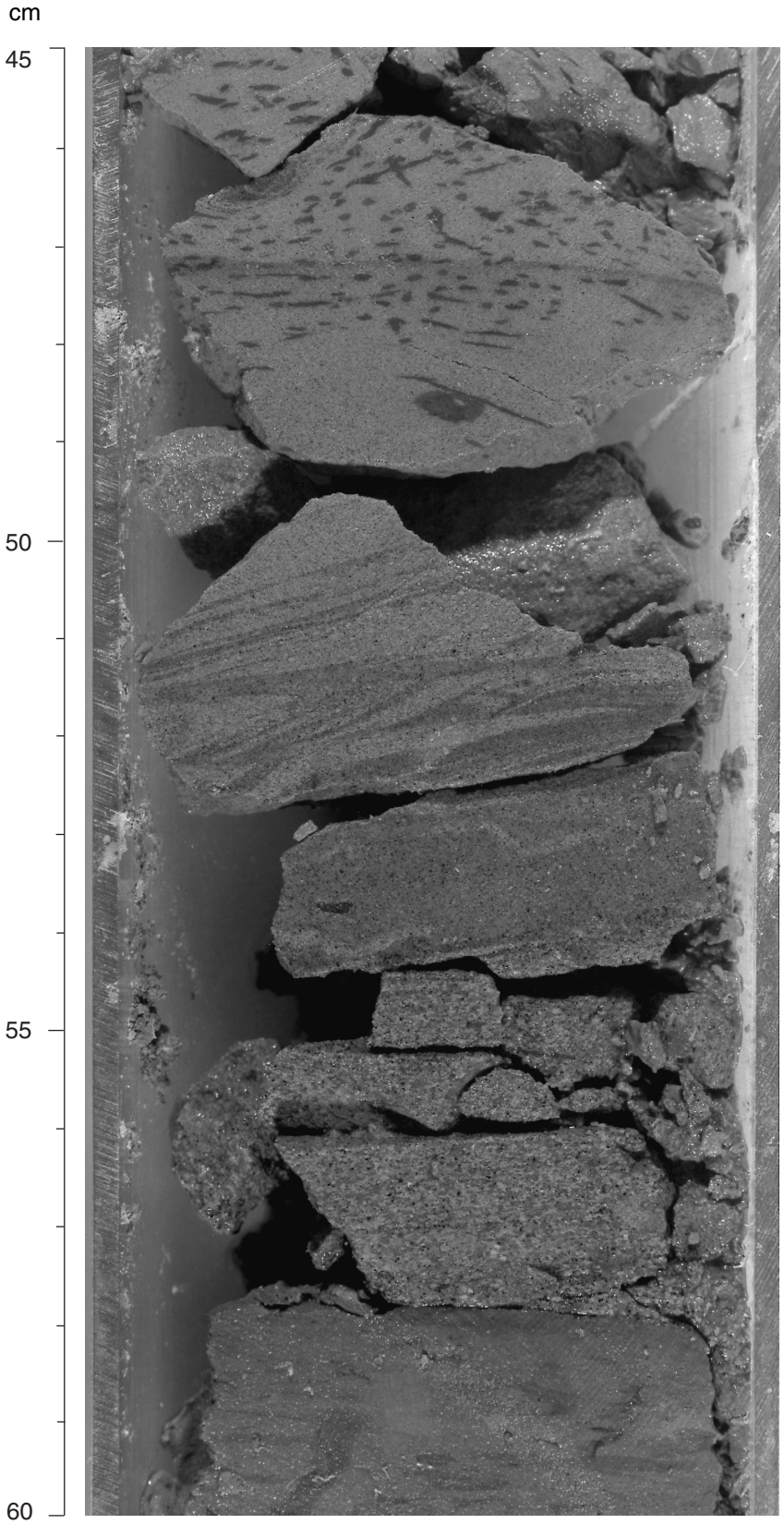

Figure F10. Burrowed nannofossil ooze in Unit III with numerous horizontal *Zoophycos* burrows (interval 182-1128D-6R-2, 110–132 cm).

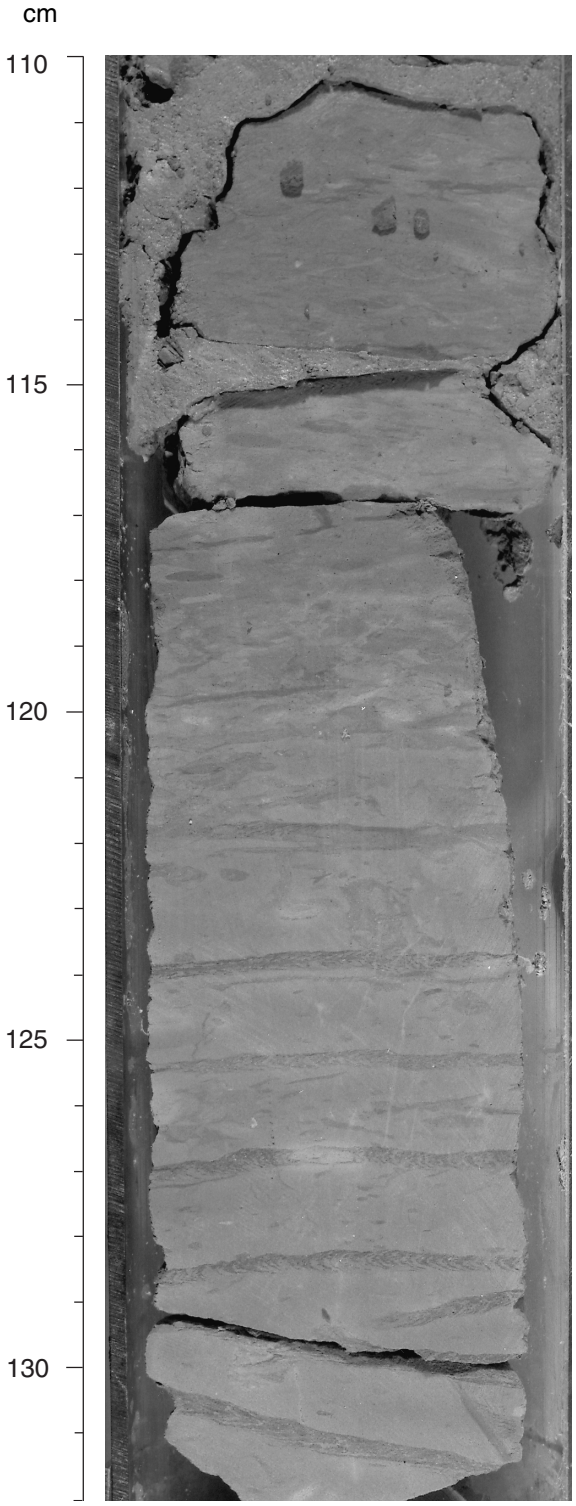

Figure F11. Stratigraphic position of calcareous nannofossil and planktonic foraminifer zones, together with benthic foraminiferal assemblages at Site 1128. Dashed boundaries imply uncertainty. No sample means that the core catcher, if recovered, did not contain enough sediment to prepare for foraminifers.

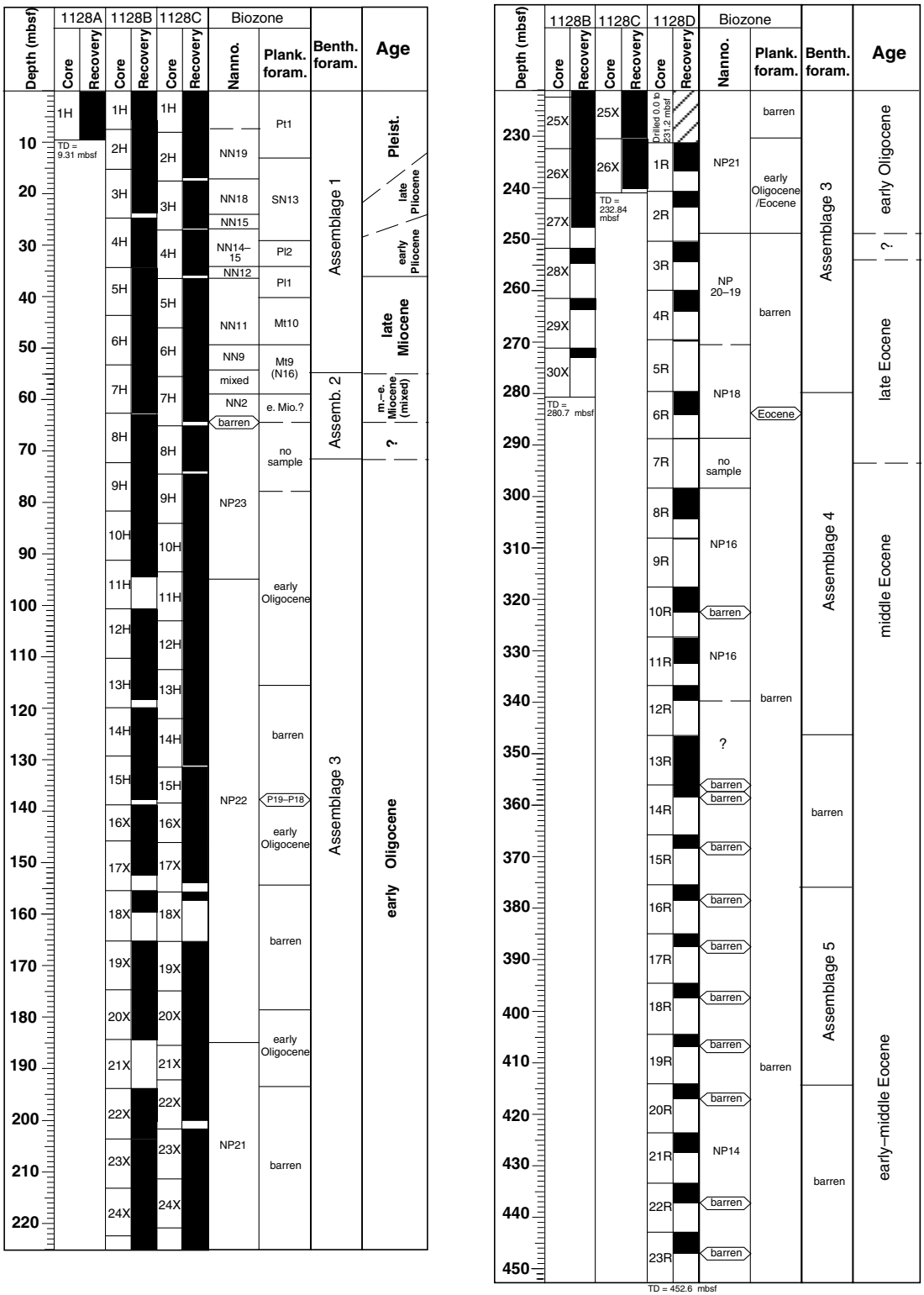

Figure F12. Sedimentation rate curve constructed from the 23 datum levels listed in Table T2, p. 90. Stratigraphic error varies between ±0.695 and ±5.175 m, as indicated by the length of the error bars.

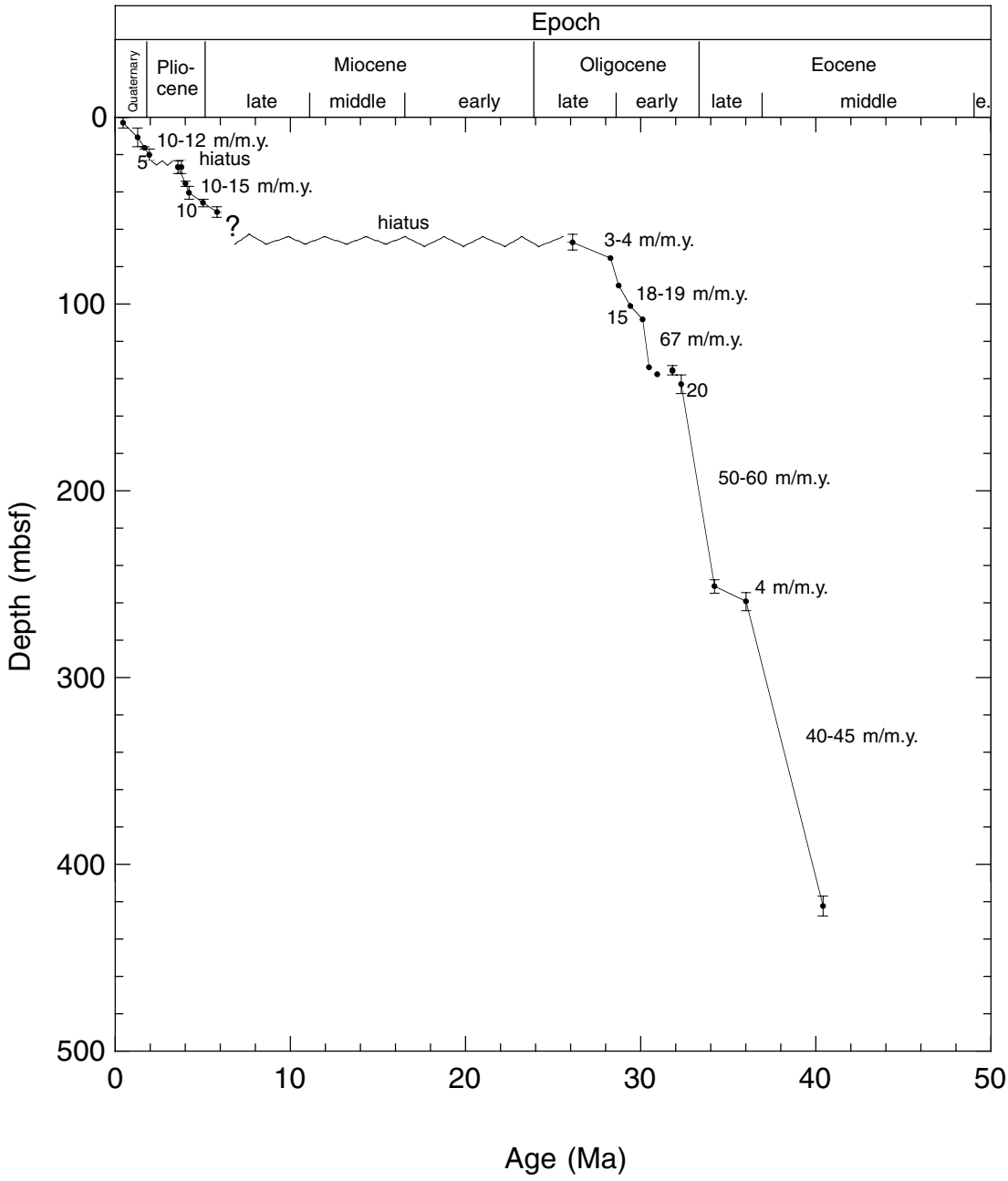

Figure F13. Alternating field demagnetization behavior of (**A**) soft sediment (Sample 182-1128B-4H-3, 63–65 cm) and (**B**) lithified (Sample 182-1128D-4R-1, 40–42 cm) discrete samples. The plot on the left shows the decrease in intensity upon demagnetization. The center panel gives the vector plots in the horizontal and north and up planes (north and east are solid symbols; north and up are open symbols). A stereographic projection of the directions is given on the right. Solid symbols represent downward directions and open symbols represent upward directions.

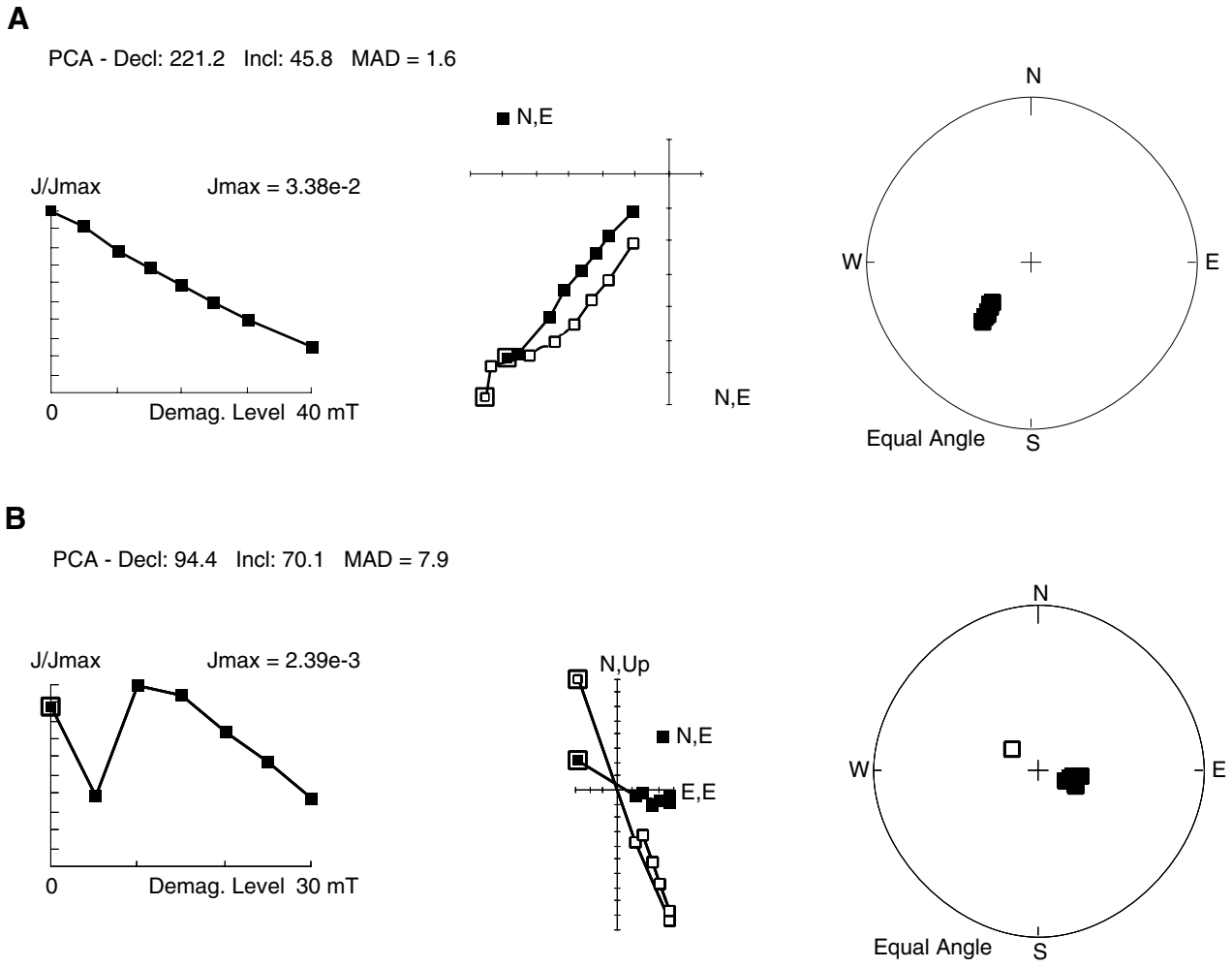

Figure F14. Plots of demagnetization of natural remanent magnetization (NRM), anhysteretic remanent magnetization (ARM), and isothermal remanent magnetization (IRM), and of the acquisition of IRM (IRM A). The plots summarize the magnetic characteristics of the samples. Closed symbols represent Core 182-1128B-3H-2, and open symbols represent Core 182-1128B-13H-2. The ratios of ARM:IRM for the shallower Core 182-1128B-3H-2 are indicative of single-domain behavior and suggest a magnetotactic origin of the magnetite. The lower ARM:IRM ratio for Core 182-1128B-13H-2 implies less single-domain (bacterial) magnetite, suggesting that it suffers dissolution with increasing depth.

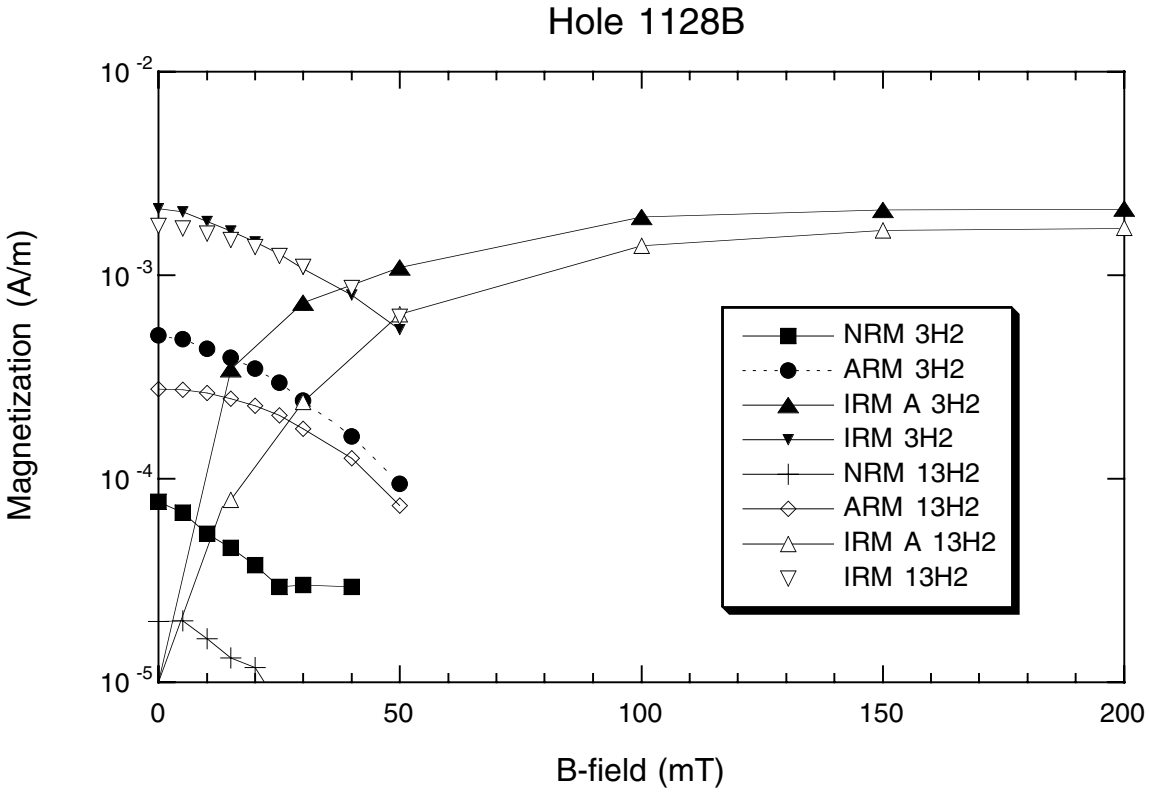

Figure F15. Magnetic susceptibility of cores from Hole 1128B. A seven-point running mean was calculated to average the data. The squares indicate the position of reversals in the Oligocene sequence, indicating subtle changes in sedimentation rate.

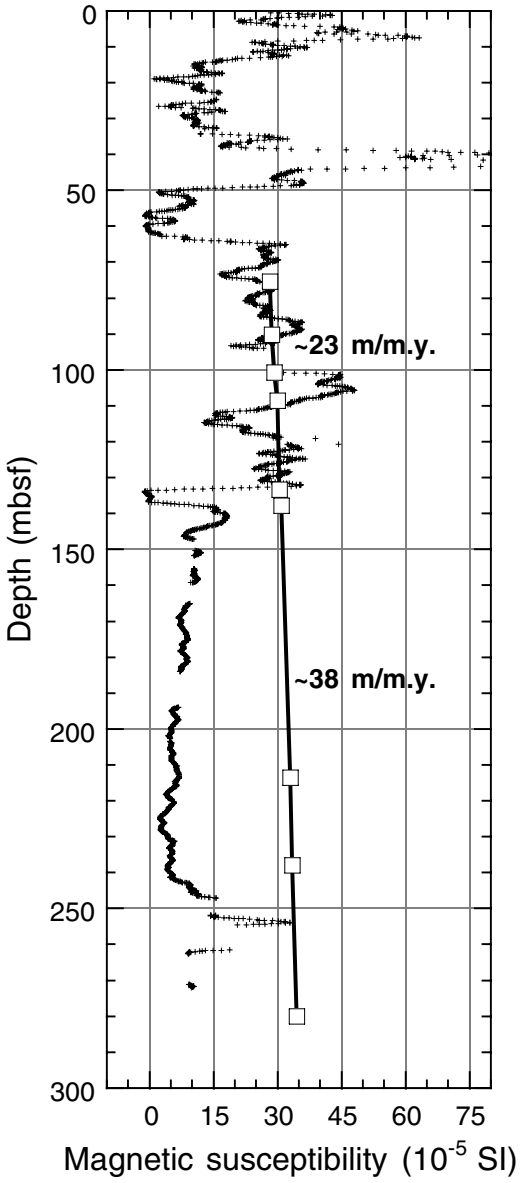

Figure F16. Pliocene–Pleistocene magnetostratigraphy from Holes 1128B and 1128C, showing tentative correlation with the geomagnetic polarity time scale (GPTS). The stratigraphic position of the main turbidites is shown by the stippled bar pattern on the right of each inclination plot.

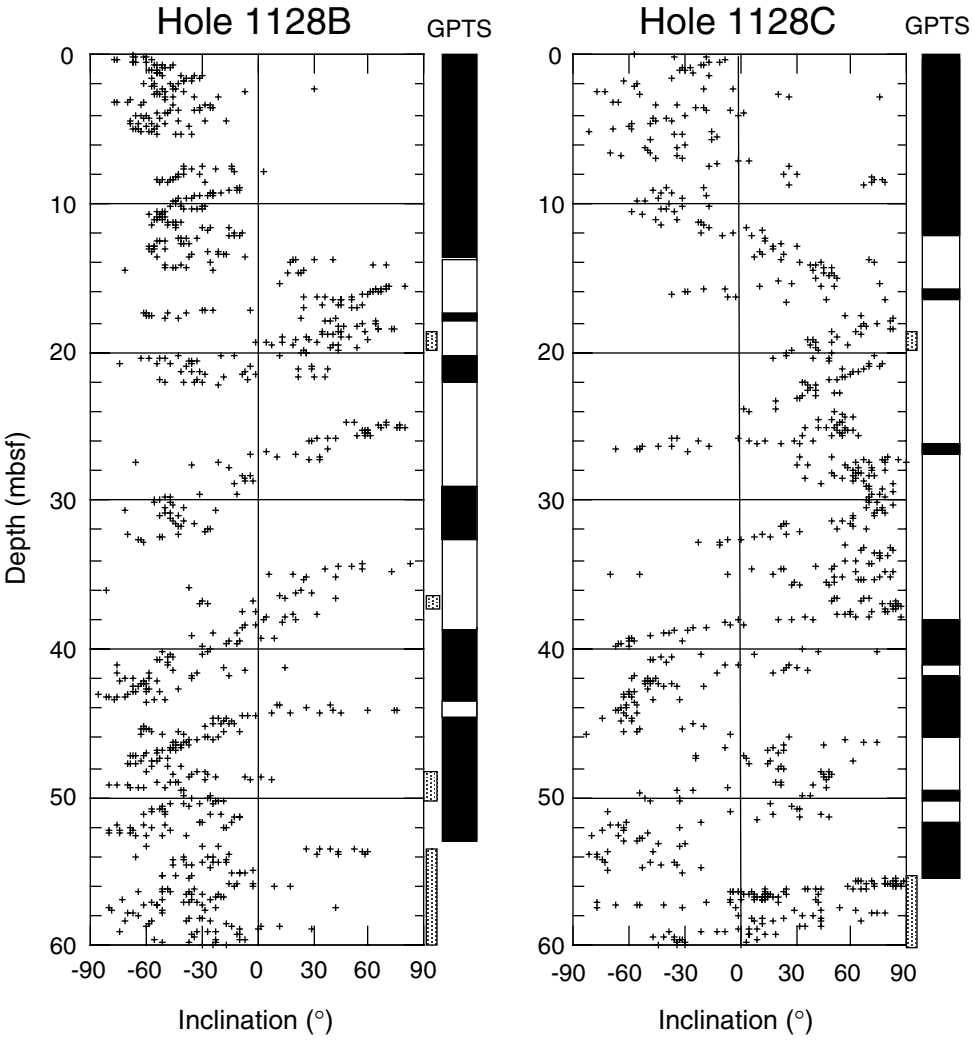

Figure F17. Complete magnetostratigraphy for Holes 1128B, 1128C, and 1128D, and correlation with the geomagnetic polarity time scale (GPTS). Long-core measurements (crosses) are compared with results from discrete samples (open squares).

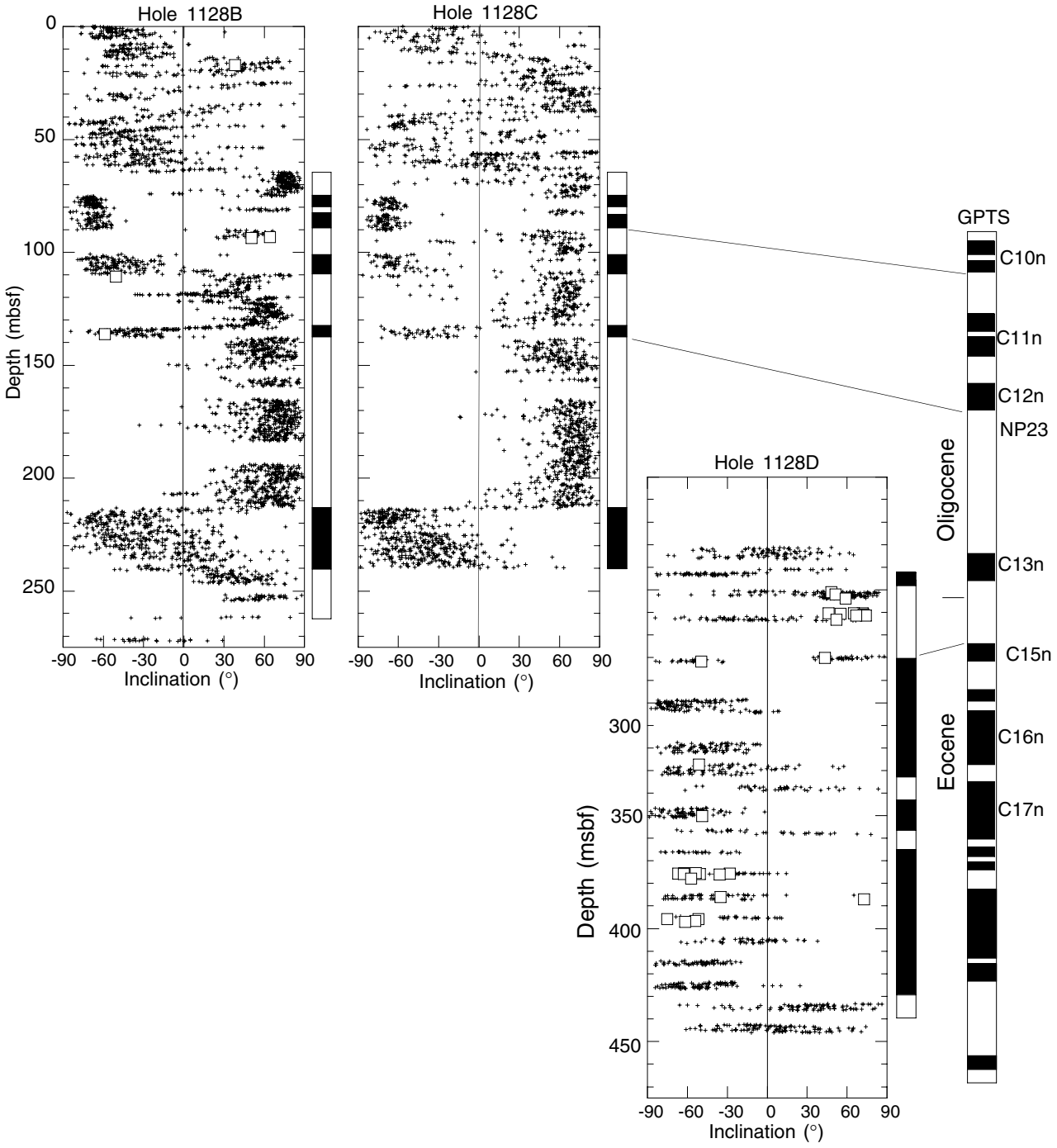

Figure F18. Composite depth section produced using the Splicer software. The black line is data from Hole 1128B, and the red line is data from Hole 1128C. Chrons are delineated by the horizontal dashed lines and identified on the right margin of the plots. Magnetic polarity is shown to the right of the chron identification. ? = magnetic intensity too low to measure. All depths use the meters composite depth (mcd) scale. For conversions from mcd to mbsf, see Table T3, p. 91. (Continued on next two pages.)

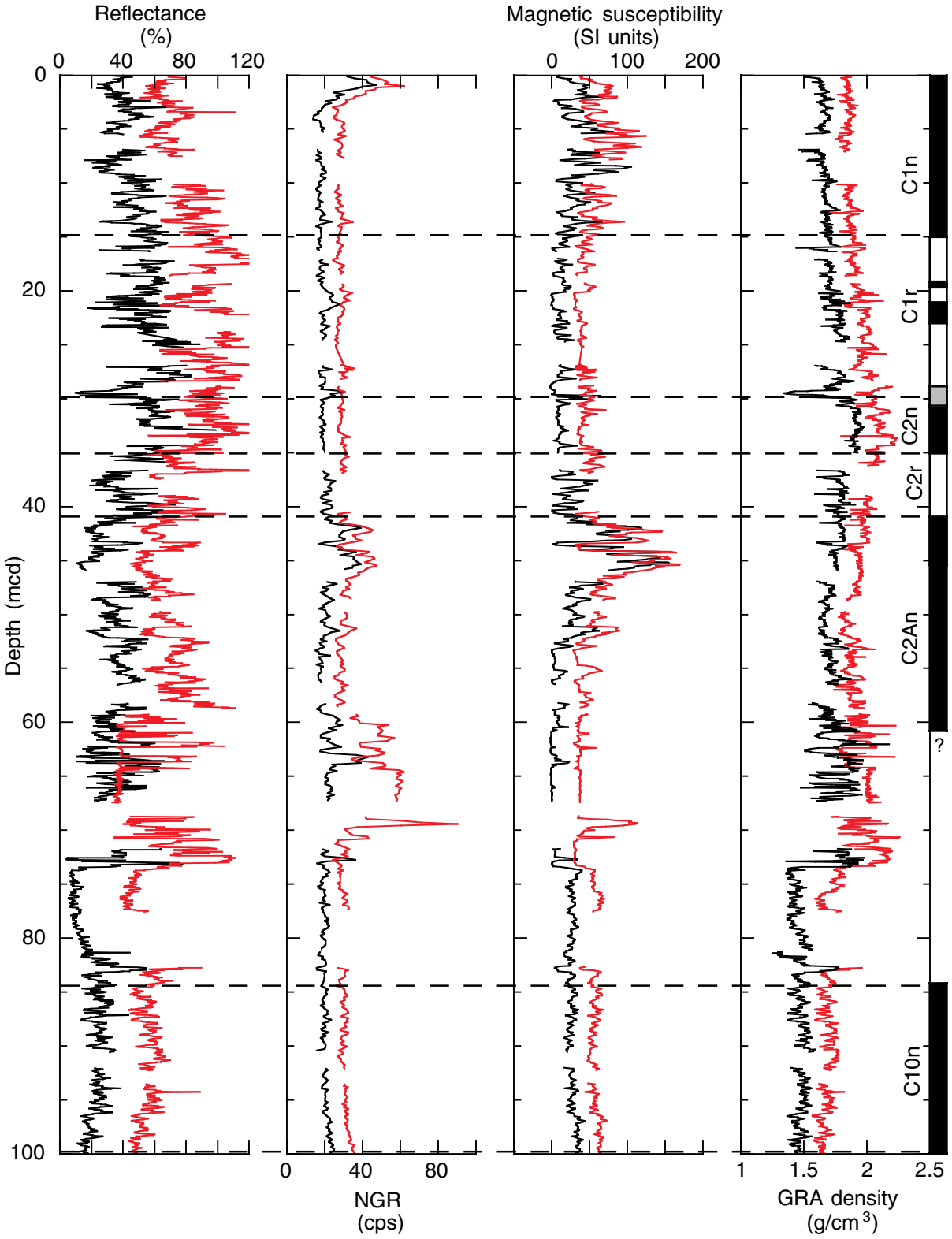

Figure F18 (continued).

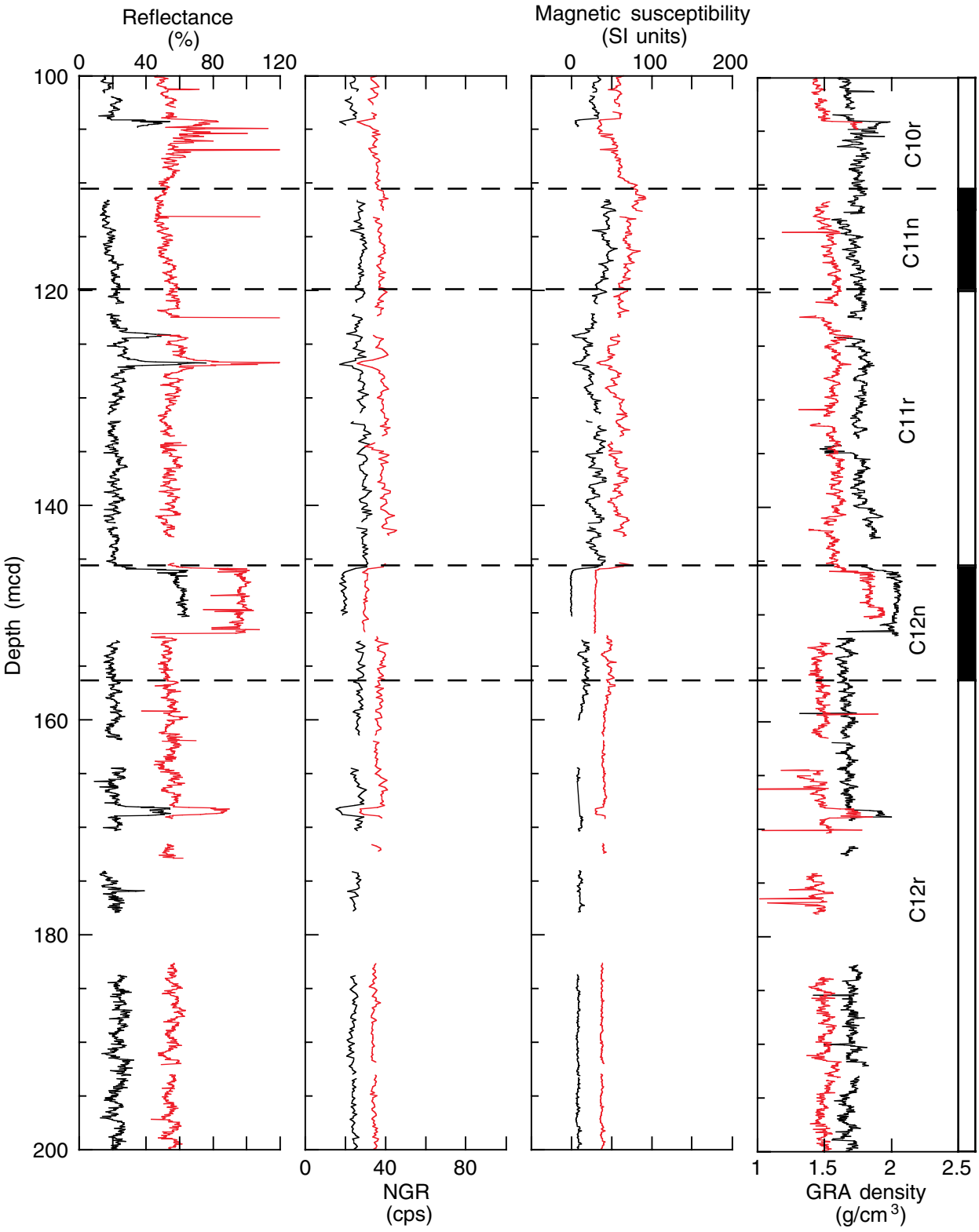

Figure F18 (continued).

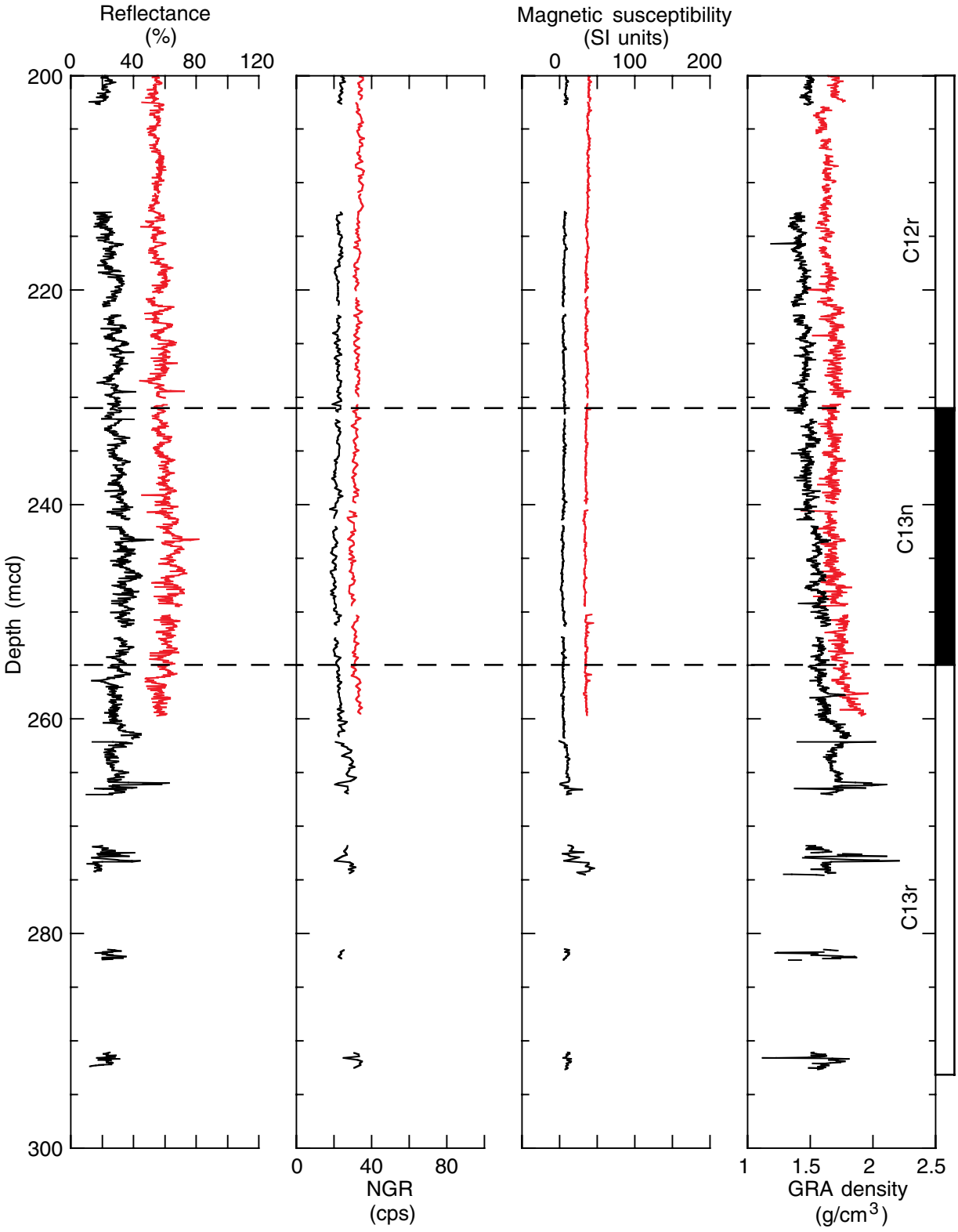

Figure F19. Spliced section of smoothed color reflectance data (400 nm) produced using the Splicer software. These data are a spliced composite of correlated data from Holes 1128B and 1128C. Ages are derived from biostratigraphic data. Lithostratigraphic units are described in "Lithostratigraphy," p. 3.

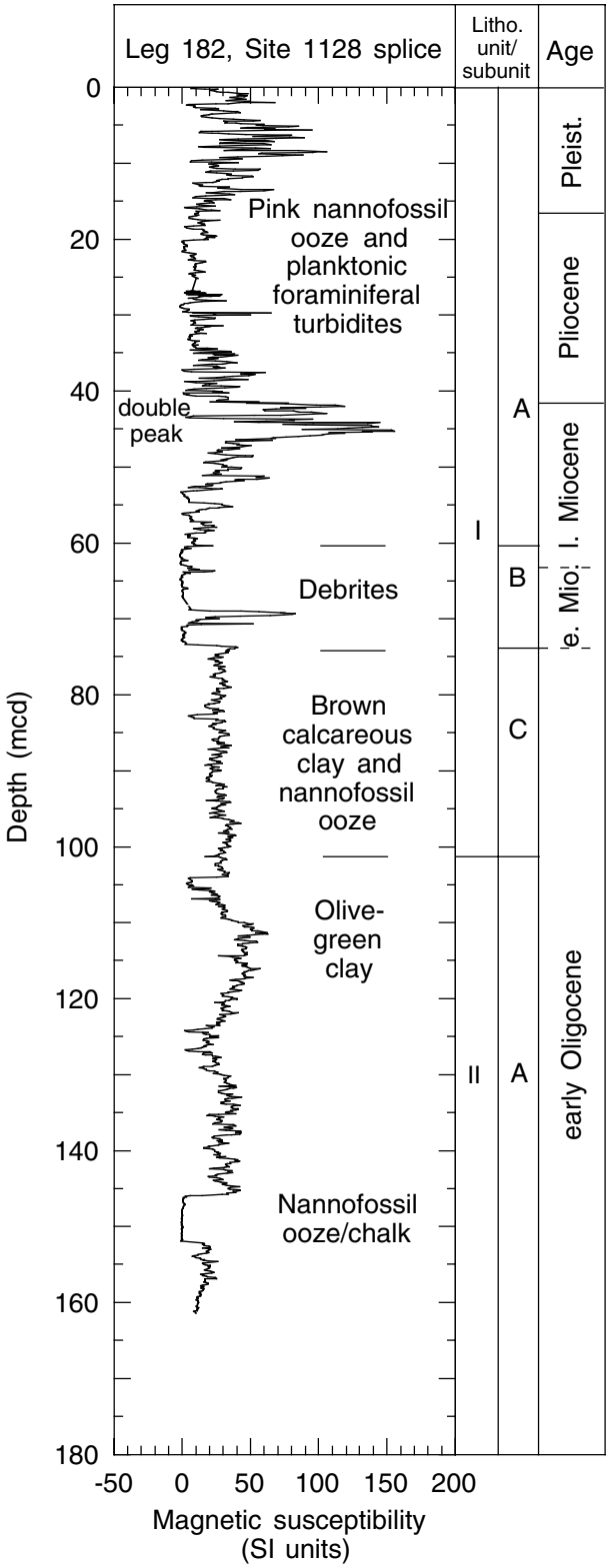

Figure F20. Calcium carbonate ($CaCO_3$) and organic carbon (C_{org}) contents in samples from Holes 1128B (solid circles) and 1128D (open circles).

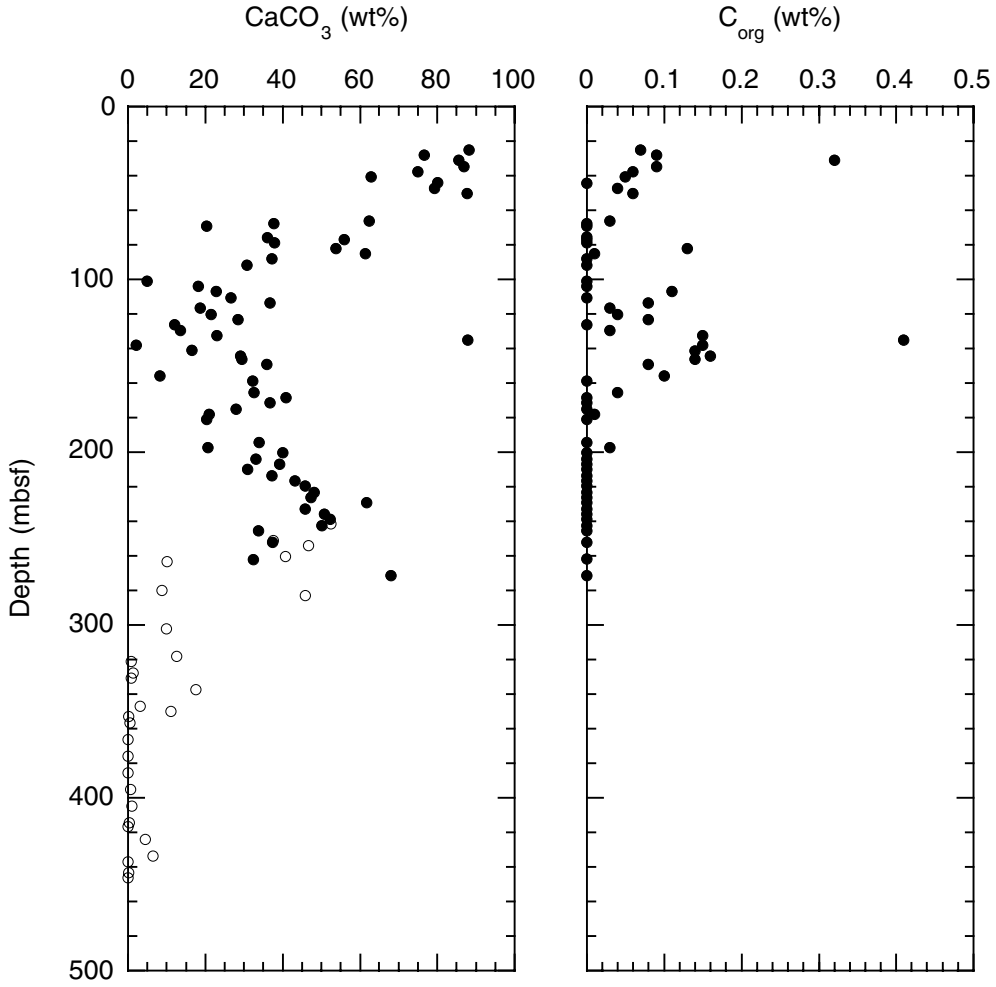

Figure F21. Summary of trends in (**A**) Cl^-, (**B**) salinity, and (**C**) Na^+/Cl^-. The horizontal line denotes the abrupt change in the Cl^- and salinity near the boundary of lithostratigraphic Units II and IV (see **"Lithostratigraphy,"** p. 3). The Na^+/Cl^- ratio, however, remains constant throughout, within the analytical precision of the techniques used (see **"Inorganic Geochemistry,"** p. 18, in the "Explanatory Notes" chapter).

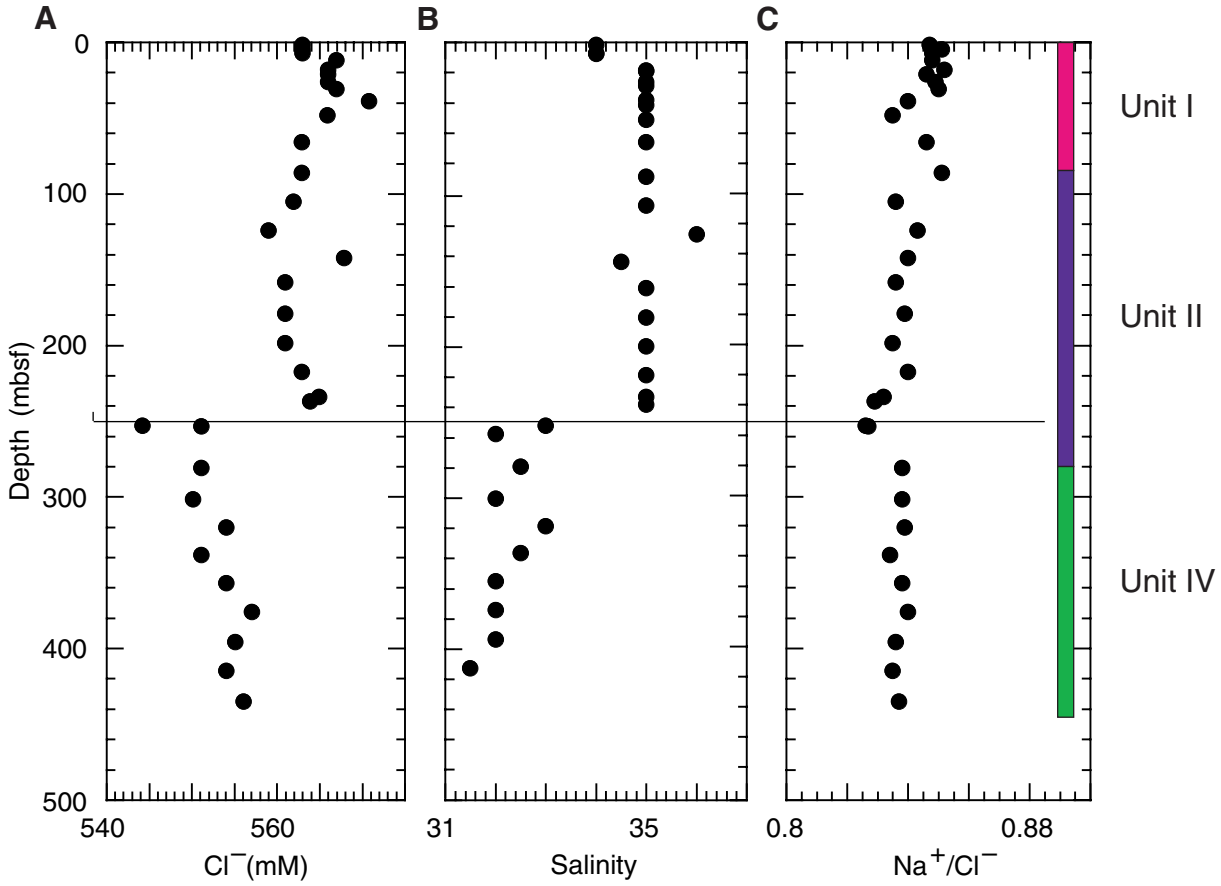

Figure F22. Relationship between salinity and Cl^- at Site 1128. If changes are a result of simple mixing of waters with different evaporative histories, then samples should fall on a line with a slope of 0.063 (dashed line). Samples falling below this line have lower salinity as a result of the removal of several minor constituents. The solid line represents a regression of the salinity and Cl^- data.

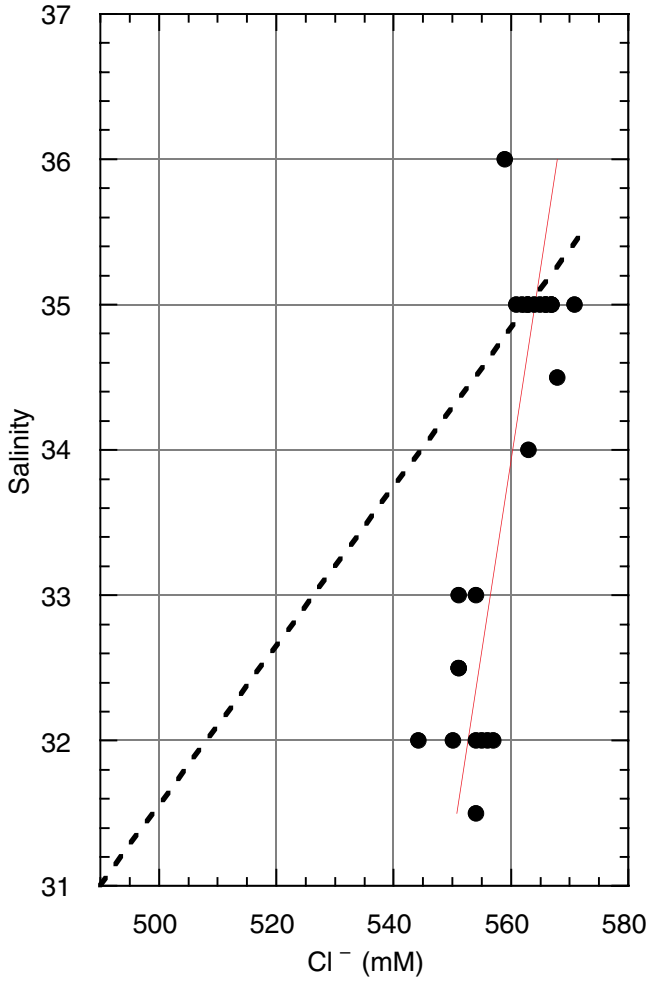

Figure F23. Summary of trends in cations (**A**) Na^+, (**B**) Mg^{2+}, Ca^{2+}, and K^+, and (**C**) Sr^{2+} and Li^+. Note the abrupt shift in the concentration of all constituents except Sr^{2+} between Cores 182-1128B-26X (236.8 mbsf) and 28X (253.1 mbsf).

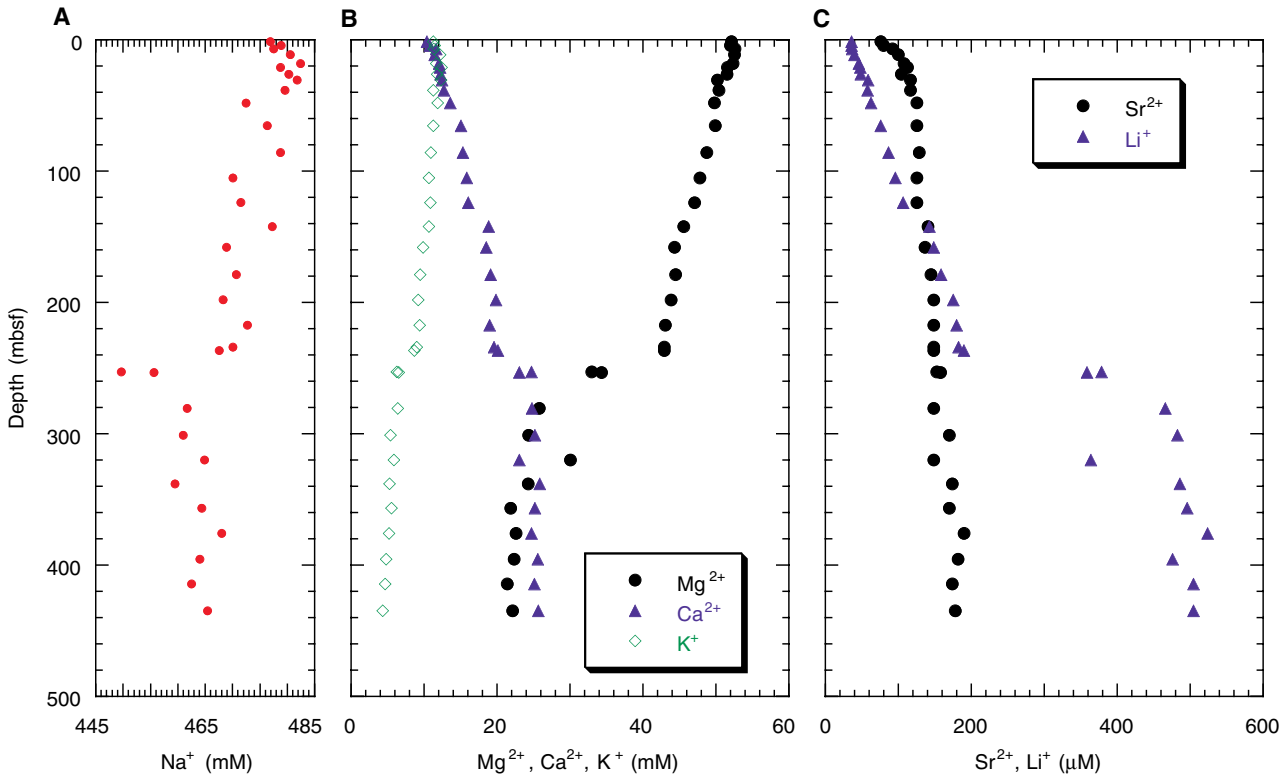

Figure F24. Variations in concentration of $H_4SiO_4^0$ with depth from Site 1128. Note the minimum between 26.2 and 38.6 mbsf and the mid-depth maximum.

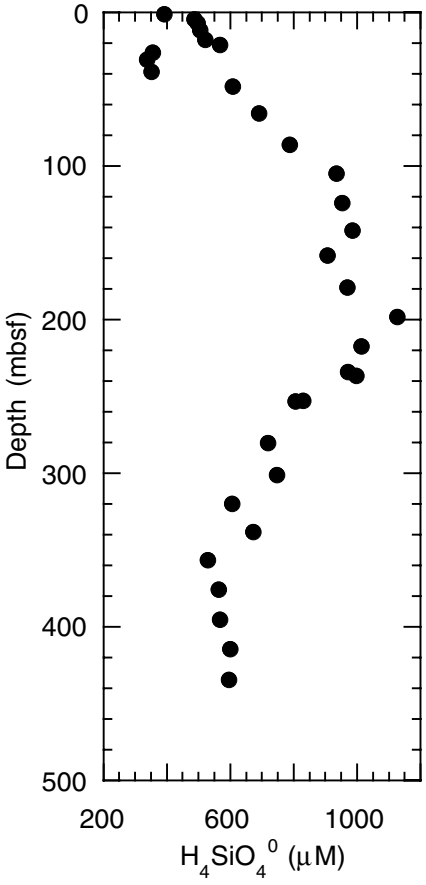

Figure F25. Variations in (A) alkalinity, (B) pH (the punch-in pH electrode values are shown by the open triangles), and (C) SO_4^{2-} from Site 1128.

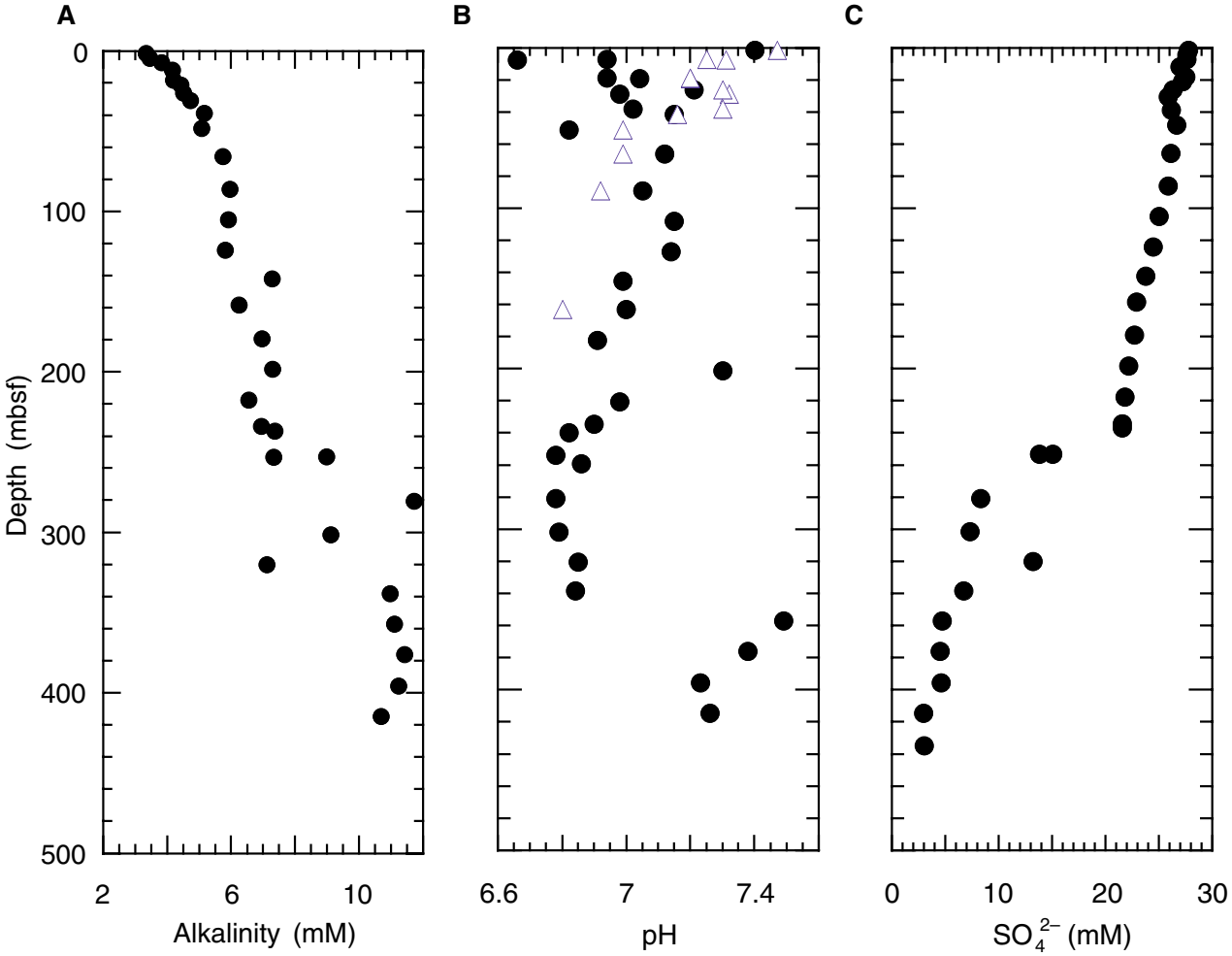

Figure F26. Variations in the ratio of low-Mg calcite (LMC) and quartz.

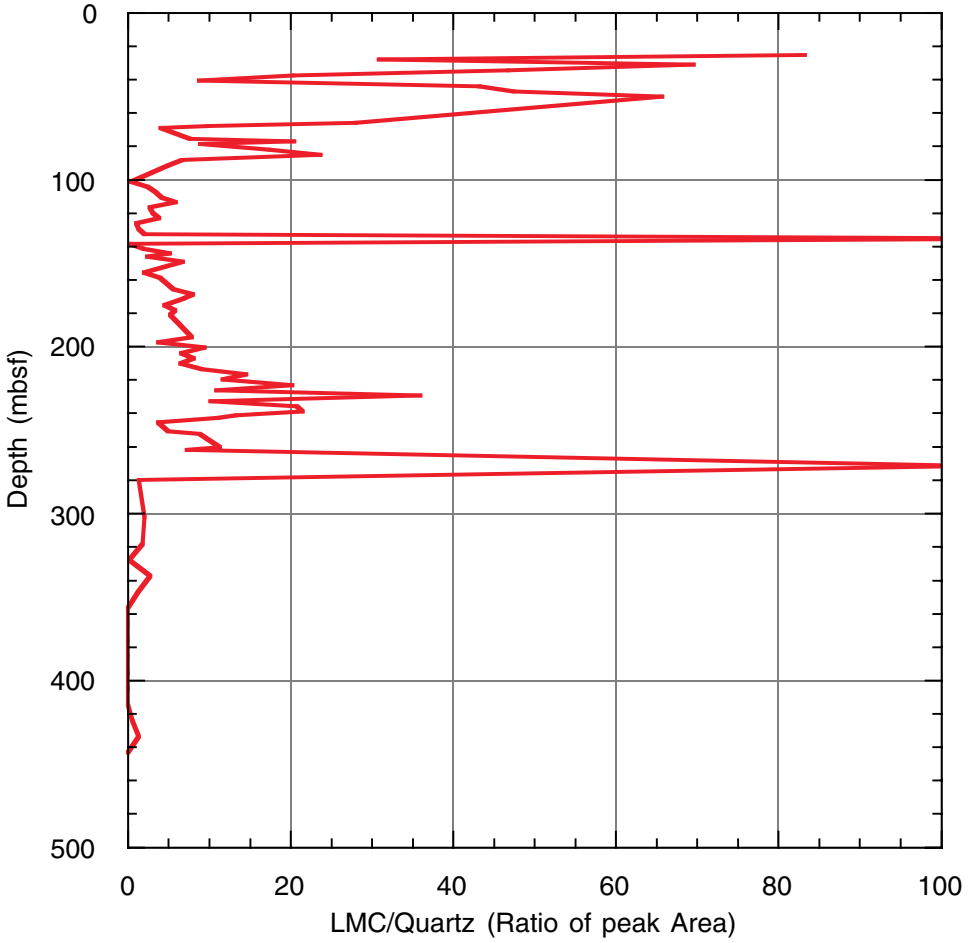

Figure F27. Combined plot of *P*-wave velocity, uncorrected gamma-ray attenuation (GRA; blue dots) and moisture-and-density (MAD; black dots) bulk densities, porosity, magnetic susceptibility, and natural gamma radiation (NGR) for Site 1128. Physical properties units (PP units) are indicated on the right.

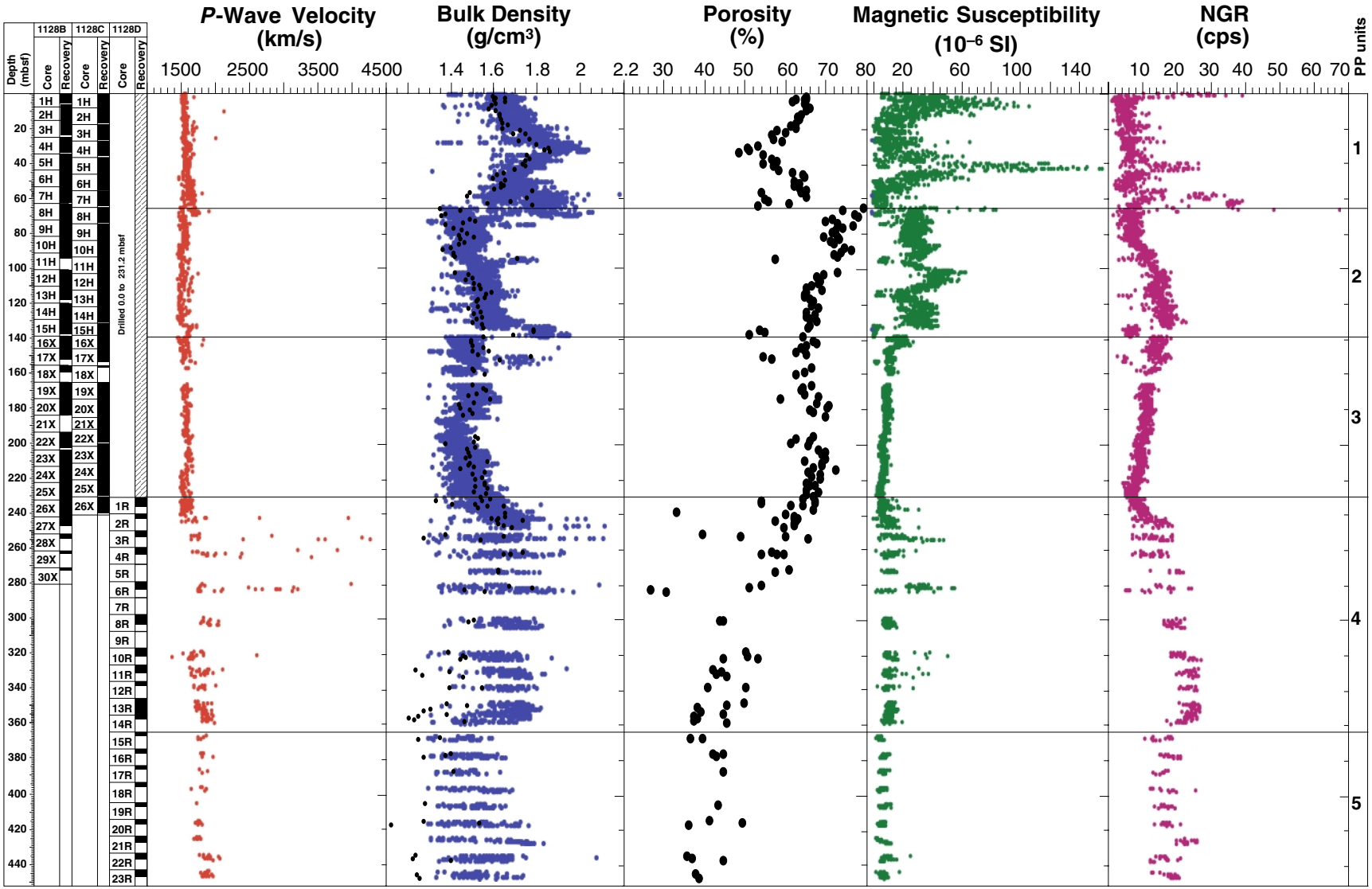

Figure F28. Combined plot of natural gamma radiation (NGR), magnetic susceptibility, uncorrected GRA (red line) and MAD (blue dots) bulk densities, and *P*-wave velocity, from the upper 270 m at Site 1128. Physical properties units (PP units) are indicated on the right.

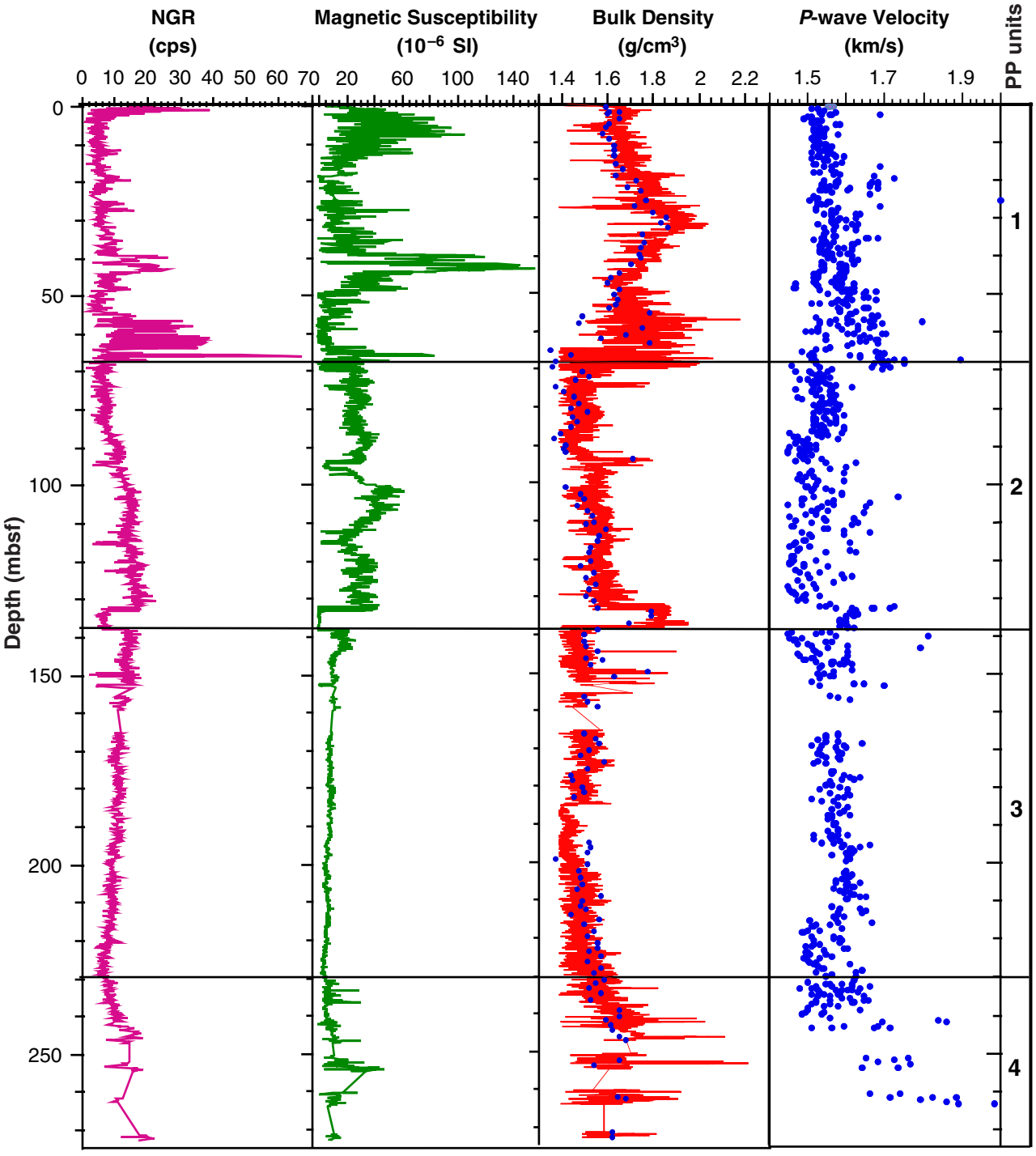

Figure F29. Comparison of downhole logging data and physical properties measurements on recovered sediments from Site 1128. **A.** Bulk density from gamma-ray attenuation densiometry (dots) and downhole measurements (line). **B.** Natural gamma-ray data from the multisensor track (blue dots) and two separate logging runs (red and green dots). **C.** *P*-wave velocity from discrete measurements (dots) and sonic log (line).

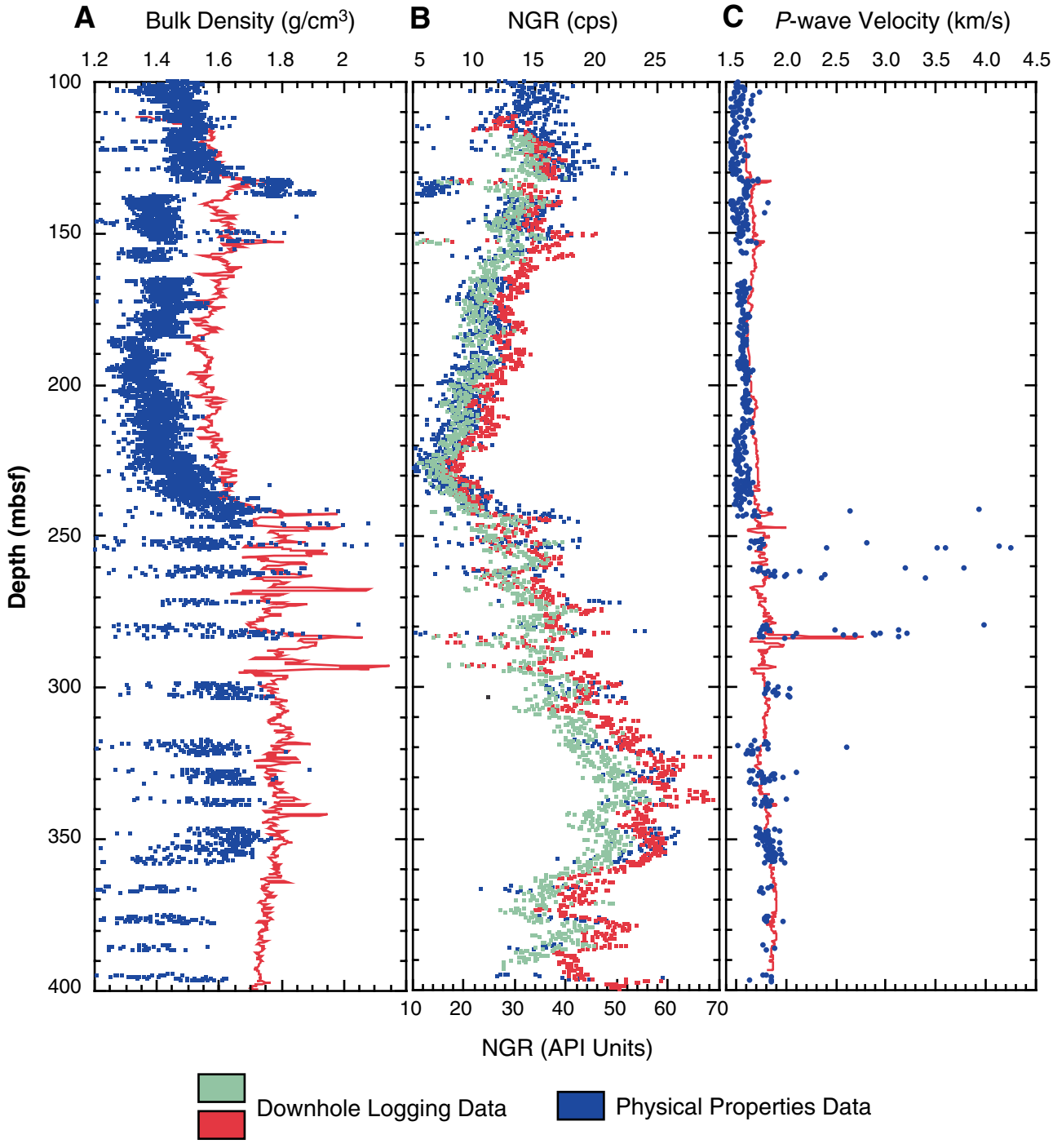

Figure F30. Shear strength (kPa; blue dots) and the ratio of undrained shear strength (S_u) to overburden stress (P'_o) from Site 1128 (red dots). This ratio provides an estimate of sediment consolidation relative to those of a gravimetrically or normally consolidated sedimentary section.

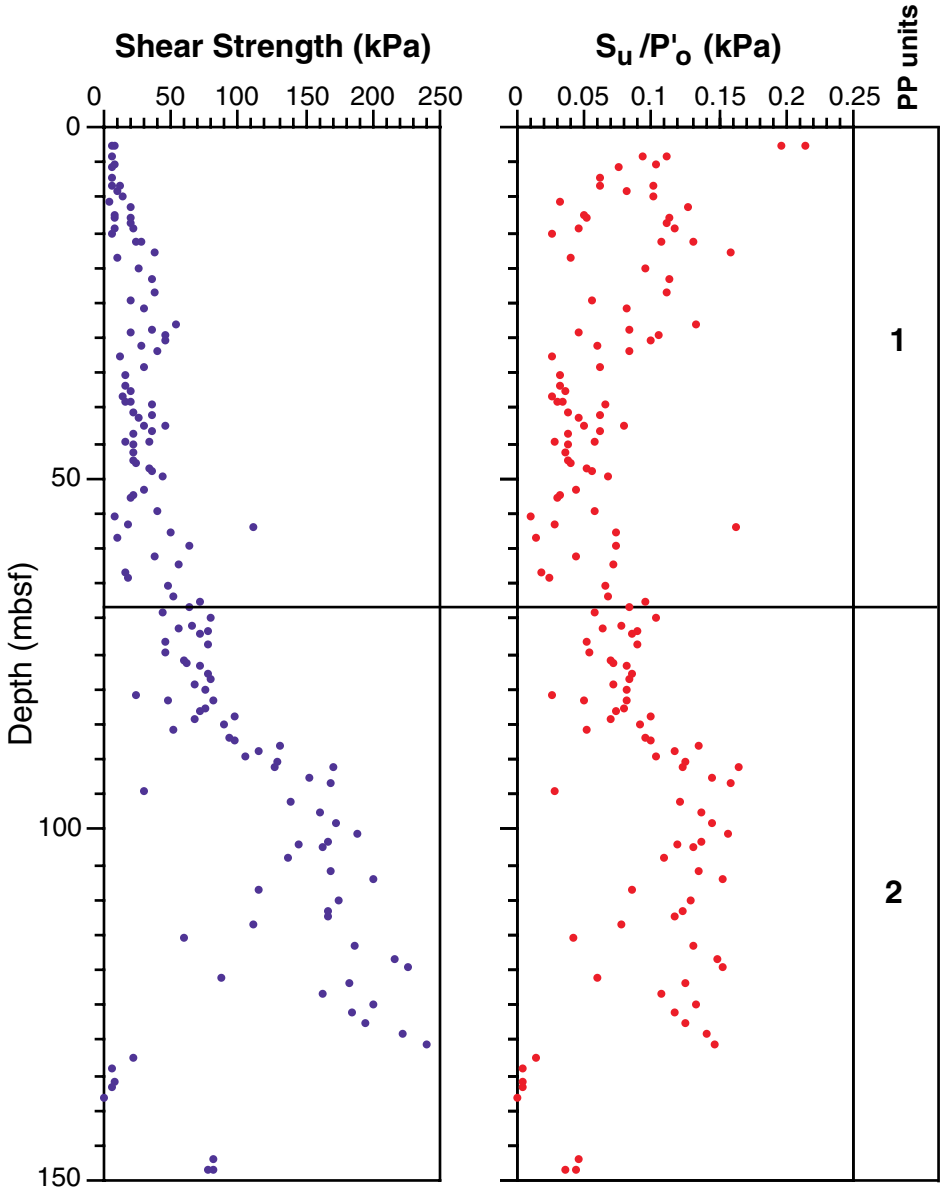

Figure F31. Thermal conductivity (blue dots) and bulk density (red dots) measurements for Site 1128. Physical properties units (PP units) are shown on the right.

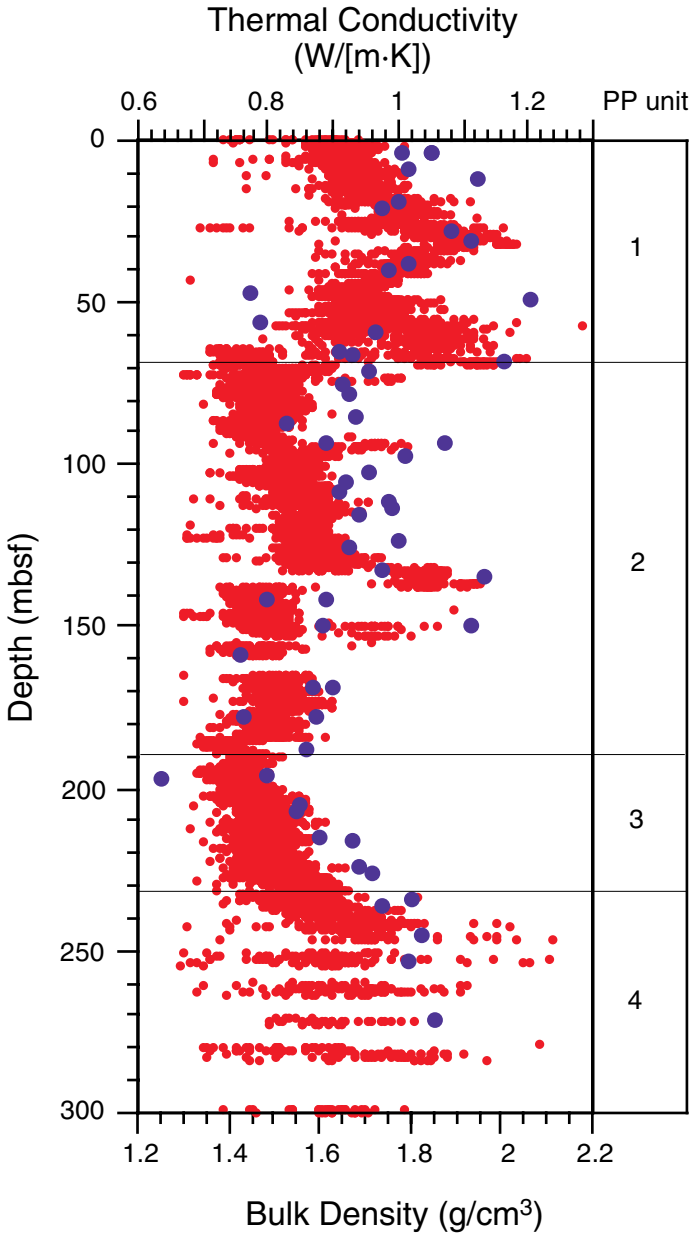

Figure F32. Variation of formation temperature with depth at Site 1128 from the Adara temperature tool (blue dots) and Davis-Villinger temperature probe (DVTP; red square).

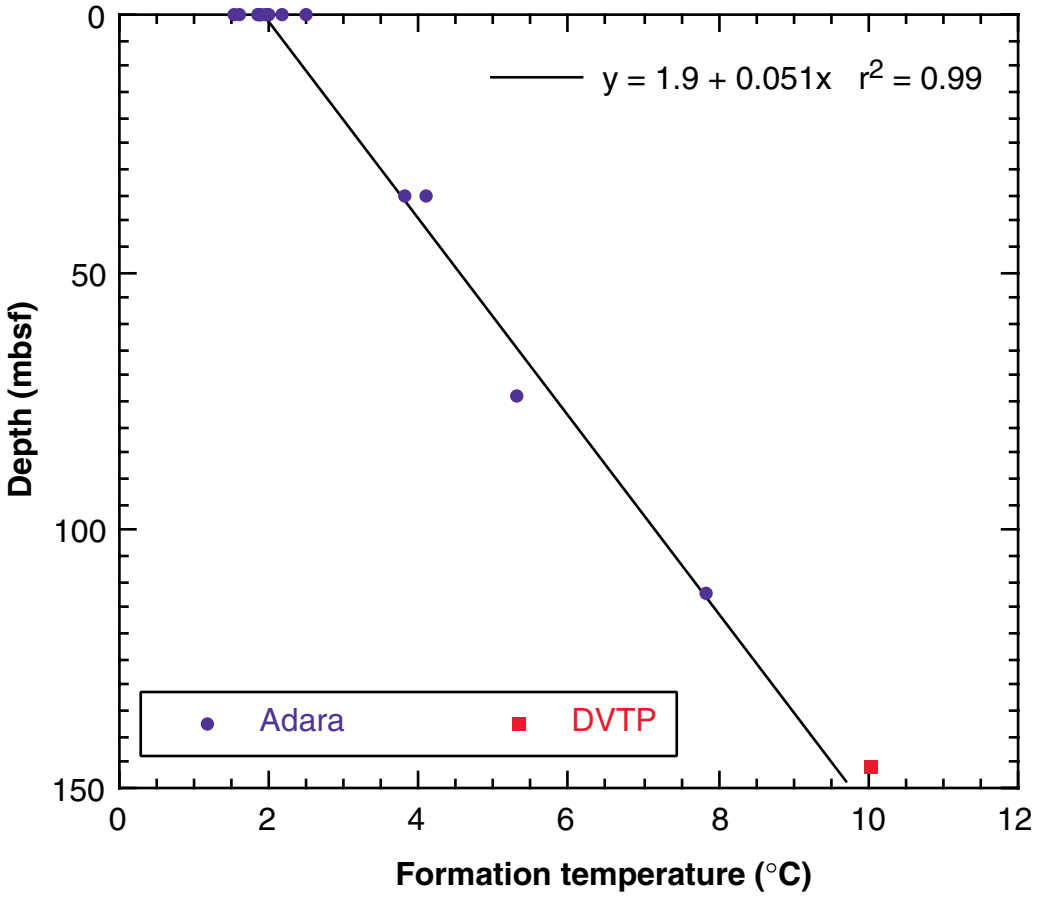

Figure F33. Summary of logging runs using the triple combination logging tool (triple combo) and the Formation MicroScanner (FMS)/sonic at Hole 1128D. Logging speed for both runs was 275 m/hr. See **"Logging Tools and Tool Strings,"** p. 27, in the "Explanatory Notes" chapter for a description of the tool strings. TD = total logging depth.

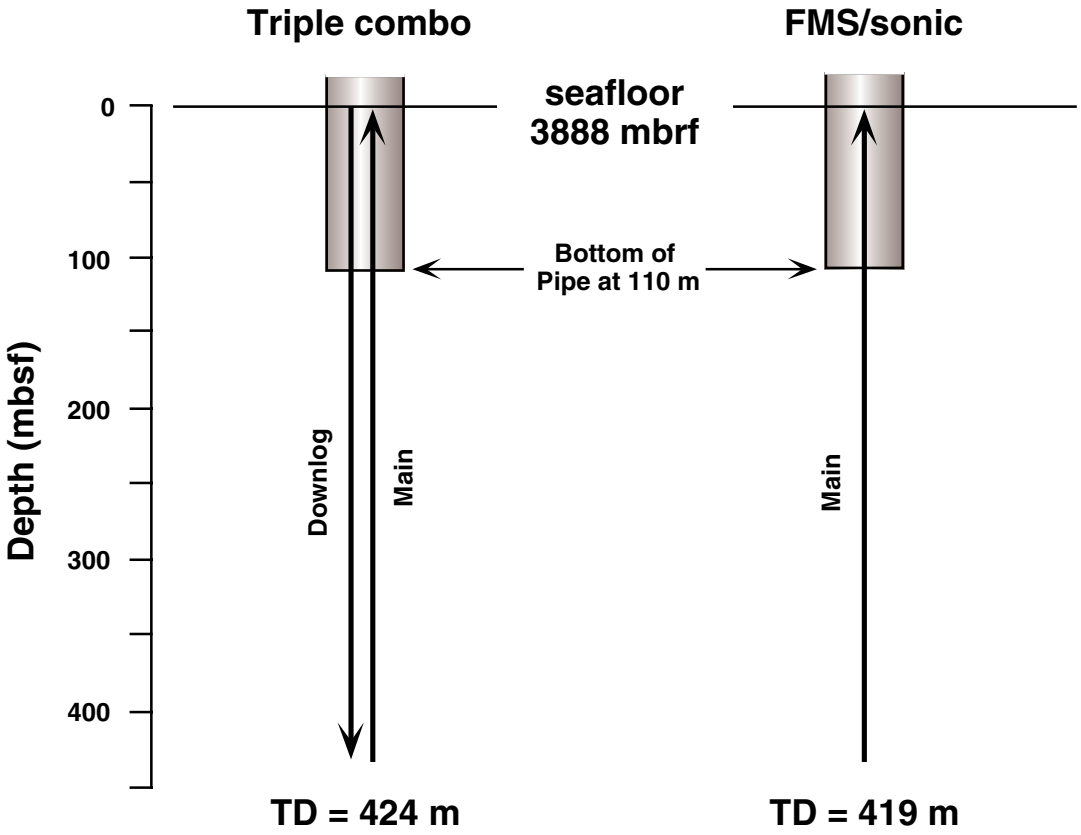

Figure F34. Summary of geophysical logs from the triple combination logging tool, plotted vs. depth for the open-hole logged interval. The data, plotted from left to right, are core recovery; caliper and total gamma radiation (HSGR); porosity and density, scaled so that the two curves will coincide for a clean limestone; photoelectric effect (PEF); shallow, medium, and deep resistivity; sonic velocity; logging units; lithostratigraphic units; and biostratigraphic ages.

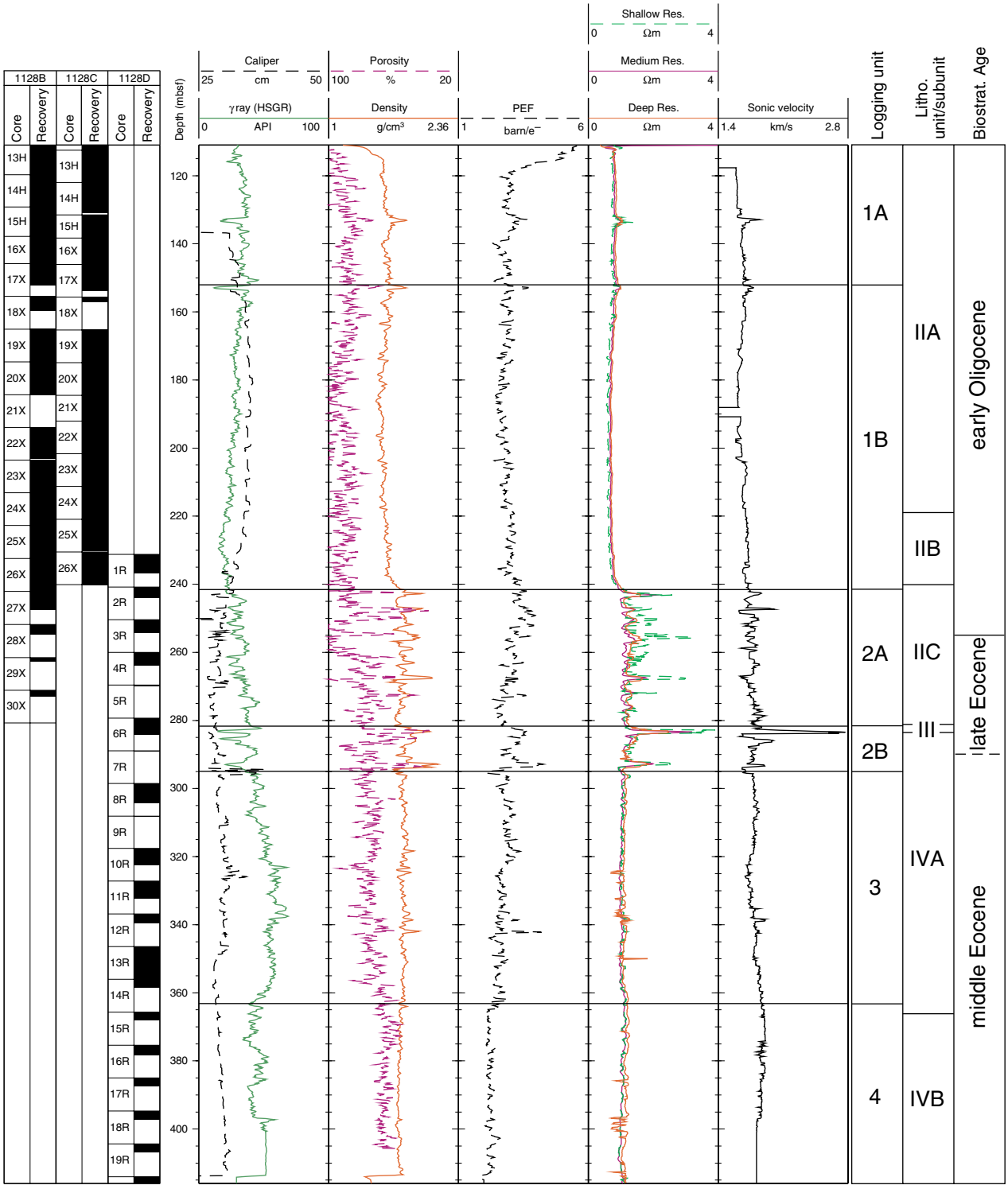

Figure F35. Summary of spectral gamma-ray logs, plotted vs. depth for the open-hole logged interval. The data, plotted from left to right, are core recovery, total gamma radiation (HSGR) and computed (uranium-free) gamma radiation (HCGR), uranium, thorium, potassium, logging units, lithostratigraphic units, and biostratigraphic ages.

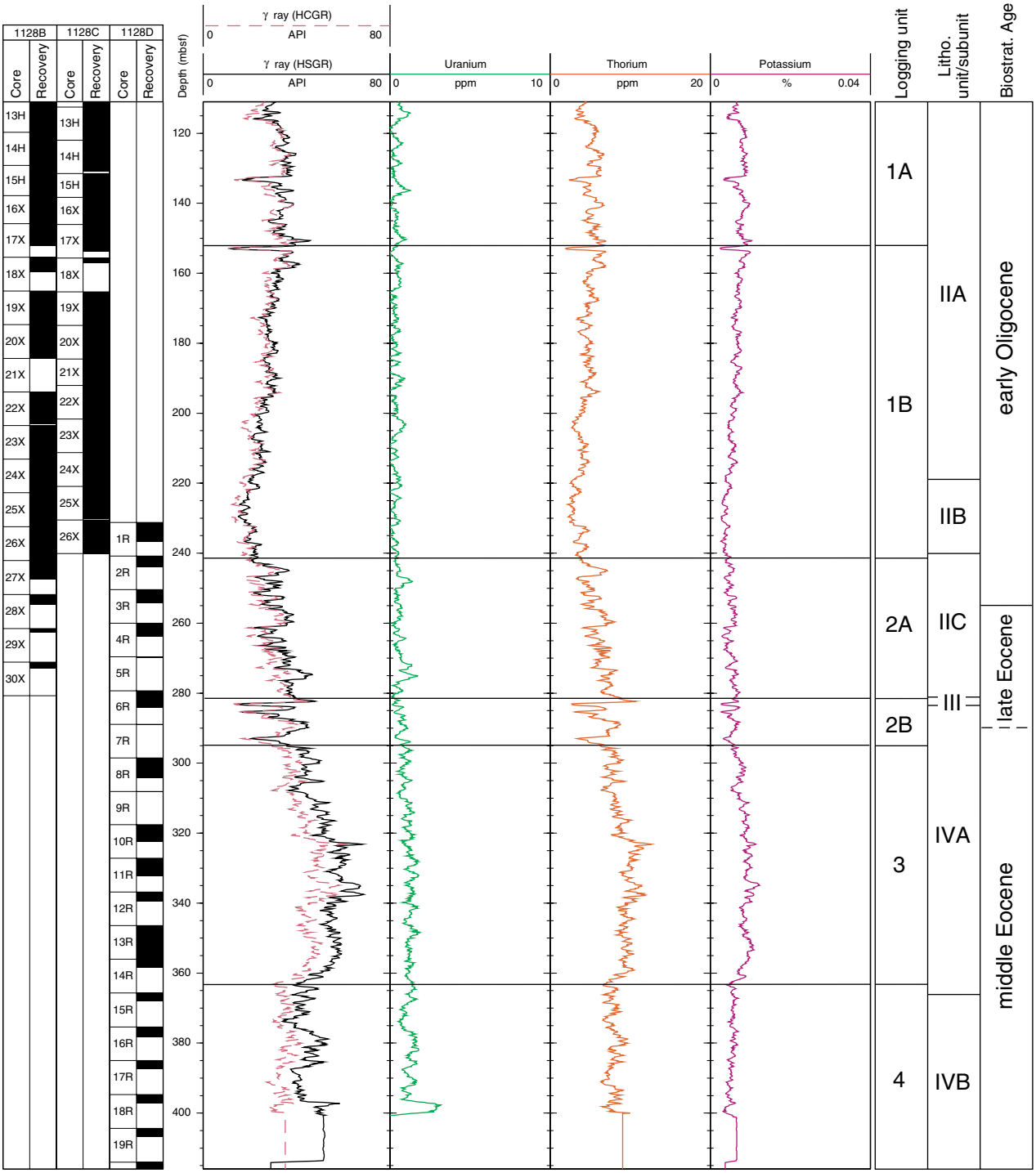

Figure F36. Summary of spectral gamma-ray logs, plotted vs. depth for the interval logged through pipe. The data, plotted from left to right, are core recovery, total gamma radiation (HSGR) and computed (uranium-free) gamma radiation (HCGR), uranium, thorium, potassium, logging units, lithostratigraphic units, and biostratigraphic ages.

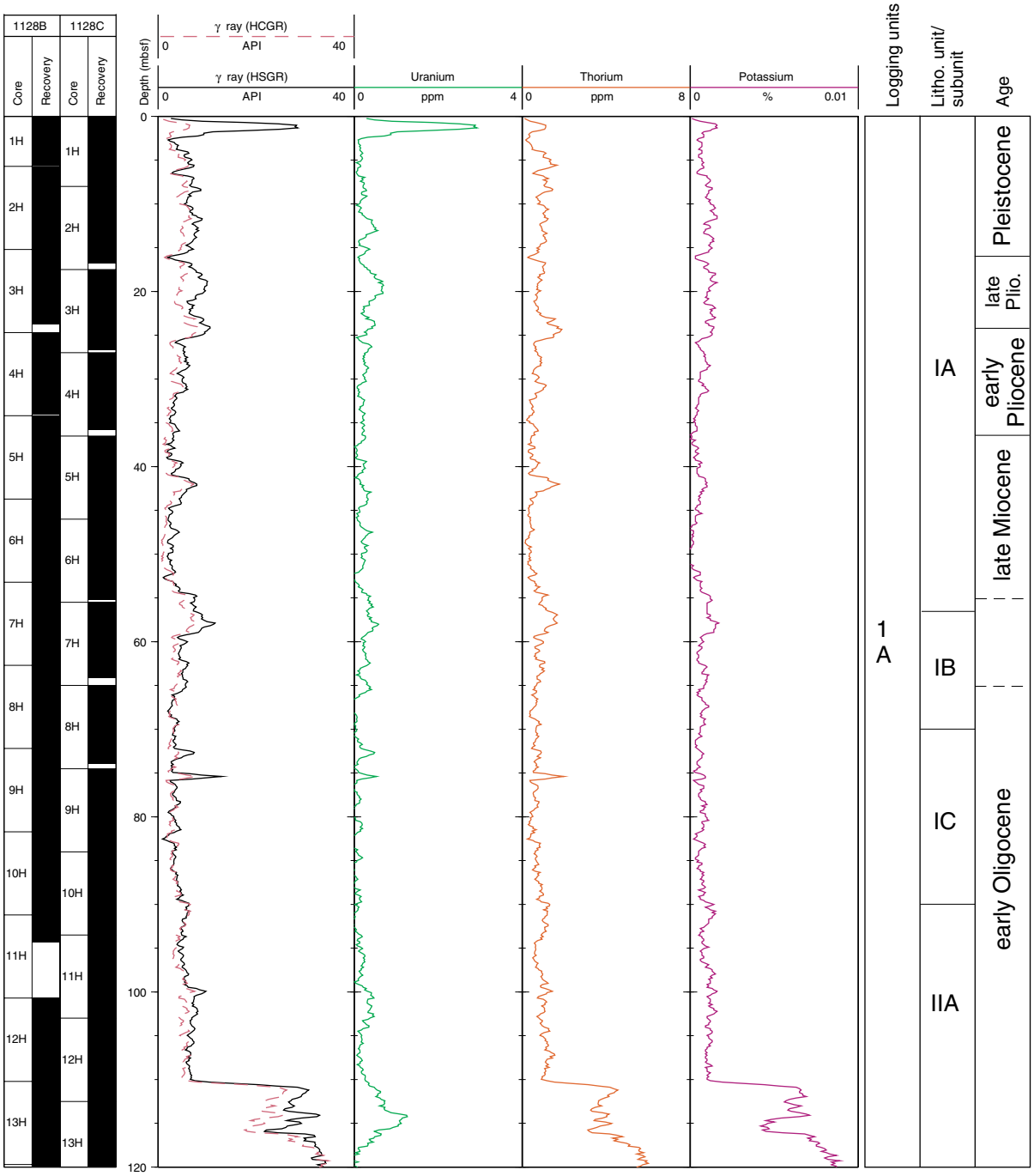

Figure F37. Log of acoustic impedance vs. depth calculated from the density and sonic logs from Site 1128. Horizontal lines indicate potential locations of seismic reflectors. Impedance data have been smoothed through a 5-m smoothing function to produce a resolution comparable to site-survey seismic data.

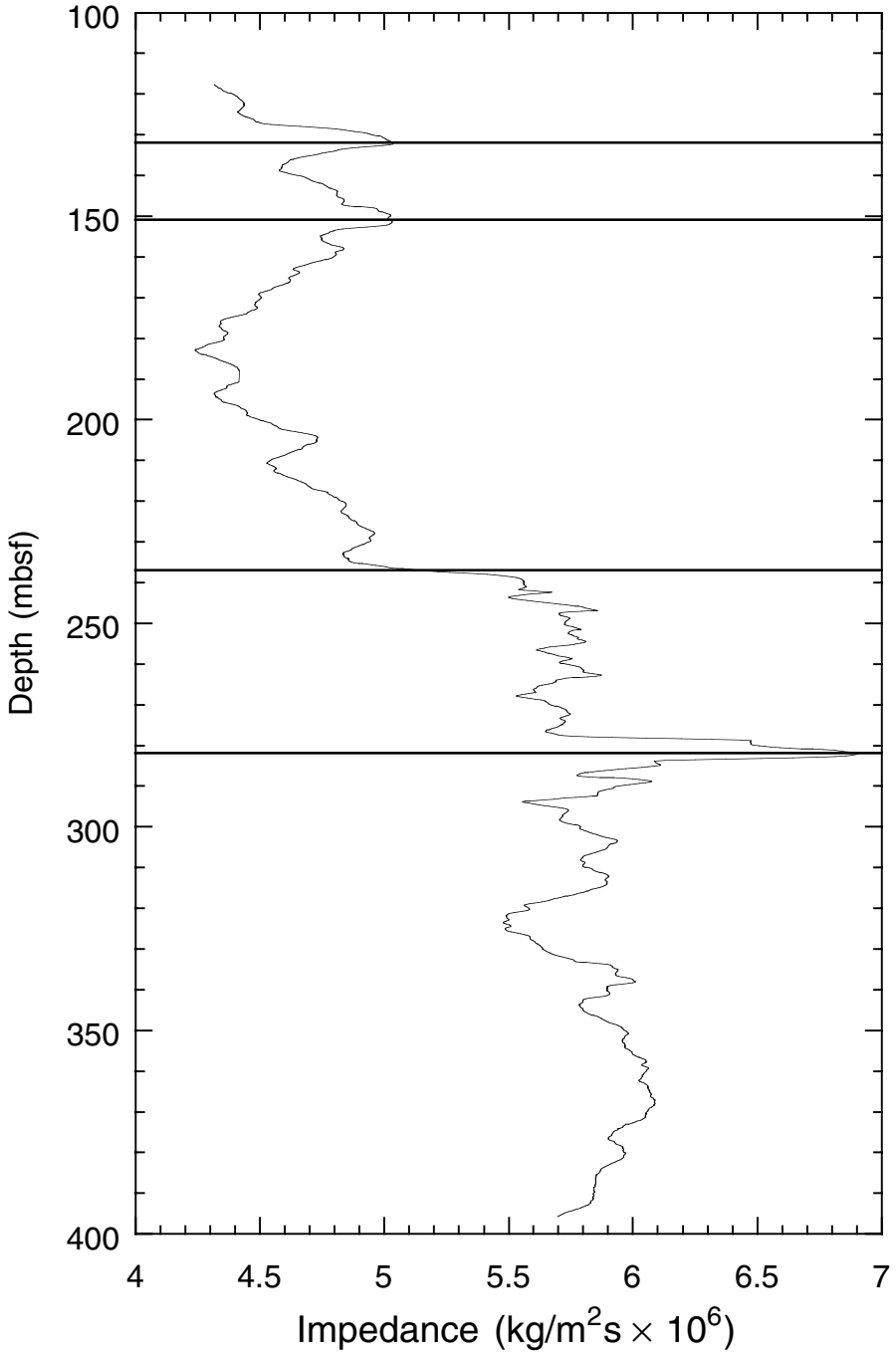

Figure F38. Map showing seismic site-survey tracks for Site 1128 (Lines AGSO169/08 and AGSO169/ 11) in relation to other Leg 182 sites and the Australian Geological Survey Organisation Survey 169 (AGSO169) site-survey seismic lines. The bold trackline (AGSO169/11e) corresponds to the seismic line segment shown in Figure F39, p. 84.

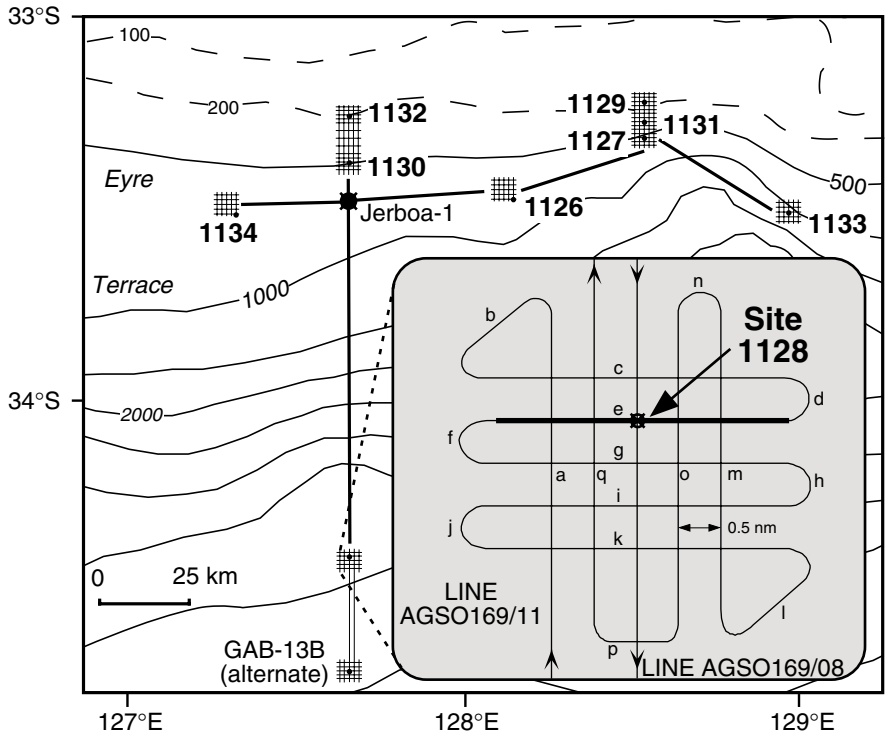

Figure F39. Portion of seismic Line AGSO169/11e showing predrill interpreted seismic stratigraphic sequences planned (shown in white) and actually intersected (shown in black) at Site 1128.

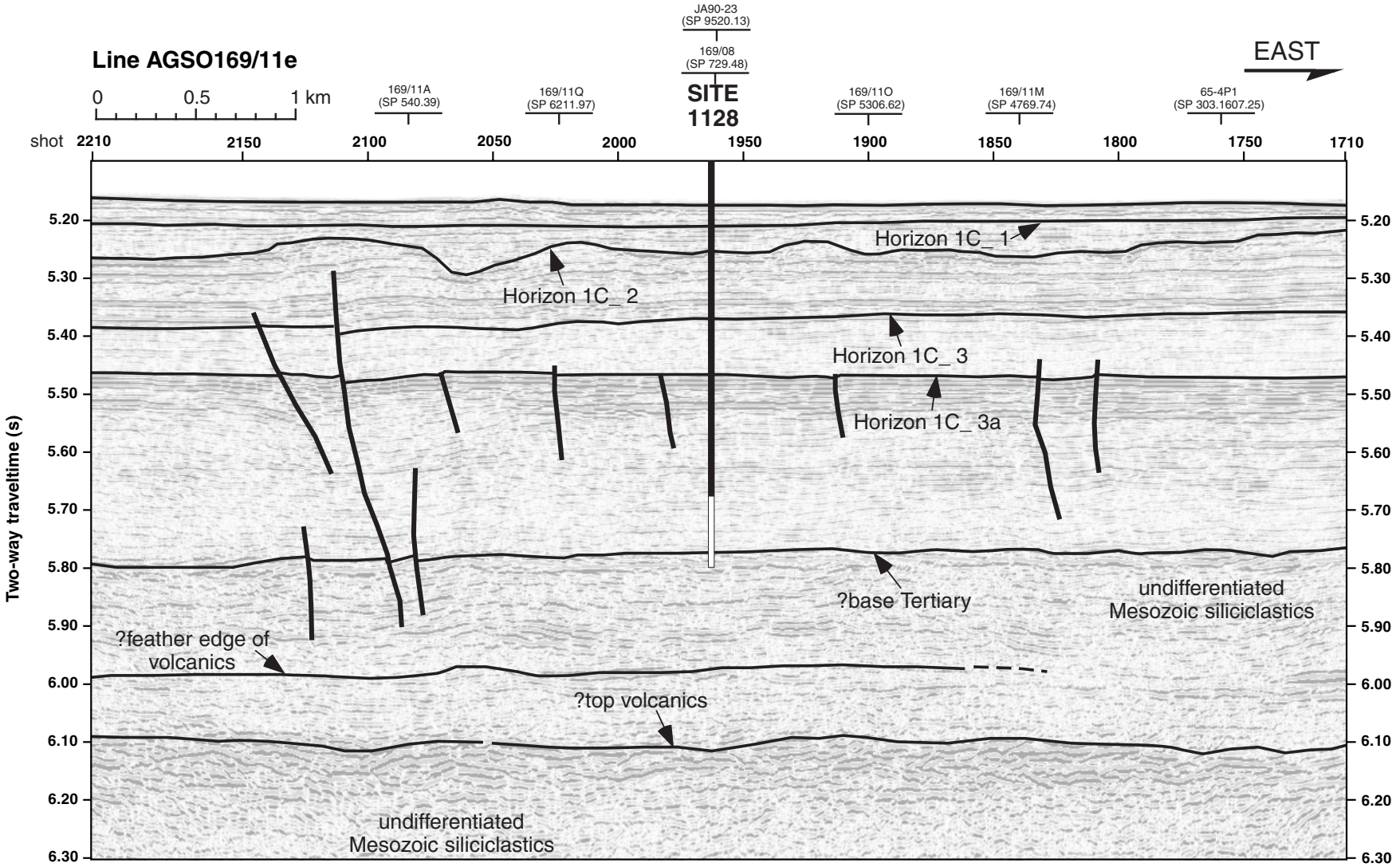

Figure F40. A. Plot showing relationship between predicted depths to key horizons and sequence boundaries (dashed) and corrected depths (arrowed). Corrected depths are based on the integrated sonic log (derived from interval transit-time data) shown plotted as a heavy dashed line relative to plots of site-survey seismic data stacking velocities. **B.** Plot of the velocity log (from compressional sonic trace) used as the basis for the integrated sonic log.

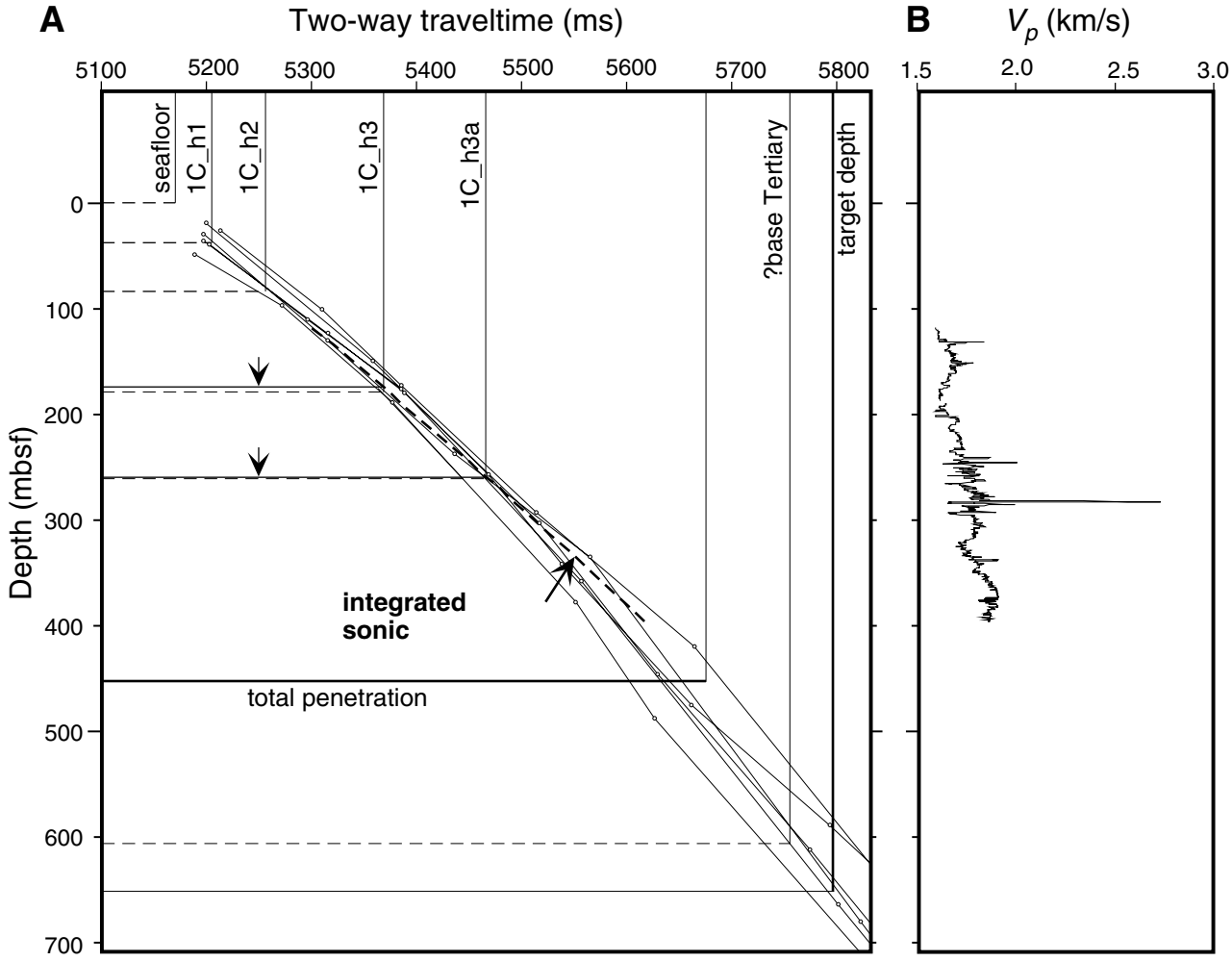

Figure F41. Tentative summary correlation between lithostratigraphic units, seismic sequences, biostratigraphic hiatuses, and ages at Site 1128. The 'IC_' horizons, derived from the local upper continental rise seismic interpretation, are shown in relation to the slope and shelf seismic stratigraphy (sequences defined in Feary and James, 1998, reprinted as **Chap. 2**) correlated using biostratigraphic data.

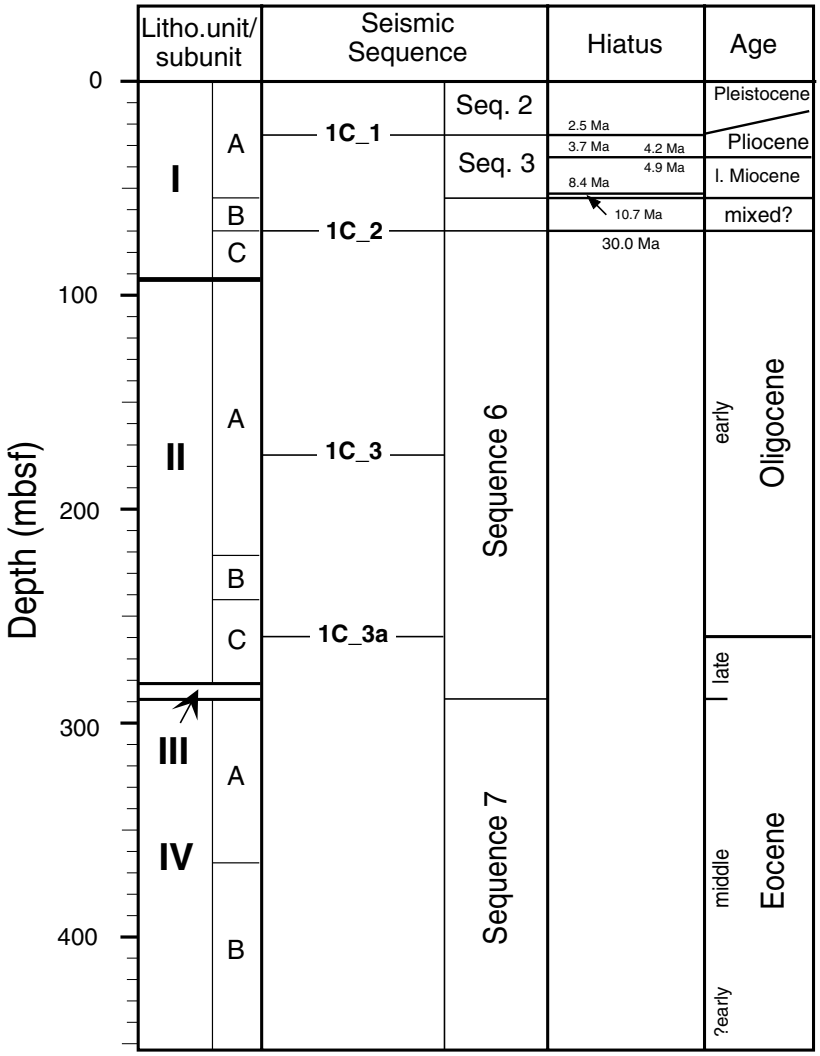

Table T1. Site 1128 coring summary. (See table notes. Continued on next two pages.)

Hole 1128A

Latitude: –34.391143° (34°23.4686′S)
Longitude: 127.5906967° (127°35.4418′E)
Seafloor (drill-pipe measurement from rig floor, mbrf): 3887.00
Distance between rig floor and sea level (m): 11.0
Water depth (drill-pipe measurement from sea level, m): 3876.0
Total depth (from rig floor, mbrf): 3896.5
Penetration (mbsf): 9.5
Total number of cores: 1
Total length of cored section (m): 9.5
Total core recovered (m): 9.31
Core recovery (%): 98.0
Remarks: Core badly disturbed by drilling; remnants of PIG found in core liner of Section 1 (location marked as void). As a result, the core was not described by sedimentologists.

Hole 1128B

Latitude: –34.391177° (34°23.4706′S)
Longitude: 127.590758° (127°35.4455′E)
Seafloor (drill-pipe measurement from rig floor, mbrf): 3885.8
Distance between rig floor and sea level (m): 11.2
Water depth (drill-pipe measurement from sea level, m): 3874.6
Total depth (from rig floor, mbrf): 4166.5
Penetration (mbsf): 280.7
Total number of cores: 30
Total length of cored section (m): 280.7
Total core recovered (m): 231.57
Core recovery (%): 82.5

Hole 1128C

Latitude: –34.391055° (34°23.4633′S)
Longitude: 127.591032° (127°35.4619′E)
Seafloor (drill-pipe measurement from rig floor, mbrf): 3885.5
Distance between rig floor and sea level (m): 11.2
Water depth (drill-pipe measurement from sea level, m): 3874.3
Total depth (from rig floor, mbrf): 4125.6
Penetration (mbsf): 240.10
Total number of cores: 26
Total length of cored section (m): 240.1
Total core recovered (m): 232.84
Core recovery (%): 97.0

Hole 1128D

Latitude: –34.390938° (34°23.4563′S)
Longitude: 127.590923° (127°35.4554′E)
Seafloor (drill-pipe measurement from rig floor, mbrf): 3885.5
Distance between rig floor and sea level (m): 11.3
Water depth (drill-pipe measurement from sea level, m): 3874.2
Total depth (from rig floor, mbrf): 4338.1
Penetration (mbsf): 452.6
Total number of cores: 23
Total length of cored section (m): 221.4
Total number of drilled intervals: 1
Total length of drilled intervals (m): 231.2
Total core recovered (m): 79.08
Core recovery (%): 35.7

Core	Date (Nov 1998)	Time (UTC + 8 hr)	Depth (mbsf)	Length cored (m)	Length recovered (m)	Recovery (%)	Comment
182-1128A-							
1H	3	1925	0.00–9.50	9.5	9.31	98.0	Disturbed core; PIG
Totals:				9.5	9.31	98.0	
182-1128B-							
1H	3	2020	0.00–5.70	5.7	5.66	99.3	
2H	3	2115	5.70–15.20	9.5	9.83	103.5	
3H	3	2220	15.20–24.70	9.5	8.52	89.7	Crushed liner; oriented
4H	3	2315	24.70–34.20	9.5	9.32	98.1	Crushed liner
5H	4	0005	34.20–43.70	9.5	9.52	100.2	Oriented
6H	4	0105	43.70–53.20	9.5	9.88	104.0	Oriented

Table T1 (continued).

Core	Date (Nov 1998)	Time (UTC + 8 hr)	Depth (mbsf)	Length cored (m)	Length recovered (m)	Recovery (%)	Comment
7H	4	0200	53.20–62.70	9.5	9.41	99.1	Split liner; oriented
8H	4	0300	62.70–72.20	9.5	9.80	103.2	Oriented
9H	4	0400	72.20–81.70	9.5	9.64	101.5	
10H	4	0500	81.70–91.20	9.5	9.95	104.7	
11H	4	0600	91.20–100.70	9.5	3.08	32.4	
12H	4	0700	100.70–110.20	9.5	9.89	104.1	
13H	4	0755	110.20–119.70	9.5	9.48	99.8	
14H	4	0855	119.70–129.20	9.5	9.91	104.3	
15H	4	0950	129.20–137.80	8.6	8.59	99.9	Sections 4 to 6 may be suck-in
16X	4	1155	137.80–145.80	8.0	9.87	123.4	
17X	4	1500	145.80–155.40	9.6	6.50	67.7	DVTP
18X	4	1730	155.40–165.10	9.7	4.26	43.9	
19X	4	1900	165.10–174.70	9.6	9.76	101.7	
20X	4	2035	174.70–184.30	9.6	9.72	101.3	
21X	4	2135	184.30–193.90	9.6	0.00	0.0	No recovery
22X	4	2230	193.90–203.50	9.6	9.29	96.8	
23X	4	2325	203.50–213.10	9.6	9.84	102.5	
24X	5	0030	213.10–222.70	9.6	9.69	100.9	
25X	5	0130	222.70–232.40	9.7	9.81	101.1	
26X	5	0305	232.40–242.10	9.7	9.73	100.3	
27X	5	0545	242.10–251.80	9.7	5.35	55.2	
28X	5	0810	251.80–261.50	9.7	2.89	29.8	
29X	5	1020	261.50–271.10	9.6	1.12	11.7	
30X	5	1310	271.10–280.70	9.6	1.76	18.3	
Totals:				280.7	231.57	82.5	
182-1128C-							
1H	5	1700	0.00–8.00	8.0	7.95	99.4	
2H	5	1800	8.00–17.50	9.5	8.77	92.3	
3H	5	1900	17.50–27.00	9.5	9.14	96.2	
4H	5	2015	27.00–36.50	9.5	8.78	92.4	Oriented/Adara
5H	5	2130	36.50–46.00	9.5	10.05	105.8	
6H	5	2245	46.00–55.50	9.5	9.18	96.6	Liner patched
7H	5	2340	55.50–65.00	9.5	8.65	91.1	Liner patched
8H	6	0120	65.00–74.50	9.5	8.97	94.4	Adara; oriented, liner patch
9H	6	0225	74.50–84.00	9.5	9.95	104.7	
10H	6	0320	84.00–93.50	9.5	9.75	102.6	
11H	6	0420	93.50–103.00	9.5	9.81	103.3	Liner patched
12H	6	0545	103.00–112.50	9.5	9.89	104.1	
13H	6	0645	112.50–122.00	9.5	9.97	105.0	
14H	6	0745	122.00–131.50	9.5	8.91	93.8	
15H	6	0845	131.50–138.30	6.8	6.83	100.4	
16X	6	1025	138.30–146.10	7.8	9.83	126.0	
17X	6	1125	146.10–155.70	9.6	7.73	80.5	
18X	6	1250	155.70–165.30	9.6	1.45	15.1	
19X	6	1350	165.30–174.90	9.6	9.88	102.9	
20X	6	1450	174.90–184.50	9.6	9.90	103.1	
21X	6	1550	184.50–192.10	7.6	8.93	117.5	
22X	6	1650	192.10–201.70	9.6	9.69	100.9	
23X	6	1745	201.70–211.30	9.6	9.76	101.7	
24X	6	1845	211.30–220.90	9.6	9.86	102.7	
25X	6	1945	220.90–230.50	9.6	9.32	97.1	
26X	6	2050	230.50–240.10	9.6	9.89	103.0	
Totals:				240.1	232.84	97.0	
182-1128D-							
			*****Drilled from 0 to 231.2 mbsf*****				
1R	7	1840	231.20–240.80	9.6	5.56	57.9	
2R	7	1950	240.80–250.40	9.6	3.08	32.1	
3R	7	2140	250.40–260.00	9.6	3.91	40.7	
4R	7	2335	260.00–269.60	9.6	3.95	41.2	
5R	8	0120	269.60–279.30	9.7	0.29	3.0	
6R	8	0300	279.30–288.90	9.6	4.76	49.6	
7R	8	0525	288.90–298.50	9.6	0.12	1.3	
8R	8	0715	298.50–308.10	9.6	5.74	59.8	
9R	8	0930	308.10–317.60	9.5	0.08	0.8	
10R	8	1100	317.60–327.20	9.6	4.89	50.9	
11R	8	1310	327.20–336.80	9.6	5.07	52.8	
12R	8	1500	336.80–346.40	9.6	2.65	27.6	

Table T1 (continued).

Core	Date (Nov 1998)	Time (UTC + 8 hr)	Depth (mbsf)	Length cored (m)	Length recovered (m)	Recovery (%)	Comment
13R	8	1705	346.40–356.00	9.6	9.56	99.6	
14R	8	1905	356.00–365.70	9.7	2.53	26.1	
15R	8	2055	365.70–375.40	9.7	2.38	24.5	
16R	8	2240	375.40–385.00	9.6	2.89	30.1	
17R	9	0035	385.00–394.70	9.7	2.35	24.2	
18R	9	0200	394.70–404.40	9.7	2.51	25.9	
19R	9	0350	404.40–414.00	9.6	2.41	25.1	
20R	9	0520	414.00–423.70	9.7	3.00	30.9	
21R	9	0800	423.70–433.30	9.6	3.65	38.0	
22R	9	0925	433.30–442.90	9.6	3.79	39.5	
23R	9	1120	442.90–452.60	9.7	3.91	40.3	
Coring totals:				221.4	79.08	35.7	
Drilling total:				231.2			
Total:				452.6			

Notes: PIG = wiper pig remnants, UTC = Universal Time Coordinated, DVTP = Davis-Villinger temperature probe, Adara = Adara temperature tool.

Table T2. Datum levels used for the calculation of the Site 1128 sedimentation rate.

Datum type	Datum level	Age (Ma)	Midpoint (mbsf)	Stratigraphic error (m)	Datum level code	Fossil group	Upper sample		Lower sample	
							Core, section, interval (cm)	Depth (mbsf)	Core, section, interval (cm)	Depth (mbsf)
							182-1128B-		182-1128B-	
T	*P. lacunosa*	0.45	2.83	2.83	1	1	1H-CC, 14-17	5.63	1H-1, 0-1	0
	Brunhes/Matuyama	0.78	14		2		2H-6, 80	14.00		
T	*H. sellii*	1.25	10.595	4.935	3	1	1H-CC, 14-17	5.63	2H-CC, 21-24	15.50
T	*C. macintyrei*	1.67	16.225	0.695	4	1	2H-CC, 21-24	15.50	3H-2, 18-22	16.88
T	*D. brouweri*	1.95	20.07	3.15	5	1	3H-2, 18-22	16.88	3H-CC, 21-24	23.19
T	*R. pseudoumbilicus*	3.75	26.525	3.305	6	1	3H-CC, 21-24	23.19	4H-4, 58-63	29.78
T	*G. margaritae*	3.58	26.525	3.305	7	4	3H-CC, 21-24	23.19	4H-4, 58-63	29.78
T	*A. tricorniculatus*	4	35.385	1.365	8	1	4H-CC, 14-17	33.99	5H-2, 101-105	36.71
T	*Z. nepenthes*	4.2	40.235	3.485	9	4	5H-2, 101-105	36.71	5H-CC, 11-13	43.70
B	*D. asymmetricus*	5.02	45.69	1.99	10	1	5H-CC, 11-13	43.70	6H-3, 98-103	47.68
T	*G. dehiscens*	5.8	50.655	2.925	11	4	6H-3, 98-103	47.68	6H-CC, 19-21	53.56
T	*C. altus*	26.1	66.82	4.21	12	1	7H-CC, 21-24	62.58	8H-6, 79-83	70.99
T	C10n	28.28	75.20		13		9H-2, 150	75.20		
B	C10n	28.745	90.00		14		9H-6, 80	90.00		
T	C11n	29.4	100.80		15		12H-1, 10	100.80		
B	C11n	30.1	108.20		16		12H-5, 150	108.20		
T	C12n	30.48	133.70		17		15H-4, 41	133.70		
T	*I. recurvus*	31.8	135.25	2.54	18	1	15H-3, 50-51	132.70	15H-CC, 11-14	137.76
B	C12n	30.94	137.50		19		15H-6, 24	137.50		
T	*R. umbilicus*	32.3	142.73	4.94	20	1	15H-CC, 11-14	137.76	16X-CC, 50-53	147.64
T	*D. saipanensis*	34.2	251.04	3.62	21	1	27X-CC, 28-31	247.42	28X-CC, 32-35	254.66
							182-1128D-		182-1128D-	
B	*I. recurvus*	36	259.11	4.83	22	1	3R-CC, 24-27	254.28	4R-CC, 11-12	263.94
T	*C. solitus*	40.4	422.17	5.175	23	1	20R-CC, 13-16	416.97	21R-CC, 20-23	427.32

Notes: T = top of taxon stratigraphic range, B = bottom of taxon stratigraphic range. Midpoint = the middle depth between the sample where the taxon occurs and the adjacent sample where it does not occur. Stratigraphic error = one-half the distance between the sample where the taxon occurs and the adjacent sample where it does not occur. Fossil groups = calcareous nannofossils (1) and planktonic foraminifers (4).

Table T3. Core and section depths in meters composite depth (mcd) and meters below seafloor (mbsf), Site 1128. (See table notes. Continued on next four pages.)

Leg	Site	Hole	Core	Type	Section	Depth (mbsf)	Offset	Depth (mcd)
182	1128	B	1	H	1	0.00	0.00	0.00
182	1128	B	1	H	2	1.50	0.00	1.50
182	1128	B	1	H	3	3.00	0.00	3.00
182	1128	B	1	H	4	4.50	0.00	4.50
182	1128	B	2	H	1	5.70	1.10	6.80
182	1128	B	2	H	2	7.20	1.10	8.30
182	1128	B	2	H	3	8.70	1.10	9.80
182	1128	B	2	H	4	10.20	1.10	11.30
182	1128	B	2	H	5	11.70	1.10	12.80
182	1128	B	2	H	6	13.20	1.10	14.30
182	1128	B	2	H	7	14.70	1.10	15.80
182	1128	B	3	H	1	15.20	1.78	16.98
182	1128	B	3	H	2	16.70	1.78	18.48
182	1128	B	3	H	3	18.20	1.78	19.98
182	1128	B	3	H	4	19.70	1.78	21.48
182	1128	B	3	H	5	21.20	1.78	22.98
182	1128	B	3	H	6	22.20	1.78	23.98
182	1128	B	4	H	1	24.70	2.14	26.84
182	1128	B	4	H	2	26.20	2.14	28.34
182	1128	B	4	H	3	27.70	2.14	29.84
182	1128	B	4	H	4	29.20	2.14	31.34
182	1128	B	4	H	5	30.70	2.14	32.84
182	1128	B	4	H	6	32.20	2.14	34.34
182	1128	B	5	H	1	34.20	2.38	36.58
182	1128	B	5	H	2	35.70	2.38	38.08
182	1128	B	5	H	3	37.20	2.38	39.58
182	1128	B	5	H	4	38.70	2.38	41.08
182	1128	B	5	H	5	40.20	2.38	42.58
182	1128	B	5	H	6	41.70	2.38	44.08
182	1128	B	5	H	7	42.70	2.38	45.08
182	1128	B	6	H	1	43.70	3.20	46.90
182	1128	B	6	H	2	45.20	3.20	48.40
182	1128	B	6	H	3	46.70	3.20	49.90
182	1128	B	6	H	4	48.20	3.20	51.40
182	1128	B	6	H	5	49.70	3.20	52.90
182	1128	B	6	H	6	51.20	3.20	54.40
182	1128	B	6	H	7	52.70	3.20	55.90
182	1128	B	7	H	1	53.20	4.98	58.18
182	1128	B	7	H	2	54.70	4.98	59.68
182	1128	B	7	H	3	55.50	4.98	60.48
182	1128	B	7	H	4	57.00	4.98	61.98
182	1128	B	7	H	5	58.50	4.98	63.48
182	1128	B	7	H	6	60.00	4.98	64.98
182	1128	B	7	H	7	61.50	4.98	66.48
182	1128	B	8	H	1	62.70	8.98	71.68
182	1128	B	8	H	2	64.20	8.98	73.18
182	1128	B	8	H	3	65.70	8.98	74.68
182	1128	B	8	H	4	67.20	8.98	76.18
182	1128	B	8	H	5	68.70	8.98	77.68
182	1128	B	8	H	6	70.20	8.98	79.18
182	1128	B	8	H	7	71.70	8.98	80.68
182	1128	B	9	H	1	72.20	8.98	81.18
182	1128	B	9	H	2	73.70	8.98	82.68
182	1128	B	9	H	3	75.20	8.98	84.18
182	1128	B	9	H	4	76.70	8.98	85.68
182	1128	B	9	H	5	78.20	8.98	87.18
182	1128	B	9	H	6	79.70	8.98	88.68
182	1128	B	9	H	7	81.20	8.98	90.18
182	1128	B	10	H	1	81.70	10.30	92.00
182	1128	B	10	H	2	83.20	10.30	93.50
182	1128	B	10	H	3	84.70	10.30	95.00
182	1128	B	10	H	4	86.20	10.30	96.50
182	1128	B	10	H	5	87.70	10.30	98.00
182	1128	B	10	H	6	89.20	10.30	99.50
182	1128	B	10	H	7	90.70	10.30	101.00
182	1128	B	11	H	1	91.20	10.68	101.88

Table T3 (continued).

Leg	Site	Hole	Core	Type	Section	Depth (mbsf)	Offset	Depth (mcd)
182	1128	B	11	H	2	92.70	10.68	103.38
182	1128	B	12	H	1	100.70	10.82	111.52
182	1128	B	12	H	2	102.20	10.82	113.02
182	1128	B	12	H	3	103.70	10.82	114.52
182	1128	B	12	H	4	105.20	10.82	116.02
182	1128	B	12	H	5	106.70	10.82	117.52
182	1128	B	12	H	6	108.20	10.82	119.02
182	1128	B	12	H	7	109.70	10.82	120.52
182	1128	B	13	H	1	110.20	11.94	122.14
182	1128	B	13	H	2	111.70	11.94	123.64
182	1128	B	13	H	3	113.20	11.94	125.14
182	1128	B	13	H	4	114.70	11.94	126.64
182	1128	B	13	H	5	116.20	11.94	128.14
182	1128	B	13	H	6	117.70	11.94	129.64
182	1128	B	13	H	7	119.20	11.94	131.14
182	1128	B	14	H	1	119.70	12.42	132.12
182	1128	B	14	H	2	121.20	12.42	133.62
182	1128	B	14	H	3	122.70	12.42	135.12
182	1128	B	14	H	4	124.20	12.42	136.62
182	1128	B	14	H	5	125.70	12.42	138.12
182	1128	B	14	H	6	127.20	12.42	139.62
182	1128	B	14	H	7	128.70	12.42	141.12
182	1128	B	15	H	1	129.20	12.80	142.00
182	1128	B	15	H	2	130.70	12.80	143.50
182	1128	B	15	H	3	132.20	12.80	145.00
182	1128	B	15	H	4	133.29	12.80	146.09
182	1128	B	15	H	5	134.76	12.80	147.56
182	1128	B	15	H	6	136.26	12.80	149.06
182	1128	B	16	X	1	137.80	14.77	152.57
182	1128	B	16	X	2	139.30	14.77	154.07
182	1128	B	16	X	3	140.80	14.77	155.57
182	1128	B	16	X	4	142.30	14.77	157.07
182	1128	B	16	X	5	143.80	14.77	158.57
182	1128	B	16	X	6	145.30	14.77	160.07
182	1128	B	17	X	1	145.80	18.63	164.43
182	1128	B	17	X	2	147.30	18.63	165.93
182	1128	B	17	X	3	148.80	18.63	167.43
182	1128	B	17	X	4	150.30	18.63	168.93
182	1128	B	18	X	1	155.40	18.63	174.03
182	1128	B	18	X	2	156.90	18.63	175.53
182	1128	B	18	X	3	158.40	18.63	177.03
182	1128	B	19	X	1	165.10	18.63	183.73
182	1128	B	19	X	2	166.60	18.63	185.23
182	1128	B	19	X	3	168.10	18.63	186.73
182	1128	B	19	X	4	169.60	18.63	188.23
182	1128	B	19	X	5	171.10	18.63	189.73
182	1128	B	19	X	6	172.60	18.63	191.23
182	1128	B	19	X	7	174.10	18.63	192.73
182	1128	B	20	X	1	174.70	18.63	193.33
182	1128	B	20	X	2	176.20	18.63	194.83
182	1128	B	20	X	3	177.70	18.63	196.33
182	1128	B	20	X	4	179.20	18.63	197.83
182	1128	B	20	X	5	180.70	18.63	199.33
182	1128	B	20	X	6	182.20	18.63	200.83
182	1128	B	20	X	7	183.70	18.63	202.33
182	1128	B	22	X	1	193.90	18.75	212.65
182	1128	B	22	X	2	195.40	18.75	214.15
182	1128	B	22	X	3	196.90	18.75	215.65
182	1128	B	22	X	4	198.40	18.75	217.15
182	1128	B	22	X	5	199.90	18.75	218.65
182	1128	B	22	X	6	201.40	18.75	220.15
182	1128	B	23	X	1	203.50	18.75	222.25
182	1128	B	23	X	2	205.00	18.75	223.75
182	1128	B	23	X	3	206.50	18.75	225.25
182	1128	B	23	X	4	208.00	18.75	226.75
182	1128	B	23	X	5	209.50	18.75	228.25
182	1128	B	23	X	6	211.00	18.75	229.75
182	1128	B	23	X	7	212.20	18.75	230.95
182	1128	B	24	X	1	213.10	18.91	232.01

Table T3 (continued).

Leg	Site	Hole	Core	Type	Section	Depth (mbsf)	Offset	Depth (mcd)
182	1128	B	24	X	2	214.60	18.91	233.51
182	1128	B	24	X	3	216.10	18.91	235.01
182	1128	B	24	X	4	217.60	18.91	236.51
182	1128	B	24	X	5	219.10	18.91	238.01
182	1128	B	24	X	6	220.60	18.91	239.51
182	1128	B	24	X	7	222.10	18.91	241.01
182	1128	B	25	X	1	222.70	19.27	241.97
182	1128	B	25	X	2	224.20	19.27	243.47
182	1128	B	25	X	3	225.70	19.27	244.97
182	1128	B	25	X	4	227.20	19.27	246.47
182	1128	B	25	X	5	228.70	19.27	247.97
182	1128	B	25	X	6	230.20	19.27	249.47
182	1128	B	25	X	7	231.70	19.27	250.97
182	1128	B	26	X	1	232.40	19.95	252.35
182	1128	B	26	X	2	233.90	19.95	253.85
182	1128	B	26	X	3	235.40	19.95	255.35
182	1128	B	26	X	4	236.90	19.95	256.85
182	1128	B	26	X	5	238.40	19.95	258.35
182	1128	B	26	X	6	239.90	19.95	259.85
182	1128	B	26	X	7	241.40	19.95	261.35
182	1128	B	27	X	1	242.10	19.95	262.05
182	1128	B	27	X	2	243.60	19.95	263.55
182	1128	B	27	X	3	245.10	19.95	265.05
182	1128	B	27	X	4	246.60	19.95	266.55
182	1128	B	28	X	1	251.80	19.95	271.75
182	1128	B	28	X	2	253.15	19.95	273.10
182	1128	B	28	X	3	254.34	19.95	274.29
182	1128	B	29	X	1	261.50	19.95	281.45
182	1128	B	29	X	2	262.13	19.95	282.08
182	1128	B	30	X	1	271.10	19.95	291.05
182	1128	B	30	X	2	272.48	19.95	292.43
182	1128	C	1	H	1	0.00	0.08	0.08
182	1128	C	1	H	2	1.50	0.08	1.58
182	1128	C	1	H	3	3.00	0.08	3.08
182	1128	C	1	H	4	4.50	0.08	4.58
182	1128	C	1	H	5	6.00	0.08	6.08
182	1128	C	1	H	6	7.50	0.08	7.58
182	1128	C	2	H	1	8.00	2.04	10.04
182	1128	C	2	H	2	9.50	2.04	11.54
182	1128	C	2	H	3	11.00	2.04	13.04
182	1128	C	2	H	4	12.50	2.04	14.54
182	1128	C	2	H	5	14.00	2.04	16.04
182	1128	C	2	H	6	15.50	2.04	17.54
182	1128	C	3	H	1	17.50	1.76	19.26
182	1128	C	3	H	2	19.00	1.76	20.76
182	1128	C	3	H	3	20.50	1.76	22.26
182	1128	C	3	H	4	22.00	1.76	23.76
182	1128	C	3	H	5	23.50	1.76	25.26
182	1128	C	3	H	6	25.00	1.76	26.76
182	1128	C	3	H	7	26.00	1.76	27.76
182	1128	C	4	H	1	27.00	1.76	28.76
182	1128	C	4	H	2	28.50	1.76	30.26
182	1128	C	4	H	3	30.00	1.76	31.76
182	1128	C	4	H	4	31.50	1.76	33.26
182	1128	C	4	H	5	33.00	1.76	34.76
182	1128	C	5	H	1	36.50	2.42	38.92
182	1128	C	5	H	2	38.00	2.42	40.42
182	1128	C	5	H	3	39.50	2.42	41.92
182	1128	C	5	H	4	41.00	2.42	43.42
182	1128	C	5	H	5	42.50	2.42	44.92
182	1128	C	5	H	6	44.00	2.42	46.42
182	1128	C	5	H	7	45.50	2.42	47.92
182	1128	C	6	H	1	46.00	3.68	49.68
182	1128	C	6	H	2	47.50	3.68	51.18
182	1128	C	6	H	3	49.00	3.68	52.68
182	1128	C	6	H	4	50.50	3.68	54.18
182	1128	C	6	H	5	52.00	3.68	55.68
182	1128	C	6	H	6	53.50	3.68	57.18
182	1128	C	6	H	7	54.30	3.68	57.98

Table T3 (continued).

Leg	Site	Hole	Core	Type	Section	Depth (mbsf)	Offset	Depth (mcd)
182	1128	C	7	H	1	55.50	3.68	59.18
182	1128	C	7	H	2	57.00	3.68	60.68
182	1128	C	7	H	3	58.50	3.68	62.18
182	1128	C	7	H	4	60.00	3.68	63.68
182	1128	C	7	H	5	61.50	3.68	65.18
182	1128	C	7	H	6	63.00	3.68	66.68
182	1128	C	8	H	1	65.00	3.68	68.68
182	1128	C	8	H	2	66.50	3.68	70.18
182	1128	C	8	H	3	68.00	3.68	71.68
182	1128	C	8	H	4	69.50	3.68	73.18
182	1128	C	8	H	5	71.00	3.68	74.68
182	1128	C	8	H	6	72.50	3.68	76.18
182	1128	C	9	H	1	74.50	8.18	82.68
182	1128	C	9	H	2	76.00	8.18	84.18
182	1128	C	9	H	3	77.50	8.18	85.68
182	1128	C	9	H	4	79.00	8.18	87.18
182	1128	C	9	H	5	80.50	8.18	88.68
182	1128	C	9	H	6	82.00	8.18	90.18
182	1128	C	9	H	7	83.50	8.18	91.68
182	1128	C	10	H	1	84.00	9.46	93.46
182	1128	C	10	H	2	85.50	9.46	94.96
182	1128	C	10	H	3	87.00	9.46	96.46
182	1128	C	10	H	4	88.50	9.46	97.96
182	1128	C	10	H	5	90.00	9.46	99.46
182	1128	C	10	H	6	91.50	9.46	100.96
182	1128	C	10	H	7	93.00	9.46	102.46
182	1128	C	11	H	1	93.50	9.88	103.38
182	1128	C	11	H	2	95.00	9.88	104.88
182	1128	C	11	H	3	96.50	9.88	106.38
182	1128	C	11	H	4	98.00	9.88	107.88
182	1128	C	11	H	5	99.50	9.88	109.38
182	1128	C	11	H	6	101.00	9.88	110.88
182	1128	C	11	H	7	102.10	9.88	111.98
182	1128	C	12	H	1	103.00	10.10	113.10
182	1128	C	12	H	2	104.50	10.10	114.60
182	1128	C	12	H	3	106.00	10.10	116.10
182	1128	C	12	H	4	107.50	10.10	117.60
182	1128	C	12	H	5	109.00	10.10	119.10
182	1128	C	12	H	6	110.50	10.10	120.60
182	1128	C	12	H	7	112.00	10.10	122.10
182	1128	C	13	H	1	112.50	11.60	124.10
182	1128	C	13	H	2	114.00	11.60	125.60
182	1128	C	13	H	3	115.50	11.60	127.10
182	1128	C	13	H	4	117.00	11.60	128.60
182	1128	C	13	H	5	118.50	11.60	130.10
182	1128	C	13	H	6	120.00	11.60	131.60
182	1128	C	13	H	7	121.50	11.60	133.10
182	1128	C	14	H	1	122.00	12.10	134.10
182	1128	C	14	H	2	123.50	12.10	135.60
182	1128	C	14	H	3	125.00	12.10	137.10
182	1128	C	14	H	4	126.50	12.10	138.60
182	1128	C	14	H	5	128.00	12.10	140.10
182	1128	C	14	H	6	129.50	12.10	141.60
182	1128	C	15	H	1	131.50	13.87	145.37
182	1128	C	15	H	2	133.00	13.87	146.87
182	1128	C	15	H	3	134.50	13.87	148.37
182	1128	C	15	H	4	136.00	13.87	149.87
182	1128	C	15	H	5	137.50	13.87	151.37
182	1128	C	16	X	1	138.30	13.87	152.17
182	1128	C	16	X	2	139.80	13.87	153.67
182	1128	C	16	X	3	141.30	13.87	155.17
182	1128	C	16	X	4	142.80	13.87	156.67
182	1128	C	16	X	5	144.30	13.87	158.17
182	1128	C	16	X	6	145.80	13.87	159.67
182	1128	C	16	X	7	147.30	13.87	161.17
182	1128	C	17	X	1	146.10	15.81	161.91
182	1128	C	17	X	2	147.60	15.81	163.41
182	1128	C	17	X	3	149.10	15.81	164.91
182	1128	C	17	X	4	150.60	15.81	166.41

Table T3 (continued).

Leg	Site	Hole	Core	Type	Section	Depth (mbsf)	Offset	Depth (mcd)
182	1128	C	17	X	5	152.10	15.81	167.91
182	1128	C	18	X	1	155.70	15.81	171.51
182	1128	C	19	X	1	165.30	17.33	182.63
182	1128	C	19	X	2	166.80	17.33	184.13
182	1128	C	19	X	3	168.30	17.33	185.63
182	1128	C	19	X	4	169.80	17.33	187.13
182	1128	C	19	X	5	171.30	17.33	188.63
182	1128	C	19	X	6	172.80	17.33	190.13
182	1128	C	19	X	7	174.30	17.33	191.63
182	1128	C	20	X	1	174.90	18.07	192.97
182	1128	C	20	X	2	176.40	18.07	194.47
182	1128	C	20	X	3	177.90	18.07	195.97
182	1128	C	20	X	4	179.40	18.07	197.47
182	1128	C	20	X	5	180.90	18.07	198.97
182	1128	C	20	X	6	182.40	18.07	200.47
182	1128	C	20	X	7	183.90	18.07	201.97
182	1128	C	21	X	1	184.50	17.95	202.45
182	1128	C	21	X	2	186.00	17.95	203.95
182	1128	C	21	X	3	187.50	17.95	205.45
182	1128	C	21	X	3	187.50	17.95	205.45
182	1128	C	21	X	4	189.00	17.95	206.95
182	1128	C	21	X	4	189.00	17.95	206.95
182	1128	C	21	X	5	190.50	17.95	208.45
182	1128	C	21	X	6	192.00	17.95	209.95
182	1128	C	22	X	1	192.10	18.85	210.95
182	1128	C	21	X	7	193.00	17.95	210.05
182	1128	C	21	X	7	193.03	17.95	210.98
182	1128	C	22	X	2	193.60	18.85	212.45
182	1128	C	22	X	3	195.10	18.85	213.95
182	1128	C	22	X	4	196.60	18.85	215.45
182	1128	C	22	X	5	198.10	18.85	216.95
182	1128	C	22	X	6	199.60	18.85	218.45
182	1128	C	22	X	7	201.10	18.85	219.95
182	1128	C	23	X	1	201.70	18.93	220.63
182	1128	C	23	X	2	203.20	18.93	222.13
182	1128	C	23	X	3	204.70	18.93	223.63
182	1128	C	23	X	4	206.20	18.93	225.13
182	1128	C	23	X	5	207.70	18.93	226.63
182	1128	C	23	X	6	209.20	18.93	228.13
182	1128	C	23	X	7	210.70	18.93	229.63
182	1128	C	24	X	1	211.30	19.29	230.59
182	1128	C	24	X	2	212.80	19.29	232.09
182	1128	C	24	X	3	214.30	19.29	233.59
182	1128	C	24	X	4	215.80	19.29	235.09
182	1128	C	24	X	5	217.30	19.29	236.59
182	1128	C	24	X	6	218.80	19.29	238.09
182	1128	C	24	X	7	220.30	19.29	239.59
182	1128	C	25	X	1	220.90	19.61	240.51
182	1128	C	25	X	2	222.40	19.61	242.01
182	1128	C	25	X	3	223.90	19.61	243.51
182	1128	C	25	X	4	225.40	19.61	245.01
182	1128	C	25	X	5	226.90	19.61	246.51
182	1128	C	25	X	6	228.40	19.61	248.01
182	1128	C	26	X	1	230.50	19.73	250.23
182	1128	C	26	X	2	232.00	19.73	251.73
182	1128	C	26	X	3	233.50	19.73	253.23
182	1128	C	26	X	4	235.00	19.73	254.73
182	1128	C	26	X	5	236.50	19.73	256.23
182	1128	C	26	X	6	238.00	19.73	257.73
182	1128	C	26	X	7	239.50	19.73	259.23

Notes: Depths are measured at the top of each section. This table is also available in **ASCII format.**

Table T4. Biostratigraphic data used for correlation, Site 1128.

Datum	Taxon	Age (Ma)	Leg, hole, core, section, interval (cm)	Depth (mbsf)	Leg, hole, core, section, interval (cm)	Depth (mbsf)
FAD	*Globorotalia truncatulinoides*	2	182-1128B-1H-CC, 14	5.63	182-1128B-2H-CC, 21	15.50
FAD	*G. truncatulinoides*	2	182-1128C-1H-CC, 11	7.93	182-1128C-2H-CC, 15	16.74
LAD	*Pseudoemiliania lacunosa*	0.45	182-1128B-1H-CC, 14	5.63	182-1128B-1H-1, 0	0.00
LAD	*P. lacunosa*	0.45	182-1128C-1H-4, 45	4.95	182-1128C-1H-CC, 11	7.93
LAD	*Calcidiscus macintyrei*	1.67	182-1128B-2H-CC, 21	15.50	182-1128B-3H-2, 18	16.88
LAD	*C. macintyrei*	1.67	182-1128C-1H-CC, 11	7.93	182-1128C-2H-CC, 15	16.74
LAD	*Reticulofenestra pseudoumbilicus*	3.75	182-1128B-3H-CC, 21	23.19	182-1128B-4H-4, 58	29.78
LAD	*R. pseudoumbilicus*	3.75	182-1128C-3H-6, 24	25.24	182-1128C-3H-CC, 0	26.61
LAD	*Globorotalia margaritae*	3.58	182-1128B-3H-CC, 21	23.19	182-1128B-4H-4, 58	29.78
LAD	*G. margaritae*	3.58	182-1128C-3H-6, 24	25.25	182-1128C-3H-CC, 0	26.61
LAD	*Globoquadrina dehiscens*	5.8	182-1128B-6H-3, 98	47.68	182-1128B-6H-CC, 19	53.56
LAD	*G. dehiscens*	5.8	182-1128C-6H-2, 104	48.54	182-1128C-6H-CC, 10	55.15
LAD	*Catinaster altus*	26.1	182-1128B-7H-CC, 21	62.58	182-1128B-8H-6, 79	70.99
LAD	*C. altus*	26.1	182-1128C-8H-CC, 0	73.95	182-1128C-9H-CC, 30	84.42
LAD	*Reticulofenestra umbilicus*	32.3	182-1128B-15H-CC, 11	137.76	182-1128B-16X-CC, 50	147.64
LAD	*R. umbilicus*	32.3	182-1128C-15H-3, 100	135.50	182-1128C-15X-CC, 13	138.30

Note: FAD = first appearance datum, LAD = last appearance datum.

Table T5. Magnetostratigraphic datums, Site 1128.

Chron boundary	Age (Ma)	Hole	Depth (mbsf)	Depth (mcd)
C1r - top	0.78	1128B	13.6	14.7
C1r - top	0.78	1128C	10-14	12-16
C2n - top	1.77	1128B	27-30	29-32
C2n - top	1.77	1128C	26-28	28-30
C2An - top	2.581	1128B	37-40	39-42
C2An - top	2.581	1128C	38	40.4
C10n - top	28.28	1128B	75.2	84.2
C10n - top	28.28	1128C	75.8	83.9
C10n - bottom	28.74	1128B	90	100.3
C10n - bottom	28.74	1128C	90.4	99.9
C11n - top	29.4	1128B	100.8	111.6
C11n - top	29.4	1128C	100.3	110.2
C11n - bottom	30.1	1128B	108.2	119
C11n - bottom	30.1	1128C	109	119.1
C12n - top	30.48	1128B	133.8	146.6
C12n - top	30.48	1128C	133	146.9
C12n - bottom	30.94	1128B	137.5	152.3
C12n - bottom	30.94	1128C	138.2	152.1
C13n - top	33.06	1128B	213.5	232.4
C13n - top	33.06	1128C	213.5	232.8

Table T6. Splice tie points, Site 1128.

Site	Hole	Core	Type	Section	Interval (cm)	Depth (mbsf)	Depth (mcd)		Site	Hole	Core	Type	Section	Interval (cm)	Depth (mbsf)	Depth (mcd)
1128	B	1	H	3	131	4.31	4.31	Tie to	1128	C	1	H	3	123	4.23	4.31
1128	C	1	H	5	107	7.07	7.15	Tie to	1128	B	2	H	1	35	6.05	7.15
1128	B	2	H	5	59	12.29	13.39	Tie to	1128	C	2	H	3	35	11.35	13.39
1128	C	2	H	5	139	15.39	17.43	Tie to	1128	B	3	H	1	42	15.65	17.43
1128	B	3	H	3	83	19.03	20.81	Tie to	1128	C	3	H	2	2	19.05	20.81
1128	C	3	H	7	3	26.03	27.79	Tie to	1128	B	4	H	1	95	25.65	27.79
1128	B	4	H	4	3	29.23	31.37	Tie to	1128	C	4	H	2	111	29.61	31.37
1128	C	4	H	6	51	35.01	36.77	Tie to	1128	B	5	H	1	19	34.39	36.77
1128	B	5	H	7	27	42.97	45.35	Tie to	1128	C	5	H	5	43	42.93	45.35
1128	C	5	H	6	131	45.31	47.73	Tie to	1128	B	6	H	1	83	44.53	47.73
1128	B	6	H	5	3	49.73	52.93	Tie to	1128	C	6	H	3	24	49.25	52.93
1128	C	6	H	7	35	54.65	58.33	Tie to	1128	B	7	H	1	13	53.35	58.33
1128	B	7	H	7	84	62.34	67.32	Append to	1128	C	8	H	1	0	65.00	68.68
1128	C	8	H	4	11	69.61	73.29	Tie to	1128	B	8	H	2	11	64.31	73.29
1128	B	8	H	7	52	72.22	81.2	Append to	1128	B	9	H	1	0	72.20	81.18
1128	B	9	H	7	12	81.32	90.3	Tie to	1128	C	9	H	6	12	82.12	90.30
1128	C	9	H	7	52	84.02	92.2	Tie to	1128	B	10	H	1	20	81.90	92.20
1128	B	10	H	3	136	86.06	96.36	Tie to	1128	C	10	H	2	140	86.90	96.36
1128	C	10	H	7	3	93.03	102.49	Tie to	1128	B	11	H	1	58	91.81	102.49
1128	B	11	H	2	67	93.37	104.05	Tie to	1128	C	11	H	1	67	94.17	104.05
1128	C	11	H	6	76	101.76	111.64	Tie to	1128	B	12	H	1	12	100.82	111.64
1128	B	12	H	5	83	107.53	118.35	Tie to	1128	C	12	H	4	75	108.25	118.35
1128	C	12	H	7	43	112.43	122.53	Tie to	1128	B	13	H	1	37	110.59	122.53
1128	B	13	H	5	75	116.95	128.89	Tie to	1128	C	13	H	4	26	117.29	128.89
1128	C	13	H	6	103	121.03	132.63	Tie to	1128	B	14	H	1	51	120.21	132.63
1128	B	14	H	5	91	126.61	139.03	Tie to	1128	C	14	H	4	43	126.93	139.03
1128	C	14	H	6	75	130.25	142.35	Tie to	1128	B	15	H	1	35	129.55	142.35
1128	B	15	H	4	27	133.56	146.36	Tie to	1128	C	15	H	1	99	132.49	146.36
1128	C	15	H	5	64	138.14	152.01	Append to	1128	C	16	X	1	0	138.30	152.17
1128	C	16	X	CC	40	148.08	161.95									

Note: This table is also available in **ASCII format.**

Table T7. Composition of headspace gases, Site 1128.

Core, section	Depth (mbsf)	C_1 (ppmv)
182-1128B-		
1H-4	4.50	2
2H-5	11.70	2
3H-5	21.20	2
4H-5	30.70	2
5H-4	38.70	2
6H-4	48.20	2
7H-2	54.70	2
8H-3	65.70	2
9H-4	76.70	2
10H-4	86.20	3
11H-2	92.70	2
12H-4	105.20	4
13H-4	114.70	3
14H-4	124.20	6
15H-5	134.76	4
16X-4	142.30	4
17X-4	150.30	5
18X-3	158.40	4
19X-4	169.60	6
20X-4	179.20	5
22X-4	198.40	4
23X-4	208.00	4
24X-4	217.60	5
25X-4	227.20	4
26X-4	236.90	4
27X-3	245.10	2
28X-2	253.15	3
29X-1	261.50	3
30X-1	272.47	4
182-1128D-		
1R-3	234.20	3
2R-2	242.30	2
3R-3	253.40	2
4R-3	263.00	3
5R-CC	269.60	3
8R-3	301.50	3
10R-3	320.60	3
11R-3	330.20	3
12R-2	338.30	2
13R-4	350.90	2
14R-2	357.05	2
15R-2	367.20	2
16R-2	376.11	2
17R-2	386.50	2
18R-2	395.67	2
19R-2	405.90	3
20R-2	414.72	3
21R-2	425.20	2
22R-2	434.80	2
23R-2	444.40	3

Note: ppmv = parts per million by volume.

Table T8. Calcium carbonate ($CaCO_3$), organic carbon (C_{org}), nitrogen (N), and sulfur (S) data, Holes 1128B and 1128D.

Core, section, interval (cm)	Depth (mbsf)	$CaCO_3$ (wt%)	C_{org} (wt%)	N (wt%)	S (wt%)
182-1128B-					
4H-1, 60-61	25.30	88.2	0.07		
4H-3, 60-61	28.30	76.7	0.09		
4H-5, 60-61	31.30	85.6	0.32		
5H-1, 57-58	34.77	87.0	0.09		
5H-3, 59-60	37.79	75.1	0.06		
5H-5, 58-59	40.78	63.0	0.05		
6H-1, 60-61	44.30	80.2			
6H-3, 60-61	47.30	79.3	0.04		
6H-5, 60-61	50.30	87.7	0.06		
8H-3, 59-60	66.29	62.4	0.03		
8H-4, 58-59	67.78	37.8			
8H-5, 59-60	69.29	20.4			
9H-3, 59-60	75.79	36.1			
9H-4, 34-35	77.04	55.9			
9H-5, 59-60	78.79	37.9			
10H-1, 59-60	82.29	53.9	0.13		
10H-3, 59-60	85.29	61.5	0.01		
10H-5, 59-60	88.29	37.3			
11H-1, 60-61	91.80	30.9			0.07
12H-1, 60-61	101.30	5.0			0.05
12H-3, 60-61	104.30	18.3			
12H-5, 60-61	107.30	22.8	0.11		0.07
13H-1, 60-61	110.80	26.6			
13H-3, 60-61	113.80	36.7	0.08		
13H-5, 60-61	116.80	18.8	0.03		
14H-1, 60-61	120.30	21.6	0.04		
14H-3, 60-61	123.30	28.5	0.08		
14H-5, 60-61	126.30	12.1			
15H-1, 60-61	129.80	13.6	0.03		
15H-3, 60-61	132.80	23.0	0.15		
15H-5, 60-61	135.36	88.0	0.41		
16X-1, 60-61	138.40	2.1	0.15		
16X-3, 60-61	141.40	16.5	0.14		0.06
16X-5, 60-61	144.40	29.1	0.16		
17X-1, 60-61	146.40	29.5	0.14		
17X-3, 59-60	149.39	35.9	0.08		
18X-1, 60-61	156.00	8.4	0.1		
18X-3, 60-61	159.00	32.3			
19X-1, 60-61	165.70	32.6	0.04		
19X-3, 60-61	168.70	40.9			
19X-5, 60-61	171.70	36.8			
20X-1, 60-61	175.30	27.9			
20X-3, 60-61	178.30	21.1	0.01		0.08
20X-5, 60-61	181.30	20.4			
22X-1, 60-61	194.50	34.0			
22X-3, 60-61	197.50	20.8	0.03		
22X-5, 60-61	200.50	40.1			
23X-1, 60-62	204.10	33.1			
23X-3, 60-62	207.10	39.2			
23X-5, 60-62	210.10	31.0			
24X-1, 60-61	213.70	37.2			
24X-3, 64-65	216.74	43.2			
24X-5, 64-65	219.74	45.9			0.21
25X-1, 59-60	223.29	48.2			
25X-3, 59-60	226.29	47.3			
25X-5, 59-60	229.29	61.8			
26X-1, 60-61	233.00	45.8			
26X-3, 60-61	236.00	50.9			
26X-5, 60-61	239.00	52.3			
27X-1, 60-61	242.70	50.1			
27X-3, 60-61	245.70	33.8			
28X-1, 59-60	252.39	37.4			
29X-1, 59-61	262.09	32.5			
30X-1, 60-61	271.70	68.0			
182-1128D-					
2R-1, 60-61	241.40	52.6	NA	NA	NA
3R-1, 59-60	250.99	37.6	NA	NA	NA
3R-3, 59-60	253.99	46.7	NA	NA	NA
4R-1, 59-60	260.59	40.8	NA	NA	NA
4R-3, 59-60	263.59	10.1	NA	NA	NA
6R-1, 59-60	279.89	8.8	NA	NA	NA
6R-3, 53-54	282.83	45.9	NA	NA	NA
8R-3, 60-61	302.10	9.9	NA	NA	NA
10R-1, 59-60	318.19	12.6	NA	NA	NA
10R-3, 59-60	321.19	0.8	NA	NA	NA
11R-1, 59-60	327.79	1.4	NA	NA	NA
11R-3, 59-60	330.79	0.8	NA	NA	NA
12R-1, 59-60	337.39	17.5	NA	NA	NA
13R-1, 59-60	346.99	3.1	NA	NA	NA
13R-3, 59-60	349.99	11.1	NA	NA	NA
13R-5, 59-60	352.99	0.2	NA	NA	NA
14R-1, 59-60	356.59	0.5	NA	NA	NA
15R-1, 59-60	366.29	0.1	NA	NA	NA
16R-1, 59-60	375.99		NA	NA	NA
17R-1, 59-60	385.59		NA	NA	NA
18R-1, 60-61	395.30	0.8	NA	NA	NA
19R-1, 60-61	405.00	1.0	NA	NA	NA
20R-1, 60-61	414.60	0.3	NA	NA	NA
20R-3, 55-56	416.77		NA	NA	NA
21R-1, 59-60	424.29	4.4	NA	NA	NA
22R-1, 60-61	433.90	6.4	NA	NA	NA
22R-3, 60-61	436.90	0.1	NA	NA	NA
23R-1, 58-59	443.48	0.2	NA	NA	NA
23R-3, 60-61	446.50	0.1	NA	NA	NA

Note: NA = not analyzed; blank = not detected.

Table T9. Interstitial water geochemistry, Site 1128.

Core, section, interval (cm)	Depth (mbsf)	pH	ppH	Alkalinity (mM)	Salinity	Cl^- (mM)	SO_4^{2-} (mM)	Na^+ (mM)	K^+ (mM)	Mg^{2+} (mM)	Ca^{2+} (mM)	Sr^{2+} (µM)	Li^+ (µM)	$H_4SiO_4^0$ (µM)	NH_4^+ (µM)	Fe (µM)
182-1128A-																
1H-1, 145-150	1.45	7.40	7.47	3.33	34.0	563	27.8	476.9	11.3	52.1	10.4	76	36	392	47	0.9
182-1128B-																
1H-3, 145-150	4.45	6.66	7.31	3.45	34.0	563	27.6	478.9	11.5	52.1	10.8	80	36	488	37	0.4
2H-1, 145-150	7.15	6.94	7.25	3.82	34.0	563	27.6	477.6	11.3	52.6	11.7	92	37	498	58	2.3
2H-4, 145-150	11.65	7.04	7.20	4.15	35.0	567	26.9	480.6	12.2	52.5	11.5	100	40	507	78	9.8
3H-2, 145-150	18.15	6.94	7.20	4.20	35.0	566	27.5	482.4	11.7	52.4	12.1	108	46	522		24.1
3H-4, 145-150	21.15	6.98	7.32	4.42	35.0	566	27.2	478.8	12.4	51.6	12.2	113	48	568	78	18.9
4H-1, 145-150	26.15	7.21	7.30	4.51	35.0	566	26.3	480.3	11.8	51.5	12.3	104	49	356	137	6.5
4H-4, 145-150	30.65	7.02	7.30	4.72	35.0	567	25.8	481.8	12.3	50.2	12.5	117	59	339	126.5	3.4
5H-3, 140-150	38.60	7.15	7.16	5.16	35.0	571	26.2	479.6	11.3	50.4	12.7	117	58	352	119	4.8
6H-3, 140-150	48.10	6.82	6.99	5.08	35.0	566	26.7	472.5	11.9	49.8	13.6	125	63	609	31	2.7
8H-2, 140-150	65.60	7.12	6.99	5.74	35.0	563	26.1	476.4	11.3	50.0	15.1	125	76	691	148	0.0
10H-3, 140-150	86.10	7.05	6.92	5.96	35.0	563	25.9	478.8	11.0	48.8	15.4	129	87	787	177	0.1
12H-3, 140-150	105.10	7.15	NM	5.91	35.0	562	25.0	470.1	10.7	47.8	15.8	125	96	935	182	13.9
14H-3, 140-150	124.10	7.14	NM	5.81	36.0	559	24.5	471.5	10.9	47.1	16.1	125	107	954	87	26.3
16H-3, 140-150	142.20	6.99	NM	7.27	34.5	568	23.7	477.2	10.7	45.6	18.9	141	143	986	260	67.3
18X-2, 145-150	158.35	7.00	6.80	6.25	35.0	561	22.9	469.0	9.9	44.4	18.5	137	149	907	263	54.5
20X-3, 140-150	179.10	6.91	NM	6.96	35.0	561	22.7	470.7	9.5	44.5	19.2	145	159	969	173	60.4
22X-3, 140-150	198.30	7.30	NM	7.30	35.0	561	22.2	468.3	9.2	43.9	19.9	149	175	1126	334	56.7
24X-3, 140-150	217.50	6.98	NM	6.54	35.0	563	21.8	472.7	9.4	43.1	19.0	149	180	1015	350	27.1
26X-3, 140-150	236.80	6.82	NM	7.36	35.0	564	21.6	467.6	8.7	42.9	20.2	149	190	998	220.1	32.6
28X-1, 125-135	253.05	6.86	NM	8.98	32.0	544	13.8	449.7	6.3	33.0	24.8	153	379	831	477.5	35.7
182-1128D-																
1R-2, 140-150	234.10	6.90	NM	6.94	35.0	565	21.6	470.1	9.0	42.9	19.6	149	183	971	196.7	23.0
3R-2, 140-150	253.30	6.78	NM	7.32	33.0	551	15.1	455.7	6.5	34.4	23.1	158	359	806	531.5	32.2
6R-1, 140-150	280.70	6.78	NM	11.73	32.5	551	8.3	461.7	6.4	25.8	24.8	149	466	719	697.1	61.9
8R-2, 140-150	301.40	6.79	NM	9.12	32.0	550	7.3	461.0	5.4	24.3	25.2	170	483	748	830.3	61.1
10R-2, 140-150	320.00	6.85	NM	7.11	33.0	554	13.2	464.9	5.9	30.1	23.1	149	364	606	805.1	54.2
12R-1, 140-150	338.20	6.84	NM	10.98	32.5	551	6.7	459.5	5.3	24.3	25.9	174	486	672	713.3	35.1
14R-1, 95-105	356.95	7.49	NM	11.11	32.0	554	4.7	464.4	5.6	21.9	25.2	170	496	530	893.3	1.2
16R-1, 61-71	376.01	7.38	NM	11.43	32.0	557	4.5	468.0	5.2	22.6	24.8	190	524	564	855.5	0.5
18R-1, 87-97	395.57	7.23	NM	11.23	32.0	555	4.6	464.0	4.8	22.3	25.6	182	476	568	927.5	0.3
20R-1, 61-72	414.61	7.26	NM	10.69	31.5	554	2.9	462.5	4.6	21.4	25.2	174	505	600	972.5	0.00
22R-2, 0-10	434.80	NM	NM	NM	32.0	556	3.0	465.5	4.4	22.2	25.7	178	505	596	985.1	

Note: NM = not measured.

Table T10. Summary of X-ray diffraction analysis, Site 1128. (See table notes. Continued on next page.)

Leg	Site	Hole	Core	Type	Section	Top (cm)	Bottom (cm)	Depth (mbsf)	LMC/quartz
182	1128	B	4	H	1	60	61	25.30	83.33
182	1128	B	4	H	3	60	61	28.30	30.88
182	1128	B	4	H	5	60	61	31.30	69.62
182	1128	B	5	H	1	57	58	34.77	46.74
182	1128	B	5	H	3	59	60	37.79	20.37
182	1128	B	5	H	5	58	59	40.78	8.73
182	1128	B	6	H	1	60	61	44.30	43.23
182	1128	B	6	H	3	60	61	47.30	47.50
182	1128	B	6	H	5	60	61	50.30	65.69
182	1128	B	8	H	3	59	60	66.29	28.07
182	1128	B	8	H	4	58	59	67.78	9.92
182	1128	B	8	H	5	59	60	69.29	4.00
182	1128	B	9	H	3	59	60	75.79	7.70
182	1128	B	9	H	4	34	35	77.04	20.46
182	1128	B	9	H	5	59	60	78.79	8.96
182	1128	B	10	H	1	59	60	82.29	17.42
182	1128	B	10	H	3	59	60	85.29	23.73
182	1128	B	10	H	5	59	60	88.29	6.71
182	1128	B	11	H	1	60	61	91.80	4.91
182	1128	B	12	H	1	60	61	101.30	0.41
182	1128	B	12	H	3	60	61	104.30	2.45
182	1128	B	12	H	5	60	61	107.30	3.41
182	1128	B	13	H	1	60	61	110.80	4.21
182	1128	B	13	H	3	60	61	113.80	5.95
182	1128	B	13	H	5	60	61	116.80	2.68
182	1128	B	14	H	1	60	61	120.30	3.11
182	1128	B	14	H	3	60	61	123.30	3.84
182	1128	B	14	H	5	60	61	126.30	1.02
182	1128	B	15	H	1	60	61	129.80	1.37
182	1128	B	15	H	3	60	61	132.80	2.04
182	1128	B	15	H	5	60	61	135.36	100.00
182	1128	B	16	X	1	60	61	138.40	0.27
182	1128	B	16	X	3	60	61	141.40	1.98
182	1128	B	16	X	5	60	61	144.40	5.23
182	1128	B	17	X	1	60	61	146.40	2.42
182	1128	B	17	X	3	59	60	149.39	6.81
182	1128	B	18	X	1	60	61	156.00	1.95
182	1128	B	18	X	3	60	61	159.00	3.96
182	1128	B	19	X	1	60	61	165.70	5.61
182	1128	B	19	X	3	60	61	168.70	8.05
182	1128	B	19	X	5	60	61	171.70	6.79
182	1128	B	20	X	1	60	61	175.30	4.53
182	1128	B	20	X	3	60	61	178.30	5.82
182	1128	B	20	X	5	60	61	181.30	5.20
182	1128	B	22	X	1	60	61	194.50	7.88
182	1128	B	22	X	3	60	61	197.50	3.76
182	1128	B	22	X	5	60	61	200.50	9.44
182	1128	B	23	X	1	60	62	204.10	6.56
182	1128	B	23	X	3	60	62	207.10	8.11
182	1128	B	23	X	5	60	62	210.10	6.44
182	1128	B	24	X	1	60	61	213.70	9.14
182	1128	B	24	X	3	64	65	216.74	14.59
182	1128	B	24	X	5	64	65	219.74	11.68
182	1128	B	25	X	1	59	60	223.29	20.25
182	1128	B	25	X	3	59	60	226.29	10.87
182	1128	B	25	X	5	59	60	229.29	36.03
182	1128	B	26	X	1	60	61	233.00	10.14
182	1128	B	26	X	3	60	61	236.00	20.83
182	1128	B	26	X	5	60	61	239.00	21.52
182	1128	D	2	R	1	60	61	241.40	13.30
182	1128	B	27	X	1	60	61	242.70	11.10
182	1128	B	27	X	3	60	61	245.70	3.76
182	1128	D	3	R	1	59	60	250.99	4.98
182	1128	B	28	X	1	59	60	252.39	8.83
182	1128	D	4	R	1	59	60	260.59	11.37
182	1128	B	29	X	1	59	61	262.09	7.26
182	1128	B	30	X	1	60	61	271.70	100.00
182	1128	D	6	R	1	59	60	279.89	1.35

Table T10 (continued).

Leg	Site	Hole	Core	Type	Section	Top (cm)	Bottom (cm)	Depth (mbsf)	LMC/quartz
182	1128	D	8	R	3	60	61	302.10	2.04
182	1128	D	10	R	1	59	60	318.19	1.85
182	1128	D	11	R	1	59	60	327.79	0.18
182	1128	D	12	R	1	59	60	337.39	2.81
182	1128	D	13	R	1	59	60	346.99	1.30
182	1128	D	14	R	1	59	60	356.59	0.02
182	1128	D	15	R	1	59	60	366.29	0.00
182	1128	D	16	R	1	59	61	375.99	0.01
182	1128	D	17	R	1	59	60	385.59	0.00
182	1128	D	18	R	1	60	61	395.30	0.00
182	1128	D	19	R	1	60	61	405.00	0.00
182	1128	D	20	R	1	60	61	414.60	0.00
182	1128	D	21	R	1	59	60	424.29	0.52
182	1128	D	22	R	1	60	61	433.90	1.34
182	1128	D	23	R	1	58	59	443.48	0.00

Notes: LMC = low-Mg calcite. This table is also available in **ASCII format.**

Table T11. *P*-wave velocity measurements from the multisensor track, Site 1128.

Leg	Site	Hole	Core	Type	Section	Interval (cm)	Depth (mbsf)	V_p (km/s)
182	1128	A	1	H	1	3.00	0.03	1.8844
182	1128	A	1	H	1	123.00	1.23	1.6825
182	1128	A	1	H	1	127.00	1.27	1.8320
182	1128	A	1	H	1	131.00	1.31	1.7960
182	1128	A	1	H	1	135.00	1.35	1.8173
182	1128	A	1	H	1	139.00	1.39	1.9721
182	1128	A	1	H	1	143.00	1.43	1.8241
182	1128	A	1	H	2	15.00	1.65	1.8152
182	1128	A	1	H	2	19.00	1.69	1.9054
182	1128	A	1	H	2	27.00	1.77	1.8078
182	1128	A	1	H	2	31.00	1.81	1.8719
182	1128	A	1	H	2	35.00	1.85	1.5141
182	1128	A	1	H	2	39.00	1.89	1.5868
182	1128	A	1	H	2	43.00	1.93	1.8073
182	1128	A	1	H	2	47.00	1.97	1.6124
182	1128	A	1	H	2	55.00	2.05	1.5799
182	1128	A	1	H	2	59.00	2.09	1.6471
182	1128	A	1	H	2	63.00	2.13	1.5314
182	1128	A	1	H	2	67.00	2.17	1.5214
182	1128	A	1	H	2	71.00	2.21	1.8113
182	1128	A	1	H	2	75.00	2.25	1.5165
182	1128	A	1	H	2	79.00	2.29	1.5130
182	1128	A	1	H	2	87.00	2.37	1.5253
182	1128	A	1	H	2	91.00	2.41	1.5137
182	1128	A	1	H	2	95.00	2.45	1.6480
182	1128	A	1	H	2	99.00	2.49	1.9036
182	1128	A	1	H	2	103.00	2.53	1.6995
182	1128	A	1	H	2	115.00	2.65	1.7083
182	1128	A	1	H	2	119.00	2.69	1.5103
182	1128	A	1	H	2	127.00	2.77	1.8279
182	1128	A	1	H	2	131.00	2.81	1.8440
182	1128	A	1	H	2	135.00	2.85	1.8707
182	1128	A	1	H	2	139.00	2.89	1.9142
182	1128	A	1	H	2	143.00	2.93	1.9780
182	1128	A	1	H	3	3.00	3.03	1.8817
182	1128	A	1	H	3	31.00	3.31	1.7349
182	1128	A	1	H	3	35.00	3.35	1.6156
182	1128	A	1	H	3	39.00	3.39	1.9522
182	1128	A	1	H	3	47.00	3.47	1.7276
182	1128	A	1	H	3	51.00	3.51	1.5155
182	1128	A	1	H	3	55.00	3.55	1.5162
182	1128	A	1	H	3	67.00	3.67	1.9762
182	1128	A	1	H	3	75.00	3.75	1.6187
182	1128	A	1	H	3	79.00	3.79	1.9798
182	1128	A	1	H	3	83.00	3.83	1.9006
182	1128	A	1	H	3	95.00	3.95	1.7809
182	1128	A	1	H	3	99.00	3.99	1.6707
182	1128	A	1	H	3	111.00	4.11	1.9290
182	1128	A	1	H	3	115.00	4.15	1.8498
182	1128	A	1	H	3	131.00	4.31	1.8235
182	1128	A	1	H	3	135.00	4.35	1.9199
182	1128	A	1	H	3	139.00	4.39	1.6945
182	1128	A	1	H	3	143.00	4.43	1.8509
182	1128	A	1	H	4	23.00	4.73	1.5939
182	1128	A	1	H	4	27.00	4.77	1.5190
182	1128	A	1	H	4	35.00	4.85	1.5190
182	1128	A	1	H	4	39.00	4.89	1.5204
182	1128	A	1	H	4	43.00	4.93	1.5223
182	1128	A	1	H	4	47.00	4.97	1.5174
182	1128	A	1	H	4	51.00	5.01	1.5156
182	1128	A	1	H	4	55.00	5.05	1.5170
182	1128	A	1	H	4	59.00	5.09	1.5202
182	1128	A	1	H	4	63.00	5.13	1.5206
182	1128	A	1	H	4	67.00	5.17	1.5255
182	1128	A	1	H	4	71.00	5.21	1.5369

Note: Only a portion of this table appears here. The complete table is available in **ASCII format.**

Table T12. Gamma-ray attenuation densiometry measurements from the multisensor track, Site 1128.

Leg	Site	Hole	Core	Type	Section	Interval (cm)	Depth (mbsf)	Density (g/cm^3)	Corrected density (g/cm^3)
182	1128	A	1	H	1	3.0	0.03	1.43	1.34
182	1128	A	1	H	1	7.0	0.07	1.42	1.33
182	1128	A	1	H	1	11.0	0.11	1.40	1.31
182	1128	A	1	H	1	15.0	0.15	1.39	1.30
182	1128	A	1	H	1	19.0	0.19	1.42	1.34
182	1128	A	1	H	1	23.0	0.23	1.52	1.45
182	1128	A	1	H	1	27.0	0.27	1.57	1.50
182	1128	A	1	H	1	31.0	0.31	1.58	1.51
182	1128	A	1	H	1	35.0	0.35	1.49	1.41
182	1128	A	1	H	1	39.0	0.39	1.43	1.34
182	1128	A	1	H	1	43.0	0.43	1.41	1.33
182	1128	A	1	H	1	47.0	0.47	1.42	1.33
182	1128	A	1	H	1	51.0	0.51	1.41	1.33
182	1128	A	1	H	1	63.0	0.63	1.52	1.45
182	1128	A	1	H	1	67.0	0.67	1.58	1.50
182	1128	A	1	H	1	71.0	0.71	1.64	1.57
182	1128	A	1	H	1	75.0	0.75	1.63	1.56
182	1128	A	1	H	1	79.0	0.79	1.65	1.58
182	1128	A	1	H	1	83.0	0.83	1.66	1.59
182	1128	A	1	H	1	87.0	0.87	1.66	1.60
182	1128	A	1	H	1	91.0	0.91	1.65	1.59
182	1128	A	1	H	1	95.0	0.95	1.68	1.61
182	1128	A	1	H	1	99.0	0.99	1.67	1.60
182	1128	A	1	H	1	103.0	1.03	1.66	1.59
182	1128	A	1	H	1	107.0	1.07	1.66	1.59
182	1128	A	1	H	1	111.0	1.11	1.65	1.58
182	1128	A	1	H	1	115.0	1.15	1.64	1.57
182	1128	A	1	H	1	119.0	1.19	1.64	1.57
182	1128	A	1	H	1	123.0	1.23	1.65	1.58
182	1128	A	1	H	1	127.0	1.27	1.66	1.59
182	1128	A	1	H	1	131.0	1.31	1.65	1.58
182	1128	A	1	H	1	135.0	1.35	1.67	1.60
182	1128	A	1	H	1	139.0	1.39	1.67	1.61
182	1128	A	1	H	1	143.0	1.43	1.66	1.59
182	1128	A	1	H	2	3.0	1.53	1.69	1.62
182	1128	A	1	H	2	7.0	1.57	1.66	1.59
182	1128	A	1	H	2	11.0	1.61	1.57	1.50
182	1128	A	1	H	2	15.0	1.65	1.72	1.65
182	1128	A	1	H	2	19.0	1.69	1.73	1.66
182	1128	A	1	H	2	23.0	1.73	1.67	1.61
182	1128	A	1	H	2	27.0	1.77	1.79	1.73
182	1128	A	1	H	2	31.0	1.81	1.69	1.63
182	1128	A	1	H	2	35.0	1.85	1.69	1.63
182	1128	A	1	H	2	39.0	1.89	1.68	1.62
182	1128	A	1	H	2	43.0	1.93	1.69	1.62
182	1128	A	1	H	2	47.0	1.97	1.68	1.62
182	1128	A	1	H	2	51.0	2.01	1.69	1.62
182	1128	A	1	H	2	55.0	2.05	1.67	1.60
182	1128	A	1	H	2	59.0	2.09	1.68	1.61
182	1128	A	1	H	2	63.0	2.13	1.67	1.60
182	1128	A	1	H	2	67.0	2.17	1.67	1.61
182	1128	A	1	H	2	71.0	2.21	1.68	1.61
182	1128	A	1	H	2	75.0	2.25	1.69	1.62
182	1128	A	1	H	2	79.0	2.29	1.66	1.59
182	1128	A	1	H	2	83.0	2.33	1.64	1.57
182	1128	A	1	H	2	87.0	2.37	1.65	1.58
182	1128	A	1	H	2	91.0	2.41	1.63	1.56
182	1128	A	1	H	2	95.0	2.45	1.63	1.56
182	1128	A	1	H	2	99.0	2.49	1.63	1.56
182	1128	A	1	H	2	103.0	2.53	1.65	1.58
182	1128	A	1	H	2	107.0	2.57	1.65	1.58
182	1128	A	1	H	2	111.0	2.61	1.62	1.55
182	1128	A	1	H	2	115.0	2.65	1.64	1.57
182	1128	A	1	H	2	119.0	2.69	1.64	1.57

Note: Only a portion of this table appears here. The complete table is available in **ASCII format.**

Table T13. Magnetic susceptibility measurements from the multisensor track, Site 1128.

Leg	Site	Hole	Core	Type	Section	Interval (cm)	Depth (mbsf)	Magnetic susceptibility (10^{-6}; SI units)	Corrected susceptibility (10^{-6}; SI units)
182	1128	A	1	H	1	3.0	0.03	18.6	18.6
182	1128	A	1	H	1	11.0	0.11	17.8	17.8
182	1128	A	1	H	1	19.0	0.19	16.5	16.5
182	1128	A	1	H	1	27.0	0.27	21.5	21.5
182	1128	A	1	H	1	35.0	0.35	18.0	18.0
182	1128	A	1	H	1	43.0	0.43	14.1	14.1
182	1128	A	1	H	1	51.0	0.51	16.6	16.6
182	1128	A	1	H	1	59.0	0.59	17.7	17.7
182	1128	A	1	H	1	67.0	0.67	21.2	21.2
182	1128	A	1	H	1	75.0	0.75	22.2	22.2
182	1128	A	1	H	1	83.0	0.83	21.1	21.1
182	1128	A	1	H	1	91.0	0.91	25.9	25.9
182	1128	A	1	H	1	99.0	0.99	33.2	33.2
182	1128	A	1	H	1	107.0	1.07	42.3	42.3
182	1128	A	1	H	1	115.0	1.15	42.7	42.7
182	1128	A	1	H	1	123.0	1.23	41.1	41.1
182	1128	A	1	H	1	131.0	1.31	33.0	33.0
182	1128	A	1	H	1	139.0	1.39	29.2	29.2
182	1128	A	1	H	2	3.0	1.53	22.0	22.0
182	1128	A	1	H	2	11.0	1.61	22.2	22.2
182	1128	A	1	H	2	35.0	1.85	41.3	41.3
182	1128	A	1	H	2	43.0	1.93	20.4	20.4
182	1128	A	1	H	2	51.0	2.01	23.0	23.0
182	1128	A	1	H	2	59.0	2.09	26.5	26.5
182	1128	A	1	H	2	67.0	2.17	36.4	36.4
182	1128	A	1	H	2	75.0	2.25	48.7	48.7
182	1128	A	1	H	2	83.0	2.33	59.4	59.4
182	1128	A	1	H	2	91.0	2.41	46.8	46.8
182	1128	A	1	H	2	99.0	2.49	36.8	36.8
182	1128	A	1	H	2	107.0	2.57	38.7	38.7
182	1128	A	1	H	2	115.0	2.65	36.2	36.2
182	1128	A	1	H	2	123.0	2.73	39.1	39.1
182	1128	A	1	H	2	131.0	2.81	58.8	58.8
182	1128	A	1	H	2	139.0	2.89	47.6	47.6
182	1128	A	1	H	2	147.0	2.97	43.0	43.0
182	1128	A	1	H	3	3.0	3.03	62.5	62.5
182	1128	A	1	H	3	11.0	3.11	82.9	82.9
182	1128	A	1	H	3	19.0	3.19	63.4	63.4
182	1128	A	1	H	3	27.0	3.27	55.3	55.3
182	1128	A	1	H	3	35.0	3.35	66.7	66.7
182	1128	A	1	H	3	43.0	3.43	78.0	78.0
182	1128	A	1	H	3	51.0	3.51	83.6	83.6
182	1128	A	1	H	3	59.0	3.59	59.0	59.0
182	1128	A	1	H	3	67.0	3.67	28.9	28.9
182	1128	A	1	H	3	75.0	3.75	31.1	31.1
182	1128	A	1	H	3	83.0	3.83	40.0	40.0
182	1128	A	1	H	3	91.0	3.91	52.8	52.8
182	1128	A	1	H	3	99.0	3.99	67.7	67.7
182	1128	A	1	H	3	107.0	4.07	58.9	58.9
182	1128	A	1	H	3	115.0	4.15	50.2	50.2
182	1128	A	1	H	3	123.0	4.23	61.6	61.6
182	1128	A	1	H	3	131.0	4.31	78.2	78.2
182	1128	A	1	H	3	139.0	4.39	72.5	72.5
182	1128	A	1	H	3	147.0	4.47	52.3	52.3
182	1128	A	1	H	4	3.0	4.53	34.2	34.2
182	1128	A	1	H	4	11.0	4.61	32.1	32.1
182	1128	A	1	H	4	19.0	4.69	33.0	33.0
182	1128	A	1	H	4	27.0	4.77	42.0	42.0
182	1128	A	1	H	4	35.0	4.85	55.9	55.9
182	1128	A	1	H	4	43.0	4.93	61.0	61.0
182	1128	A	1	H	4	51.0	5.01	60.4	60.4
182	1128	A	1	H	4	59.0	5.09	50.6	50.6
182	1128	A	1	H	4	67.0	5.17	43.0	43.0
182	1128	A	1	H	4	75.0	5.25	29.7	29.7

Note: Only a portion of this table appears here. The complete table is available in **ASCII format.**

Table T14. Natural gamma-ray measurements from the multisensor track, Site 1128.

Leg	Site	Hole	Core	Type	Section	Interval (cm)	Depth (mbsf)	NGR (cps)
182	1128	A	1	H	1	11.0	0.11	13.89
182	1128	A	1	H	1	27.0	0.27	14.42
182	1128	A	1	H	1	43.0	0.43	10.04
182	1128	A	1	H	1	59.0	0.59	7.04
182	1128	A	1	H	1	75.0	0.75	5.58
182	1128	A	1	H	1	91.0	0.91	4.73
182	1128	A	1	H	1	107.0	1.07	2.69
182	1128	A	1	H	1	123.0	1.23	3.46
182	1128	A	1	H	2	11.0	1.61	2.50
182	1128	A	1	H	2	27.0	1.77	2.19
182	1128	A	1	H	2	43.0	1.93	1.73
182	1128	A	1	H	2	59.0	2.09	2.92
182	1128	A	1	H	2	75.0	2.25	5.23
182	1128	A	1	H	2	91.0	2.41	5.77
182	1128	A	1	H	2	107.0	2.57	5.19
182	1128	A	1	H	2	123.0	2.73	6.42
182	1128	A	1	H	2	139.0	2.89	8.19
182	1128	A	1	H	3	11.0	3.11	9.62
182	1128	A	1	H	3	27.0	3.27	5.92
182	1128	A	1	H	3	43.0	3.43	8.58
182	1128	A	1	H	3	59.0	3.59	5.58
182	1128	A	1	H	3	75.0	3.75	2.23
182	1128	A	1	H	3	91.0	3.91	4.81
182	1128	A	1	H	3	107.0	4.07	5.77
182	1128	A	1	H	3	123.0	4.23	7.00
182	1128	A	1	H	3	139.0	4.39	7.85
182	1128	A	1	H	4	11.0	4.61	4.96
182	1128	A	1	H	4	27.0	4.77	3.50
182	1128	A	1	H	4	43.0	4.93	6.27
182	1128	A	1	H	4	59.0	5.09	4.46
182	1128	A	1	H	4	75.0	5.25	2.39
182	1128	A	1	H	4	91.0	5.41	4.89
182	1128	A	1	H	4	107.0	5.57	7.12
182	1128	A	1	H	4	123.0	5.73	4.15
182	1128	A	1	H	4	139.0	5.89	6.23
182	1128	A	1	H	5	11.0	6.11	5.23
182	1128	A	1	H	5	27.0	6.27	6.00
182	1128	A	1	H	5	43.0	6.43	4.15
182	1128	A	1	H	5	59.0	6.59	6.92
182	1128	A	1	H	5	75.0	6.75	6.65
182	1128	A	1	H	5	91.0	6.91	6.08
182	1128	A	1	H	5	107.0	7.07	3.04
182	1128	A	1	H	5	123.0	7.23	4.58
182	1128	A	1	H	5	139.0	7.39	6.23
182	1128	A	1	H	6	11.0	7.61	4.27
182	1128	A	1	H	6	27.0	7.77	5.62
182	1128	A	1	H	6	43.0	7.93	3.50
182	1128	A	1	H	6	59.0	8.09	4.23
182	1128	A	1	H	6	75.0	8.25	3.50
182	1128	A	1	H	7	11.0	8.61	4.85
182	1128	A	1	H	7	27.0	8.77	5.35
182	1128	A	1	H	7	43.0	8.93	3.08
182	1128	A	1	H	7	59.0	9.09	4.15
182	1128	B	1	H	1	11.0	0.11	18.62
182	1128	B	1	H	1	27.0	0.27	22.96
182	1128	B	1	H	1	43.0	0.43	29.08
182	1128	B	1	H	1	59.0	0.59	29.27
182	1128	B	1	H	1	75.0	0.75	30.81
182	1128	B	1	H	1	91.0	0.91	34.04
182	1128	B	1	H	1	107.0	1.07	26.92
182	1128	B	1	H	1	123.0	1.23	23.54
182	1128	B	1	H	2	11.0	1.61	11.69
182	1128	B	1	H	2	27.0	1.77	17.12
182	1128	B	1	H	2	43.0	1.93	12.92

Notes: NGR = natural gamma radiation. Only a portion of this table appears here. The complete table is available in **ASCII format.**

Table T15. Thermal conductivity measurements, Site 1128.

Leg	Site	Hole	Core	Core	Section	Interval (cm)	Depth (mbsf)	Thermal conductivity (W/[m·K])
182	1128	B	1	H	3	75.0	3.75	1.003
182	1128	B	2	H	3	75.0	9.45	1.014
182	1128	B	3	H	3	75.0	18.95	1.001
182	1128	B	4	H	3	75.0	28.45	1.084
182	1128	B	5	H	3	75.0	37.95	1.016
182	1128	B	6	H	3	75.0	47.45	0.775
182	1128	B	7	H	3	75.0	56.25	0.787
182	1128	B	8	H	3	75.0	66.45	0.929
182	1128	B	9	H	3	75.0	75.95	0.915
182	1128	B	10	H	3	75.0	85.45	0.936
182	1128	B	11	H	2	50.0	93.20	0.887
182	1128	B	11	H	2	110.0	93.80	1.073
182	1128	B	12	H	2	78.0	102.98	0.956
182	1128	B	13	H	3	75.0	113.95	0.989
182	1128	B	14	H	3	75.0	123.45	0.999
182	1128	B	15	H	3	75.0	132.95	0.973
182	1128	B	16	X	3	75.0	141.55	0.795
182	1128	B	17	X	3	75.0	149.55	1.113
182	1128	B	18	X	3	75.0	159.15	0.756
182	1128	B	19	X	3	75.0	168.85	0.869
182	1128	B	20	X	3	75.0	178.45	0.760
182	1128	B	22	X	3	75.0	197.65	0.634
182	1128	B	23	X	3	75.0	207.25	0.842
182	1128	B	24	X	3	75.0	216.85	0.928
182	1128	B	25	X	3	78.0	226.48	0.961
182	1128	B	26	X	3	75.0	236.15	0.974
182	1128	B	27	X	3	75.0	245.85	1.038
182	1128	B	28	X	2	75.0	253.90	1.014
182	1128	B	30	X	1	75.0	271.85	1.056
182	1128	C	1	H	3	75.0	3.75	1.050
182	1128	C	2	H	3	75.0	11.75	1.121
182	1128	C	3	H	3	75.0	21.25	0.976
182	1128	C	4	H	3	75.0	30.75	1.113
182	1128	C	5	H	3	75.0	40.25	0.987
182	1128	C	6	H	3	75.0	49.75	1.204
182	1128	C	7	H	3	75.0	59.25	0.963
182	1128	C	8	H	3	75.0	68.75	1.163
182	1128	C	8	H	1	75.0	65.75	0.907
182	1128	C	8	H	5	75.0	71.75	0.957
182	1128	C	9	H	3	75.0	78.25	0.926
182	1128	C	10	H	3	75.0	87.75	0.827
182	1128	C	12	H	2	75.0	105.25	0.921
182	1128	C	11	H	3	75.0	97.25	1.010
182	1128	C	12	H	4	75.0	108.25	0.910
182	1128	C	12	H	6	75.0	111.25	0.987
182	1128	C	13	H	3	75.0	116.25	0.938
182	1128	C	14	H	3	75.0	125.75	0.924
182	1128	C	15	H	3	75.0	135.25	1.134
182	1128	C	16	X	3	75.0	142.05	0.891
182	1128	C	17	X	3	75.0	149.85	0.882
182	1128	C	19	X	3	75.0	169.05	0.898
182	1128	C	20	X	3	75.0	178.65	0.874
182	1128	C	21	X	3	75.0	188.25	0.860
182	1128	C	22	X	3	75.0	195.85	0.797
182	1128	C	23	X	3	75.0	205.45	0.850
182	1128	C	24	X	3	75.0	215.05	0.881
182	1128	C	25	X	3	75.0	224.65	0.939
182	1128	C	26	X	3	75.0	234.25	1.023
182	1128	C	1	H	3	75.0	3.75	1.050
182	1128	C	2	H	3	75.0	11.75	1.121
182	1128	C	3	H	3	75.0	21.25	0.976
182	1128	C	4	H	3	75.0	30.75	1.113
182	1128	C	5	H	3	75.0	40.25	0.987

Note: Only a portion of this table appears here. The complete table is available in **ASCII format.**

Table T16. Discrete *P*-wave velocity measurements using PWS1, PWS2, and PWS3, Site 1128.

Leg	Site	Hole	Core	Type	Section	Interval (cm)	Depth (mbsf)	PWS 1, 2, or 3	V_p (km/s)
182	1128	B	1	H	1	33.8	0.34	2	1.5649
182	1128	B	1	H	1	56.2	0.56	2	1.5578
182	1128	B	1	H	1	97.5	0.98	2	1.5266
182	1128	B	1	H	2	25.1	1.75	2	1.5414
182	1128	B	1	H	2	59.2	2.09	2	1.5334
182	1128	B	1	H	2	78.5	2.29	2	1.5709
182	1128	B	1	H	2	89.2	2.39	2	1.5578
182	1128	B	1	H	2	100.6	2.51	2	1.6882
182	1128	B	1	H	2	114.8	2.65	2	1.5357
182	1128	B	1	H	2	131.9	2.82	2	1.5601
182	1128	B	1	H	3	32.5	3.33	2	1.4984
182	1128	B	1	H	3	76.5	3.77	2	1.5081
182	1128	B	1	H	3	100.1	4.00	2	1.5226
182	1128	B	1	H	3	124.4	4.24	2	1.5260
182	1128	B	1	H	4	17.5	4.68	2	1.5198
182	1128	B	1	H	4	46.6	4.97	2	1.5087
182	1128	B	1	H	4	79.0	5.29	2	1.5721
182	1128	B	2	H	1	61.9	6.32	2	1.5165
182	1128	B	2	H	1	90.9	6.61	2	1.5178
182	1128	B	2	H	1	134.9	7.05	2	1.5305
182	1128	B	2	H	2	36.6	7.57	2	1.5426
182	1128	B	2	H	2	52.8	7.73	2	1.5769
182	1128	B	2	H	2	68.1	7.88	1	1.5267
182	1128	B	2	H	2	68.1	7.88	1	1.5217
182	1128	B	2	H	2	68.4	7.88	2	1.5300
182	1128	B	2	H	2	86.1	8.06	2	1.5323
182	1128	B	2	H	2	105.5	8.26	2	1.5232
182	1128	B	2	H	2	118.1	8.38	2	1.5391
182	1128	B	2	H	2	118.4	8.38	1	1.5267
182	1128	B	2	H	2	118.6	8.39	2	1.5391
182	1128	B	2	H	2	140.3	8.60	2	1.5331
182	1128	B	2	H	3	19.7	8.90	2	1.5125
182	1128	B	2	H	3	52.5	9.23	1	1.5228
182	1128	B	2	H	3	52.5	9.23	2	1.5159
182	1128	B	2	H	3	82.5	9.53	2	1.5238
182	1128	B	2	H	3	107.3	9.77	1	1.5273
182	1128	B	2	H	3	108.5	9.79	2	1.5236
182	1128	B	2	H	3	133.7	10.04	2	1.5294
182	1128	B	2	H	4	18.4	10.38	2	1.5311
182	1128	B	2	H	4	39.9	10.60	1	1.5480
182	1128	B	2	H	4	40.0	10.60	2	1.5438
182	1128	B	2	H	4	40.3	10.60	2	2.1142
182	1128	B	2	H	4	65.2	10.85	2	1.5153
182	1128	B	2	H	4	103.2	11.23	1	1.5451
182	1128	B	2	H	4	103.4	11.23	2	1.5461
182	1128	B	2	H	5	28.1	11.98	2	1.5392
182	1128	B	2	H	5	64.7	12.35	2	1.5566
182	1128	B	2	H	5	81.3	12.51	2	1.5323
182	1128	B	2	H	5	96.6	12.67	2	1.5311
182	1128	B	2	H	5	131.8	13.02	2	1.5649
182	1128	B	2	H	6	9.4	13.29	2	1.5513
182	1128	B	2	H	6	30.8	13.51	2	1.5294
182	1128	B	2	H	6	42.0	13.62	2	1.5715
182	1128	B	2	H	6	62.4	13.82	2	1.5253
182	1128	B	2	H	6	105.7	14.26	2	1.5490
182	1128	B	2	H	6	131.1	14.51	2	1.5514
182	1128	B	3	H	1	38.5	15.59	2	1.5721
182	1128	B	3	H	1	55.1	15.75	2	1.5198
182	1128	B	3	H	1	99.4	16.19	2	1.5625
182	1128	B	3	H	1	99.4	16.19	2	1.5625
182	1128	B	3	H	1	121.6	16.42	2	1.5390
182	1128	B	3	H	2	62.1	17.32	2	1.5643
182	1128	B	3	H	2	97.2	17.67	2	1.5727
182	1128	B	3	H	2	120.8	17.91	2	1.5328

Note: Only a portion of this table appears here. The complete table is available in **ASCII format.**

Table T17. Index properties measurements, Site 1128.

Leg	Site	Hole	Core	Type	Section	Top (cm)	Bottom (cm)	Depth (mbsf)	Bulk water content (%)	Dry water content (%)	Bulk density (g/cm^3)	Dry density (g/cm^3)	Grain density (g/cm^3)	Porosity (%)	Void ratio
182	1128	B	1	H	1	88.0	90.0	0.88	41.9	72.1	1.59	0.93	2.67	65.2	1.88
182	1128	B	1	H	2	69.0	71.0	2.19	38.7	63.2	1.65	1.01	2.70	62.5	1.67
182	1128	B	1	H	2	89.0	91.0	2.39	41.6	71.3	1.61	0.94	2.71	65.3	1.89
182	1128	B	1	H	2	128.0	130.0	2.78	41.4	70.8	1.60	0.94	2.66	64.8	1.84
182	1128	B	1	H	3	89.0	91.0	3.89	38.3	62.1	1.65	1.02	2.66	61.8	1.62
182	1128	B	1	H	4	89.0	91.0	5.39	41.0	69.6	1.61	0.95	2.68	64.6	1.82
182	1128	B	2	H	1	69.0	71.0	6.39	42.1	72.6	1.59	0.92	2.66	65.3	1.89
182	1128	B	2	H	2	69.0	71.0	7.89	42.7	74.6	1.58	0.90	2.65	65.9	1.93
182	1128	B	2	H	3	69.0	71.0	9.39	41.5	70.8	1.61	0.94	2.69	65.1	1.86
182	1128	B	2	H	4	69.0	71.0	10.89	40.2	67.3	1.63	0.97	2.70	63.9	1.77
182	1128	B	2	H	5	69.0	71.0	12.39	39.8	66.0	1.63	0.98	2.66	63.1	1.71
182	1128	B	2	H	6	69.0	71.0	13.89	39.7	65.9	1.63	0.98	2.68	63.3	1.73
182	1128	B	3	H	1	69.0	71.0	15.89	39.2	64.5	1.64	1.00	2.67	62.7	1.68
182	1128	B	3	H	2	69.0	71.0	17.39	37.8	60.8	1.67	1.04	2.70	61.5	1.60
182	1128	B	3	H	3	69.0	71.0	18.89	39.1	64.2	1.64	1.00	2.66	62.5	1.67
182	1128	B	3	H	4	69.0	71.0	20.39	34.4	52.5	1.72	1.13	2.69	57.9	1.38
182	1128	B	3	H	5	69.0	71.0	21.89	36.4	57.3	1.69	1.08	2.70	60.1	1.51
182	1128	B	3	H	6	69.0	71.0	22.89	33.2	49.7	1.75	1.17	2.69	56.6	1.31
182	1128	B	4	H	1	89.0	91.0	25.59	33.2	49.6	1.77	1.18	2.76	57.2	1.34
182	1128	B	4	H	2	75.0	77.0	26.95	35.2	54.3	1.72	1.11	2.72	59.0	1.44
182	1128	B	4	H	3	89.0	91.0	28.59	30.4	43.6	1.80	1.25	2.68	53.3	1.14
182	1128	B	4	H	4	89.0	91.0	30.09	28.0	38.8	1.86	1.34	2.71	50.7	1.03
182	1128	B	4	H	5	89.0	91.0	31.59	28.5	39.9	1.84	1.31	2.69	51.1	1.05
182	1128	B	4	H	6	49.0	51.0	32.69	26.7	36.4	1.86	1.37	2.65	48.5	0.94
182	1128	B	5	H	1	39.0	41.0	34.59	31.7	46.5	1.75	1.20	2.62	54.3	1.19
182	1128	B	5	H	2	89.0	91.0	36.59	32.8	48.8	1.76	1.19	2.72	56.5	1.30
182	1128	B	5	H	3	89.0	91.0	38.09	34.0	51.4	1.75	1.15	2.74	57.9	1.37
182	1128	B	5	H	4	89.0	91.0	39.59	32.0	47.2	1.74	1.18	2.59	54.4	1.19
182	1128	B	5	H	5	59.0	61.0	40.79	33.4	50.1	1.75	1.16	2.70	56.9	1.32
182	1128	B	5	H	6	89.0	91.0	42.59	35.0	53.9	1.70	1.10	2.64	58.2	1.39
182	1128	B	6	H	1	79.0	81.0	44.49	38.4	62.3	1.65	1.02	2.66	61.8	1.62
182	1128	B	6	H	2	79.0	81.0	45.99	40.6	68.4	1.62	0.96	2.67	64.1	1.79
182	1128	B	6	H	3	79.0	81.0	47.49	41.3	70.5	1.60	0.94	2.65	64.6	1.82
182	1128	B	6	H	4	79.0	81.0	48.99	38.5	62.7	1.65	1.02	2.69	62.2	1.65
182	1128	B	6	H	5	79.0	81.0	50.49	39.8	66.2	1.63	0.98	2.69	63.5	1.74
182	1128	B	6	H	6	59.0	61.0	51.79	38.8	63.4	1.65	1.01	2.67	62.3	1.65
182	1128	B	6	H	7	39.0	41.0	53.09	39.7	65.7	1.64	0.99	2.70	63.4	1.73
182	1128	B	7	H	1	69.0	71.0	53.89	41.5	70.9	1.61	0.94	2.69	65.1	1.86
182	1128	B	7	H	2	54.0	56.0	55.24	31.1	45.2	1.78	1.23	2.68	54.1	1.18
182	1128	B	7	H	3	69.0	71.0	56.19	43.9	78.4	1.49	0.84	2.31	63.9	1.77
182	1128	B	7	H	4	69.0	71.0	57.69	45.1	82.1	1.48	0.81	2.32	65.0	1.86
182	1128	B	7	H	5	69.0	71.0	59.19	32.0	47.1	1.75	1.19	2.64	54.8	1.21
182	1128	B	7	H	6	79.0	81.0	60.79	34.1	51.8	1.68	1.10	2.51	55.9	1.27
182	1128	B	7	H	7	49.0	51.0	61.99	39.7	65.9	1.57	0.95	2.43	61.0	1.56
182	1128	B	8	H	1	69.0	71.0	63.39	30.7	44.3	1.78	1.24	2.65	53.4	1.15
182	1128	B	8	H	2	69.0	71.0	64.89	59.9	149.6	1.35	0.54	2.59	79.1	3.78
182	1128	B	8	H	3	69.0	71.0	66.39	52.4	110.2	1.44	0.69	2.63	73.9	2.83
182	1128	B	8	H	4	69.0	71.0	67.89	57.2	133.7	1.38	0.59	2.56	77.0	3.34
182	1128	B	8	H	5	69.0	71.0	69.39	58.8	142.7	1.36	0.56	2.53	77.9	3.52
182	1128	B	8	H	6	69.0	71.0	70.89	49.2	96.9	1.49	0.76	2.66	71.5	2.51
182	1128	B	8	H	7	39.0	41.0	72.09	47.1	88.9	1.52	0.80	2.65	69.7	2.30
182	1128	B	9	H	1	79.0	81.0	72.99	51.1	104.6	1.46	0.71	2.63	72.8	2.68
182	1128	B	9	H	2	79.0	81.0	74.49	57.1	133.0	1.38	0.59	2.54	76.8	3.30
182	1128	B	9	H	3	79.0	81.0	75.99	53.6	115.7	1.41	0.66	2.52	74.0	2.85
182	1128	B	9	H	4	79.0	81.0	77.49	51.1	104.3	1.45	0.71	2.57	72.3	2.61
182	1128	B	9	H	5	79.0	81.0	78.99	49.5	97.9	1.48	0.75	2.62	71.5	2.51
182	1128	B	9	H	6	79.0	81.0	80.49	51.8	107.6	1.44	0.69	2.55	72.8	2.68
182	1128	B	9	H	7	29.0	31.0	81.49	47.0	88.8	1.51	0.80	2.62	69.4	2.27
182	1128	B	10	H	1	79.0	81.0	82.49	51.8	107.3	1.45	0.70	2.59	73.0	2.71
182	1128	B	10	H	2	79.0	81.0	83.99	49.7	98.6	1.47	0.74	2.56	71.1	2.46
182	1128	B	10	H	3	79.0	81.0	85.49	51.3	105.5	1.44	0.70	2.50	72.0	2.58
182	1128	B	10	H	4	79.0	81.0	86.99	54.5	119.7	1.40	0.64	2.49	74.4	2.91
182	1128	B	10	H	5	79.0	81.0	88.49	57.3	134.0	1.36	0.58	2.46	76.3	3.21
182	1128	B	10	H	6	79.0	81.0	89.99	53.3	113.9	1.42	0.66	2.51	73.6	2.79
182	1128	B	10	H	7	39.0	41.0	91.09	52.2	109.2	1.41	0.68	2.42	72.1	2.58

Note: Only a portion of this table appears here. The complete table is available in **ASCII format.**

Table T18. Undrained shear strength measurements, Site 1128.

Leg	Site	Hole	Core	Type	Section	Interval (cm)	Depth (mbsf)	Maximum shear strength (kPa)	Peak (kPa)	Overburden stress (kPa)	S_u/P'_o
182	1128	B	1	H	2	123.3	2.73	6.93	8.45	42.9	0.2
182	1128	B	1	H	3	116.8	4.17	5.13	6.26	67.6	0.1
182	1128	B	1	H	4	82.6	5.33	7.11	8.67	84.3	0.1
182	1128	B	2	H	2	125.8	8.46	10.98	13.39	131.1	0.1
182	1128	B	2	H	2	126.8	8.47	6.66	8.12	131.2	0.1
182	1128	B	2	H	3	116.0	9.86	12.96	15.81	155.6	0.1
182	1128	B	2	H	4	116.6	11.37	18.99	23.16	181.6	0.1
182	1128	B	2	H	5	112.5	12.82	8.73	10.65	204.7	0.1
182	1128	B	2	H	5	116.6	12.87	18.99	23.16	205.5	0.1
182	1128	B	2	H	6	112.5	14.32	8.73	10.65	229.5	0.0
182	1128	B	2	H	6	120.8	14.41	22.23	27.11	230.9	0.1
182	1128	B	3	H	1	111.8	16.32	23.67	28.87	267.3	0.1
182	1128	B	3	H	2	132.1	18.02	38.43	46.87	295.1	0.2
182	1128	B	4	H	1	120.3	25.90	29.70	36.22	449.1	0.1
182	1128	B	4	H	3	126.7	28.97	34.74	42.37	511.2	0.1
182	1128	B	4	H	3	147.5	29.17	19.62	23.93	531.6	0.0
182	1128	B	4	H	4	112.1	30.32	44.73	54.55	546.6	0.1
182	1128	B	4	H	5	120.7	31.91	39.51	48.19	575.3	0.1
182	1128	B	5	H	1	112.5	35.33	15.93	19.43	607.8	0.0
182	1128	B	5	H	2	124.8	36.95	16.74	20.42	640.0	0.0
182	1128	B	5	H	3	111.6	38.32	14.31	17.45	656.6	0.0
182	1128	B	5	H	4	94.6	39.65	36.09	44.02	676.7	0.1
182	1128	B	5	H	5	94.6	41.15	36.09	44.02	705.1	0.1
182	1128	B	5	H	5	121.8	41.42	26.10	31.83	691.5	0.0
182	1128	B	5	H	6	75.5	42.46	46.26	56.42	708.8	0.1
182	1128	B	5	H	7	71.9	43.42	36.18	44.13	724.8	0.1
182	1128	B	6	H	1	118.7	44.89	33.84	41.27	712.4	0.1
182	1128	B	6	H	2	114.9	46.35	20.97	25.58	735.5	0.0
182	1128	B	6	H	3	103.6	47.74	24.48	29.86	750.1	0.0
182	1128	B	6	H	4	69.6	48.90	35.73	43.58	794.2	0.1
182	1128	B	6	H	4	69.6	48.90	35.73	43.58	794.2	0.1
182	1128	B	6	H	5	9.5	49.79	44.28	54.01	798.4	0.1
182	1128	B	6	H	6	123.3	52.43	22.32	27.22	846.9	0.0
182	1128	B	6	H	7	27.5	52.97	20.70	25.25	851.5	0.0
182	1128	B	7	H	1	136.4	54.56	40.59	49.51	860.4	0.1
182	1128	B	7	H	2	64.1	55.34	7.74	9.44	967.7	0.0
182	1128	B	7	H	3	114.5	56.65	18.27	22.28	828.5	0.0
182	1128	B	7	H	4	81.4	57.81	49.95	60.92	837.9	0.1
182	1128	B	7	H	5	117.8	59.68	62.64	76.40	1027.2	0.1
182	1128	B	7	H	6	131.4	61.31	36.81	44.90	1009.7	0.0
182	1128	B	7	H	7	66.4	62.16	56.16	68.49	959.6	0.1
182	1128	B	8	H	1	83.2	63.53	16.29	19.87	1110.9	0.0
182	1128	B	8	H	1	137.0	64.07	17.19	20.97	850.3	0.0
182	1128	B	8	H	2	110.4	65.30	47.07	57.41	866.3	0.1
182	1128	B	8	H	3	108.7	66.79	52.38	63.88	946.3	0.1
182	1128	B	8	H	4	125.8	68.46	62.91	76.73	925.7	0.1
182	1128	B	8	H	5	99.4	69.69	79.02	96.38	928.0	0.1
182	1128	B	8	H	6	116.8	71.37	55.17	67.29	1043.5	0.1
182	1128	B	8	H	7	22.6	71.93	77.58	94.62	1071.5	0.1
182	1128	B	9	H	1	127.3	73.47	44.73	54.55	1052.6	0.1
182	1128	B	9	H	2	117.7	74.88	44.91	54.77	1012.6	0.1
182	1128	B	9	H	3	107.3	76.27	61.74	75.30	1058.3	0.1
182	1128	B	9	H	4	103.9	77.74	76.95	93.85	1107.6	0.1
182	1128	B	9	H	5	125.6	79.46	68.40	83.42	1154.0	0.1
182	1128	B	9	H	6	101.3	80.71	23.31	28.43	1140.5	0.0
182	1128	B	9	H	7	37.6	81.58	48.51	59.16	1210.4	0.0
182	1128	B	10	H	1	131.4	83.01	71.64	87.37	1177.9	0.1
182	1128	B	10	H	2	106.2	84.26	68.22	83.20	1213.0	0.1
182	1128	B	10	H	3	116.2	85.86	50.67	61.80	1211.6	0.1
182	1128	B	10	H	4	100.5	87.21	97.38	118.77	1198.1	0.1
182	1128	B	10	H	5	122.7	88.93	114.93	140.17	1191.1	0.1
182	1128	B	10	H	6	107.0	90.27	129.06	157.41	1254.3	0.1
182	1128	B	10	H	7	26.3	90.96	126.54	154.33	1263.9	0.1
182	1128	B	12	H	1	136.3	102.06	144.72	176.51	1489.3	0.1

Note: Only a portion of this table appears here. The complete table is available in **ASCII format.**

Table T19. In situ formation temperature estimates, Site 1128.

Leg, core, section	Depth (mbsf)	Mudline temperature (°C)	Formation temperature (°C)	Fitting error (°C)
182-1128C-4H	0	2.16		
	0	2.48		
	35.00		3.81	0.020
	35.00		4.10	0.007
182-1128C-8H	0	1.84		
	0	1.90		
	74.00		5.29	0.010
182-1128C-12H	0	1.90		
	0	2.00		
	112.50		7.84	0.020
182-1128C-17X	0	1.85		
	0	1.95		
	0	1.52		
	0	1.60		
	146.00		10.03	0.010

Notes: Average mudline temperature = 1.92°C. This table is also available in **ASCII format.**

Table T20. Differences between depths to seismic horizons and corrected depths.

Seismic horizons	Predicted intersection (mbsf)	ITT corrected depth (mbsf)	Difference (m)
Horizon 1C_1	38		
Horizon 1C_2	83		
Horizon 1C_3	179	182	+3
Horizon 1C_3a	261	267	+6
Base of Cenozoic	602		

Notes: Predicted intersection depths were derived using high-resolution site-survey seismic data stacking velocities. Corrected depths were based on interval transit-time (ITT) data.